Comparative Investigation of Detection Techniques for Chloride-induced Corrosion of Loaded Reinforced Concrete Slabs

by

Parham Chabi

This thesis is submitted to the Faculty of Graduate and Postdoctoral Studies in partial fulfilment of requirements for the degree of

Master of Applied Science

Department of Civil Engineering

University of Ottawa

Ottawa, Ontario, Canada

The Master of Applied Science in Civil Engineering is a joint program with the Carleton University, administered by Ottawa-Carleton Institute for Civil and Environmental Engineering

Abstract

This study involved a comparative investigation of chloride-induced corrosion detection techniques on loaded reinforced concrete slabs which were exposed to deicing salts and wetting-drying cycles to simulate typical aggressive environments in cold climates. The studied techniques involved linear polarization technique, galvanostatic pulse technique, electrochemical impedance spectroscopy, half-cell potential and concrete electrical resistivity mapping. The results showed that concrete quality and moisture content have a direct effect on corrosion activity, and these properties are represented well with concrete electrical resistivity. The galvanostatic pulse technique was shown to correlate well with electrochemical impedance spectroscopy, which was used as a benchmark for corrosion rate measurements in this study; however, the galvanostatic pulse technique was not capable of detecting corrosion activity in saturated concrete accurately. The results of this research do not support the criteria provided by the ASTM C876-09 standard for using half-cell potentials to estimate the probability of reinforcing steel corrosion in reinforced concrete structures.

Acknowledgements

First, I would like to thank my supervisors Prof. Beatriz Martin-Perez and Prof. Burkan Isgor, for providing support throughout this project. Without their support it was quite impossible to accomplish this research. It was a fantastic opportunity for me to work under their supervision.

I am also thankful to Dr. Pouria Ghods for his contributions and support throughout this research.

I would like to appreciate the unlimited support of my family, especially my father, mother and my sister which kept me inspired throughout my MASc studies. I am forever in gratitude to them.

I would like to express my gratitude to Dr. Glen Chabi, who has been always supporting me.

I would like to thank Mr. Burak Gunay for his technical assistance throughout this research.

Many people have been helpful in various ways toward the accomplishment of this work, and I would like to appreciate their support.

Finally, I would also like to thank the financial support of this research by Natural Science and Engineering Research Council of Canada (NSERC) and the Faculty of Engineering at the University of Ottawa.

Table of Contents

List of Figures

List of Tables

List of Symbols

Symbols&Acronyms	***Explanation***
A	Area [m^2]
AC	Alternating current
C_{dl}	Double layer capacitance [F/m^2]
E	Potential (V)
E_{corr}	Free corrosion potential [V]
I	Current (A)
I_{corr}	Corrosion current [A]
i_{corr}	Corrosion current density [$\mu A/cm^2$]
β_a	Anodic Tafel constant [V/dec]
β_c	Cathodic Tafel constant [V/dec]
M	Molar mass [kg mol−1]
μ	Mean value
R_P	Polarisation resistance [kOhm×cm^2]
R_Ω	Ohmic concrete resistance [Ohm]
ρ	Concrete electrical resistivity [kOhm×cm]
T	Temperature [C]
t	Time [s]
ω	Angular frequency
Ag/AgCl	Silver-silver chloride (reference electrode)
CSE	Copper-copper sulfate (reference electrode)
EIS	Electrochemical impedance spectroscopy
GPR	Galvanostatic polarization resistance
LPR	Linear polarization resistance
SCE	Saturated Calomel electrode (reference electrode)
w/c	Water/cement-ratio

1. Introduction

1.1 Background

Concrete is the most common construction material used all over the world. Availability of aggregates and raw materials to produce portland cement, as well as ease of producing concrete in large quantities made reinforced concrete construction a universal technique for building civil engineering infrastructure.

Nowadays, many of the concrete structures, such as bridges, are exposed to aggressive environments that cause severe serviceability and safety problems. For instance, the increase in the use of chloride-containing de-icing salts on the roads has resulted in extensive steel corrosion in reinforced concrete transportation infrastructure (e.g. bridge decks), causing their premature failure. The scale of this problem has reached to alarming levels, especially in cold regions, such as most parts of Canada, where de-icing salts are extensively used. In a recent study by Koch et al. (2002) on the cost of corrosion, $8.3 billion was estimated as the annual cost of corrosion of US highway bridges. According to the National Association of Corrosion Engineers International (NACE 2002), the direct cost of corrosion in infrastructure is about $22.6 billion/year.

The corrosion of reinforcing steel in concrete is an electrochemical process at the concrete/steel interface in which the steel is oxidized in the concrete pore solution. This process leads to metal loss, but, within the highly alkaline environment provided by concrete, steel is covered with a protective oxide film (passive layer) so that under ideal conditions losses are typically less than 1 μm/year. Losses of this magnitude are not significant and do not raise any concerns about structural integrity. However, under less-than-ideal service conditions, steel can depassivate and lose the protective oxide film, which can lead to higher rates of metal loss (i.e., corrosion) and concerns for the structural integrity of reinforced concrete structures. Key factors affecting the depassivation and corrosion of steel in concrete include the chloride content and the pH of the pore solution around the reinforcement, the physical and the chemical properties of concrete, the surface characteristics and the chemical composition of the steel, and the presence of mechanical stresses (Bertolini et al. 2004).

The corrosion of steel reinforcement due to chloride ingress affects the durability of reinforced concrete structures in different ways, as illustrated in Figure 1.1. These processes include increased stress in the rebar due to reduced cross sectional area of steel; cracking, delamination and spalling of concrete cover as a result of the expansive corrosion products; reduction of the bond strength between steel and concrete; and deterioration of structural ductility as a result of diminished steel elongation capacity at maximum load. Chloride ingress into concrete depends on various parameters: concrete cover depth, quality and properties of concrete (porosity, permeability and W/C) and environmental conditions (e.g. presence of wetting/drying cycles and temperature) (Bertolini et al. 2004).

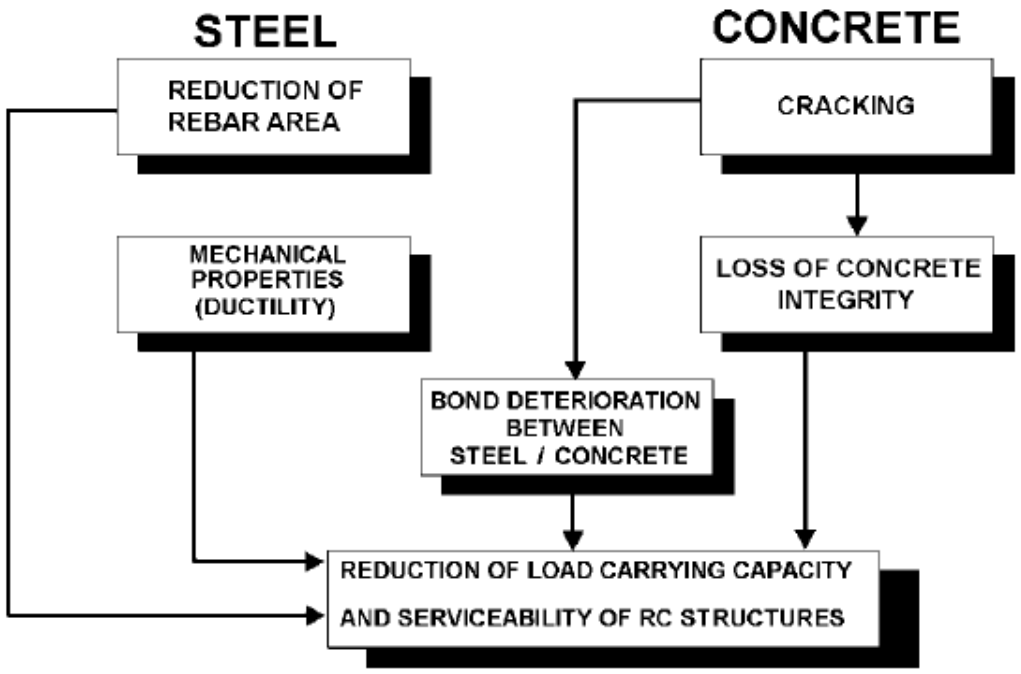

Figure 1-1: Effect of corrosion on the structural performance of reinforced concrete structures (Mong et al. 2002).

1.2 Problem definition

As shown in Figure 1.2, service life of reinforced concrete structures in aggressive environments can be divided into two distinct periods: initiation and propagation. In the first stage, ingress of aggressive agents (e.g. chloride salts) into the concrete cover takes place. Propagation stage starts when concentration of aggressive ions (e.g. chloride) at the level of reinforcement reaches to a critical level (chloride threshold), beyond which the passive film on the steel surface breaks down (depassivation), leaving reinforcement without protection against extensive corrosion.

The propagation stage can also be classified into three parts with respect to the level of structural damage: non-detectable, detectable and visible damage, which may involve corrosion-induced cracking, rust stains along cracks in concrete, delaminaton and spalling of concrete cover. Regular inspections of reinforced concrete structures, which generally take place in the form of visual inspection, mostly detect steel corrosion in the last stage, during which the damage is visible. In most cases, when the damage is visible, repair and rehabilitation options for the structure are difficult and costly. Destructive techniques that are based on actual steel mass loss measurements and that may detect corrosion at early stages are accepted widely as not practical (Hansson 1984).

The important role of non-destructive detection of corrosion activity in reinforced concrete structures has been recognized by most structure owners. Early detection of corrosion activity in concrete structures before they experience extensive damage is critical for developing efficient mitigation, repair and rehabilitation strategies. In recent decades, a number of non-destructive testing techniques (NDTs) and standards (e.g. ASTM C876 for half-cell potential mapping) have been developed to address this issue. These techniques have been generally studied in small-scale laboratory specimens with simplified reinforcement detailing and without any service loading. However, the success of these methods in accurately detecting corrosion activity in reinforced concrete structures is still a subject of debate for structures under service conditions. This gap in research provides the main motivation for this research.

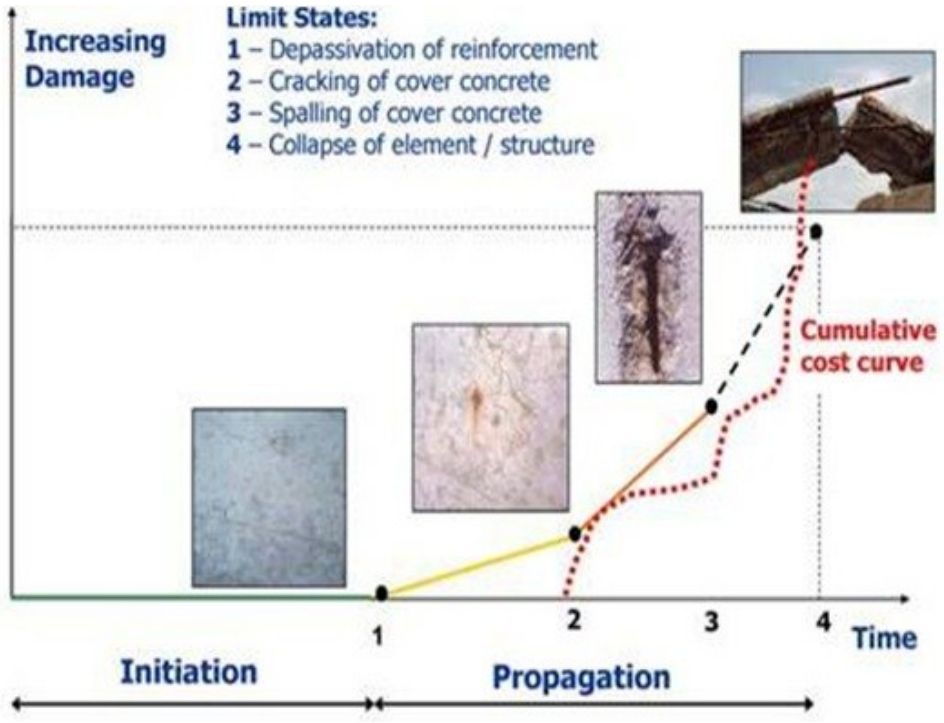

Figure 1-2: Service life of steel in reinforced concrete structures in aggressive environments (Legat 2009).

1.3 Research objectives and scope

The overall objective of this investigation is to study comparatively the most common corrosion detection techniques used in practice on realistically detailed reinforced concrete slabs that are loaded at service level. The study is designed to investigate important parameters that may affect steel corrosion in reinforced concrete such as W/C of concrete, moisture content of concrete, load-induced cracking and mechanical stresses. To control these parameters systematically and accurately, three large-scale concrete slabswere previously designed and built in the laboratory (Deif 2010). The slabs were loaded and

exposed to chloride-containing salts and wetting and drying cycles to initiate reinforcement corrosion. Half-cell potential mapping, as prescribed by ASTM C876, was used to predict the probability of steel corrosion in the slabs and to study the validity of the standard in service conditions. Practical and commercially-available linear polarization (LPR) and galvanostatic pulse (GPR) techniques were used to measure corrosion rates in the slabs, and these measurements were compared with corrosion rate measurements obtained from electrochemical impedance spectroscopy (EIS), which is an advanced technique that is suitable for laboratory studies. It was assumed that corrosion rate measurements through EIS were relatively accurate; therefore, comparisons were carried out against the EIS measurements. Electrical resistivity of concrete was mapped for each slab at different conditions so that its correlation with steel corrosion in the studied slabs is investigated.

1.4 Organization of the thesis

The thesis consists of six chapters: Chapter 1 presents the background, problem definition, research objectives and scope of this research. Chapter 2 presents theoretical and literature review on corrosion of steel in concrete with focus on electrochemical corrosion detection techniques and factors affecting the corrosion process. Chapter 3 presents the experimental program and setup to achieve the objectives discussed in Chapter 1. Chapter 4 is devoted to present the results of the experimental study. Chapter 5 presents discussions on the results and compares corrosion detection techniques. The main conclusions of this experimental research along with recommendations for future work are presented in Chapter 6.

2. Theoretical and Literature Review

2.1 General

This chapter presents a brief background on the theory of corrosion of steel in concrete to establish a base for the discussions provided in this thesis. This theoretical review is not intended to be comprehensive in its scope because of the vast nature of the subject, but more detailed information can be found in Bentur et al. (1997), Broomfield (1997) and Bohni (2005). In addition to the theoretical review, a literature review on the previous experimental studies dealing with detection and measurement of corrosion of steel in concrete is presented in this chapter.

2.2 Corrosion of steel in concrete

Corrosion of reinforcing steel is one of the most prevalent and costly deterioration problems in concrete infrastructure. The corrosion of steel rebars in concrete can be triggered by either carbonation of the concrete cover or penetration of chloride ions into the concrete (Broomfield 1997). Carbonation of concrete leads to a reduction of the natural alkalinity of the concrete, leading to steel depassivation once the carbonation front has

reached the reinforcement. Chloride-induced corrosion initiates once the content of chloride ions on the surface of steel exceeds a threshold value, which shows high degree of variability as reported in numerous studies (Angst et al. 2009; Ghods 2010).

Corrosion is a destructive electrochemical process consisting of two half-cell reactions: oxidation and reduction. In the case of corrosion of steel in the alkaline environment of concrete, oxidation and reduction reactions can be expressed by Eqs. 2.1 and 2.2, respectively (Bertolini et al. 2004):

$$Fe \rightarrow Fe^{2+} + 2e^{-} \qquad \textit{Eq. 2.1}$$

$$\frac{1}{4}O_2 + \frac{1}{2}H_2O + e^{-} \rightarrow OH^{-} \qquad \textit{Eq. 2.2}$$

The oxidation reaction takes place at the anodes, and the reduction reaction takes place at the cathodes. The electrons produced at the anodes are consumed at the cathodes, and the process is completed by the migration of hydroxide ions from the cathodes to the anodes, as illustrated in Figure 2.1

If the anodic reaction given in Eq.2.1 were the only reaction that took place during the corrosion process, there would be no cracking and spalling of the concrete surrounding the steel. However, Fe^{2+} ions react within the pore solution to form the common rust. The following reactions represent the formation of the so-called “red rust” after iron dissolution occurs at the anodic sites on the reinforcement (Broomfield 1997):

$$Fe^{2+} + 2OH^{-} \rightarrow Fe(OH)_2 \qquad \textit{Eq. 2.3}$$

$$4Fe(OH)_2 + 2H_2O + O_2 \rightarrow 4Fe(OH)_3 \qquad \textit{Eq. 2.4}$$

$$2Fe(OH)_3 \rightarrow 2H_2O + Fe_2O_3.H_2O \qquad \textit{Eq. 2.5}$$

Fe_2O_3, or red rust, is the corrosion product whose volume is three to four times larger than the volume of the steel with the same mass. Therefore, the formation of red rust causes internal stresses and generally leads to the cracking and spalling of the concrete surrounding the reinforcement. Additional reactions other than the ones given in reactions 2.1 to 2.5 may take place during the course of the corrosion process, (e.g., hydrogen evolution in the absence of oxygen or the formation of black rust); further details on these can be found in Uhlig's corrosion handbook (2011).

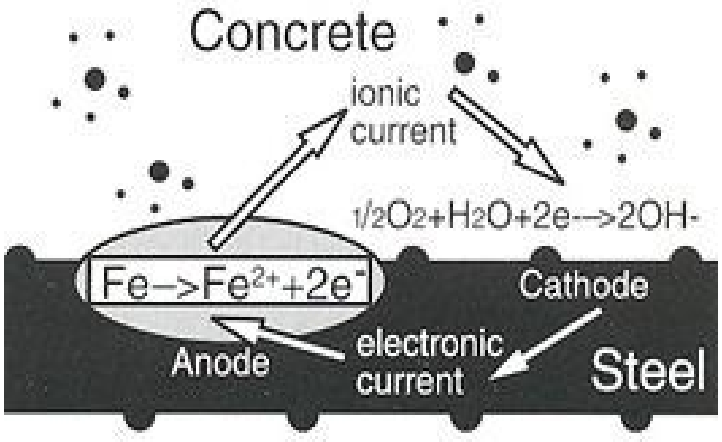

Figure 2-1: Anodic and cathodic reactions in reinforced concrete (Broomfield. 1997).

The corrosion of steel reinforcement in concrete is affected by the material properties of steel and concrete as well as the environmental factors that surround them. A comprehensive review of these factors is provided by Ghods (2010); therefore, they are not

repeated here in detail. This section provides a brief review of major concepts that are relevant to the study presented in this thesis.

Due to the high alkalinity of the concrete (pH>13), carbon steel reinforcement rapidly passivates after casting in concrete: Iron oxides and hydroxides form a nano-scale (around ~10 nm thick) protective layer on the surface of the rebar, which is called the passive film (Ghods 2010). In the passive state the corrosion rates of steel are insignificant – typically at levels smaller than 1 μm/year. If the alkalinity of the concrete decreases, the passive layer may break down, and in the presence of the water and oxygen, the corrosion rates may significantly increase. A possible mechanism that can reduce the alkalinity of concrete is its carbonation due to the access CO_2 in the atmosphere (Bertolini et al. 2004).

In addition to the pH-reducing processes like carbonation, chlorides are also well known to cause loss of passivity (i.e., depassivation) if they are present in concrete in sufficient concentrations (i.e., above a chloride threshold). Chloride ions can be found in concrete in different forms: dissolved (free) chloride ions in the concrete pore solution, physically adsorbed to the concrete pore walls, and chemically bound to the concrete hydration products (Neville 1996). Only free chloride ions in the pore solution of the concrete are generally assumed to be responsible for initiation of the corrosion process (Tuutti, 1982).

Chloride thresholds in concrete are generally represented in terms of chloride content as a percentage of mass of cement in concrete (ASTM C114 2009, BS1881, 1988). A number of researchers have demonstrated the dependence of chloride thresholds on alkalinity (Hausmann 1967, Goni and Andrade 1990, Venu et al. 1965, Li and Sagues 2001); therefore, it is also common to represent chloride thresholds as chloride-to-

hydroxide concentration ratio, Cl^-/OH^-. In spite of numerous studies conducted to establish a common chloride threshold responsible for depassivation of steel embedded in concrete, there is significant variability in the chloride threshold values (Angst et al. 2009). Figure 2.2 shows that the reported threshold Cl^-/OH^- values vary in a wide range from 0.01 to 45. Table 2.1 provides a description of the abbreviations used in Figure 2.2. It can be observed from Figure 2.2 that a large number of factors play a role in chloride thresholds; these factors include chemical and physical properties of concrete, surface conditions of steel and environmental conditions. However, it is also critical to note that corrosion detection and measurement techniques also influence how chloride thresholds are determined (Karadakis 2010).

Table 2-1: Abbreviations in Figure 2.2 (reproduced from Ghods 2010).

Exposure medium	**Steel condition**	**Corrosion detection and measurement techniques**
FA - Fly ash *GGBS* - Ground granulated blast furnace slag *OPC* - Ordinary portland cement *SF* - Silica fume *SRPC* - Sulfate resistant Portland cement	*ABR* - Abraded *AR* - As-received *CL* – Cleaned or degreased *MIL* - Mill-scaled *P* - Polished *PR* - Pre-rusted *RIB* - Ribbed steel bars *SB* - Sandblasted *SM* - Smooth steel bars	*E* – Potential *EIS* - Electrochemical impedance spectroscopy *GP* - Galvanostatic polarisation *LR*P - Linear polarisation resistance *MC* - Macro-cell current *PC* - Potentiostatic control *PDP* - Potentiodynamic polarisation *VI* - Visual inspection *WL* - Weight loss

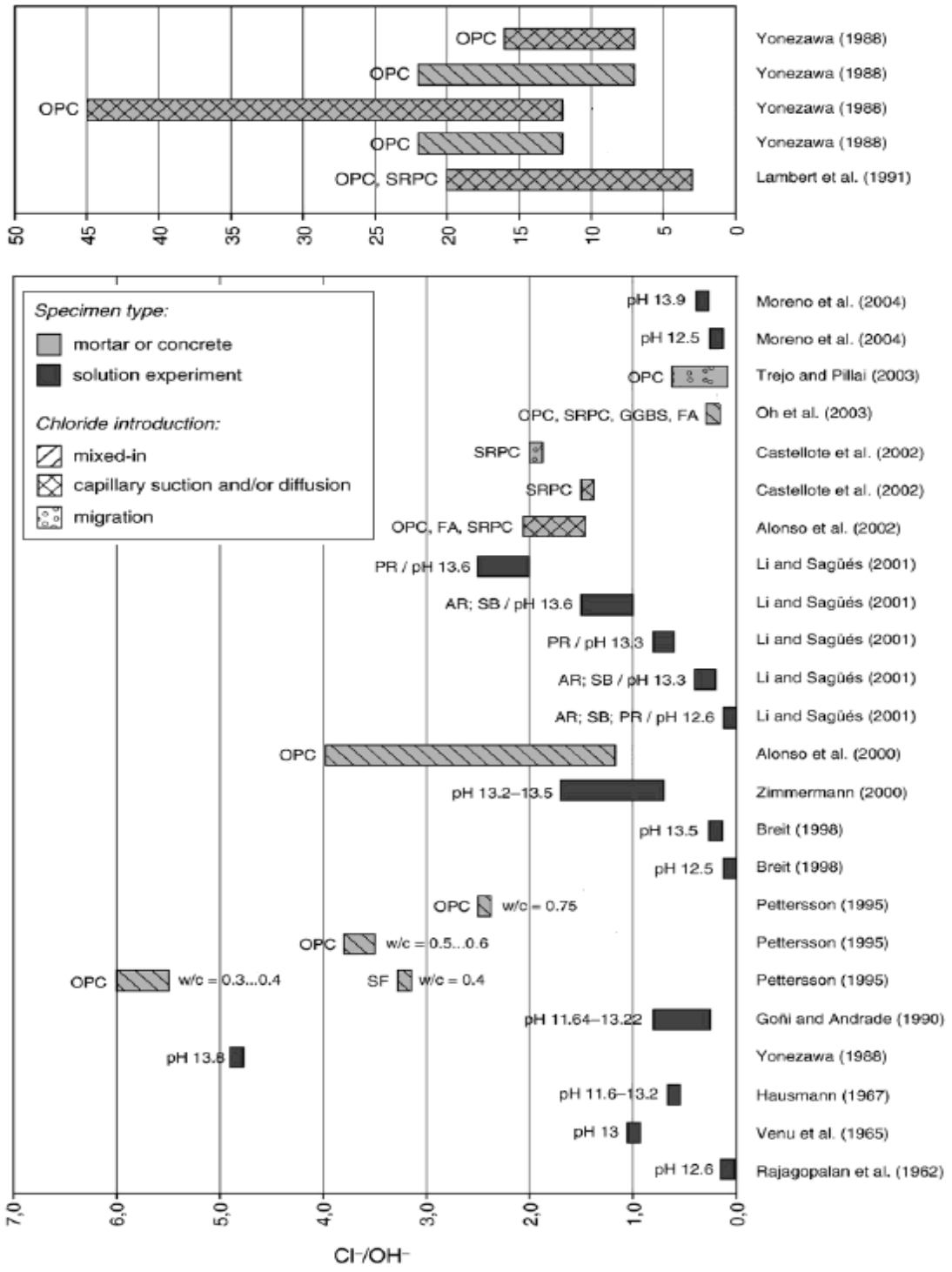

Figure 2-2: Reported chloride thresholds (taken from Angst et al. 2009), abbreviations are given in Table 2.1.

A widely accepted observation among studies on corrosion is that the corrosion process is highly correlated with concrete quality; for instance, a higher water-to-cement ratio will lead to a higher probability of corrosion activity. Chloride ions penetrate into concrete through the porous structure of concrete; therefore, the chloride permeability of concrete is a factor affecting corrosion. Water-to-binder ratio (w/b) of concrete reflects the relationship of porosity distribution and permeability (Sanberg. 1995). Figure 2.3 (A) shows the relationship of chloride diffusivity and water-to-binder ratio (w/b) for normal concrete. Figure 2.3 (B) illustrates the relationship between concrete water-to-cement ratio (w/c) and average content of chloride by mass of cement (%) on drilled concrete cores taken from existing concrete structures exposed to a chloride environment. Previous studies on chloride thresholds have revealed that the chloride threshold increases by reducing the water-to-binder (w/b) ratio of concrete (Hansson and Sorensen 1990, Pettersson and Sandbeerg 1997, Poupard et al. 2004). In addition, because of the direct effect of supplementary cementious materials (SCMs) on the quality concrete, they have a direct influence on the chloride thresholds (Pettersson 1993, 1996).

Environmental conditions such as relative humidity, temperature, wetting/drying of concrete and oxygen availability affect the corrosion process. Pettersson (1996) investigated the effect of relative humidity on the chloride concentration threshold; the results of this study are summarized in Figure 2.4. The results show that by increasing the relative humidity up to 90%, the chloride threshold decreases; however, by increasing the relative humidity beyond 90% the chloride thresholds increase. This happens due to the reduction of gas permeability (particularly oxygen) as the concrete is saturated; oxygen diffusivity in concrete decreases with increasing moisture content of concrete. Tuutti

(1982) investigated oxygen diffusivity in concrete as a function of concrete relative humidity, as illustrated in Figure 2.5, and found that diffusivity of oxygen reduces by increasing the relative humidity.

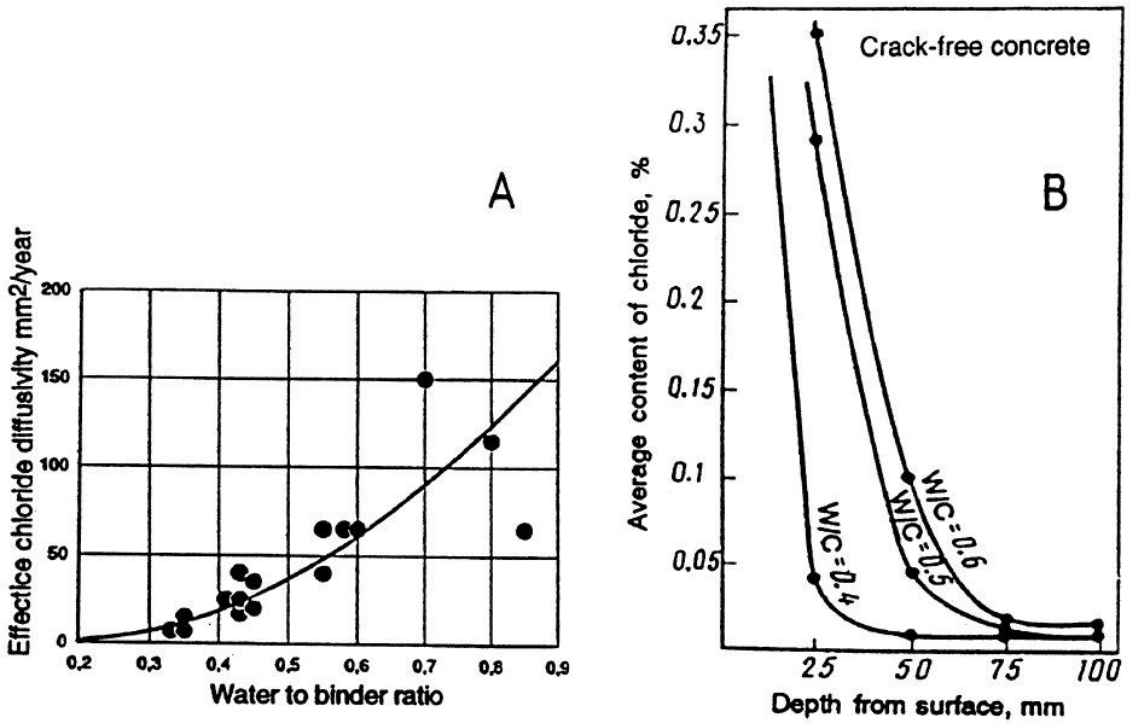

Figure 2-3: (A) Relationship between water-to-binder ratio and chloride diffusivity. (B) Relationship of concrete water-to-cement ratio and average content of chloride, measured on concrete cores taken from existing concrete structure after 830 days exposure to salts (Taken from Sandberg. 1995).

Ambient temperature also affects the corrosion initiation and propagation by affecting the diffusion of oxygen and chloride ions into the concrete. Increase of ambient temperature leads to an increase of chloride mobility into concrete, facilitating the accumulation of chloride ions at the concrete-rebar interface. Previous studies (Tuutti 1982, Schiessl and Raupach 1988, 1990) have shown that there is a linear relation between the

corrosion rate and ambient temperature; increasing the ambient temperature leads to an increase of the corrosion rate.

Concrete exposed to wetting/drying cycles has also a higher risk of reinforcing steel corrosion (Page et al. 1991). The cycles of drying and wetting of the concrete cover lead respectively to an accumulation of salts at the surface and subsequent fast penetration by capillary absorption. Cycles of wetting and drying also facilitate carbonation of the concrete cover. Moreover, reduction of the concrete resistivity due to wetting/drying cycles has been reported (Rehm et al. 1981).

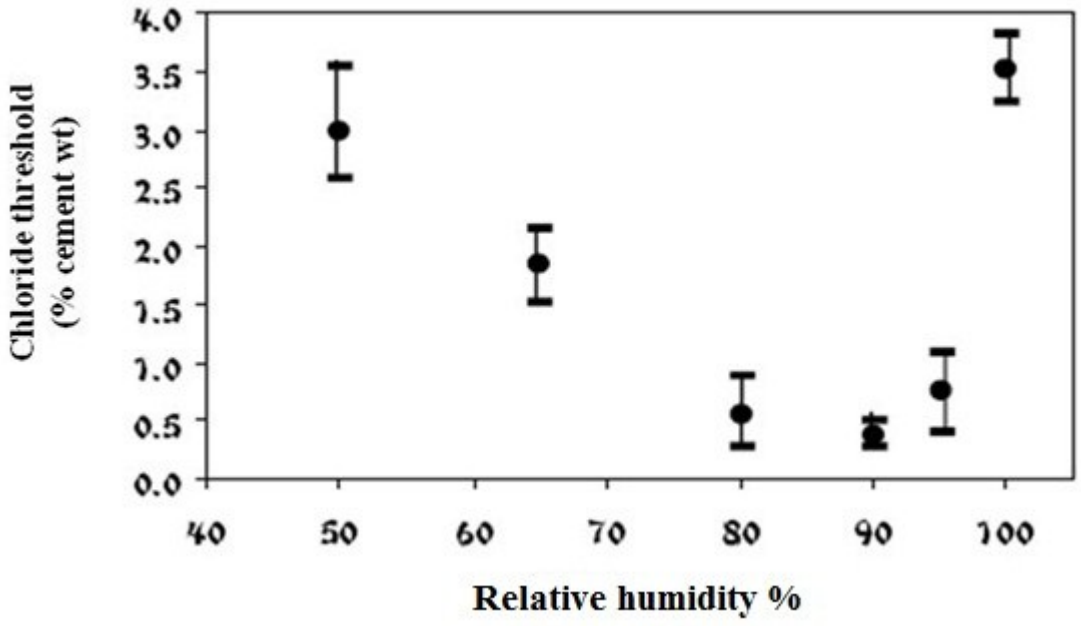

Figure 2-4: The effect of relative humidity on the chloride threshold of a concrete with 0.5 water-to-cement ratio (Taken from Pettersson 1996).

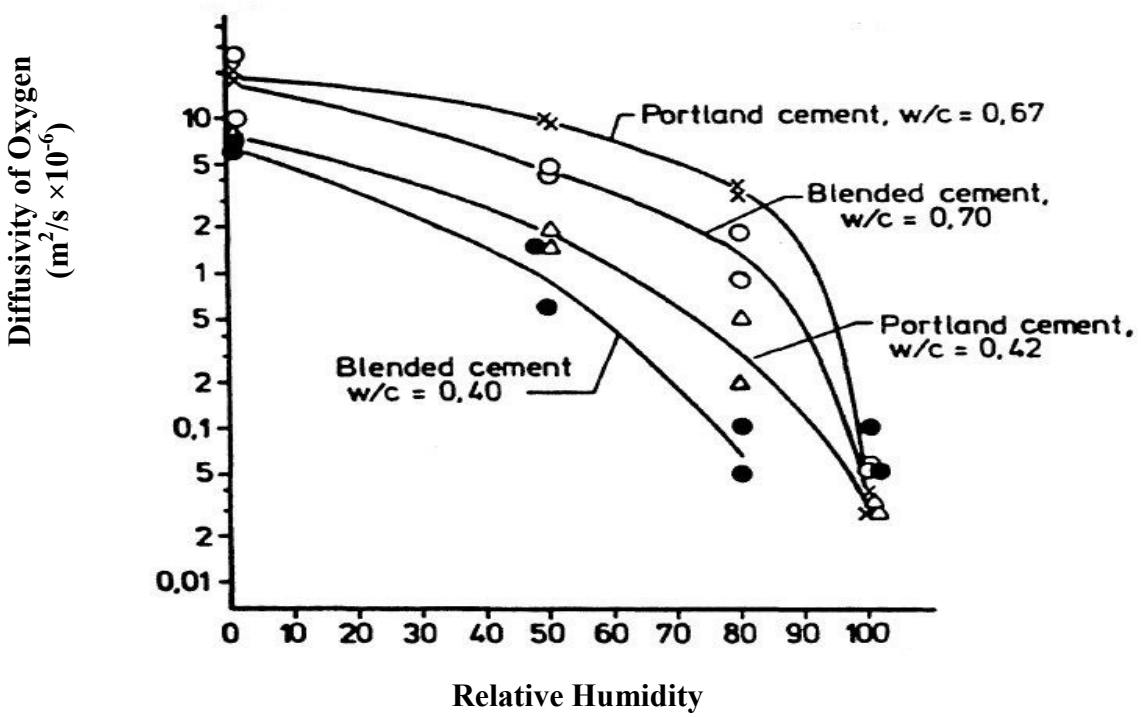

Figure 2-5: Relationship between oxygen diffusivity and concrete relative humidity (Taken from Tuutti 1982).

2.3 Detection and measurement of steel corrosion in concrete

Early studies on non-destructive tests to develop concrete corrosion detection techniques were carried out in the 1950`s and 1960`s (Stratfull 1957, Jones and Greene 1966, Monfore 1968). Corrosion rate measurements using electrochemical techniques were developed from corrosion studies of metal in aqueous solutions, and then it was standardized in ASTM G3-84. Early application of electrochemical techniques in reinforced concrete structures has been reported in studies related to cathodic protection of steel rebar in concrete (Stratfull 1983, Schell et al. 1985, Gonzalez et al. 1985). The application of advanced electrochemical techniques goes back to the seventies and eighties

(Andrade et al. 1996). This section provides a background on the commonly used corrosion rate detection and measurement techniques in concrete structures.

2.3.1 Half-cell potential mapping

Half-cell potential mapping is the most common non-destructive technique for detecting corrosion in reinforced concrete structures. The early utilization of half-cell potential measurements to assess steel corrosion in concrete was first reported by Spellman and Stratfull (1973) and Stratfull et al. (1975). Later in 1977 this method was standardized as ASTM C876-77. This standard provides information and guidelines for measuring and interpreting the results. The last version of this standard has been published in 2009 as ASTM C876 – 09 (2009).

As described in section 2.1, corrosion in concrete is an electrochemical process; active and passive areas along the rebar embedded in concrete show differences in electrical potential. This is due to the current flow between the anode and the cathode. Actively corroding areas on the rebar act as anodes (showing more negative half-cell potential), while passive areas on the rebar act as cathodes (showing more positive half-cell potential). The surface of the steel is not accessible for potential measurements, but potentials can be measured easily on the accessible surface of concrete. If it is assumed that the concrete cover thickness is not extremely large and resistivity of concrete is not very high, negative potentials on the corroding areas of steel can be observed from the concrete surface. A typical half-cell potential is a contour plot of the potentials on the concrete surface.

In half-cell potential mapping, the potential difference between an external reference electrode (e.g. $Cu/CuSO_4$, Ag/AgCl) located at the surface of concrete and the embedded reinforcement is measured with a high impedance voltmeter. A solid electrical connection between the reinforcement and the voltmeter, and a wet connection between the external electrode and the reinforcement through the concrete cover are essential for obtaining reliable readings. Figure 2.6 schematically illustrates the test setup for a typical half-cell potential test in reinforced concrete structures.

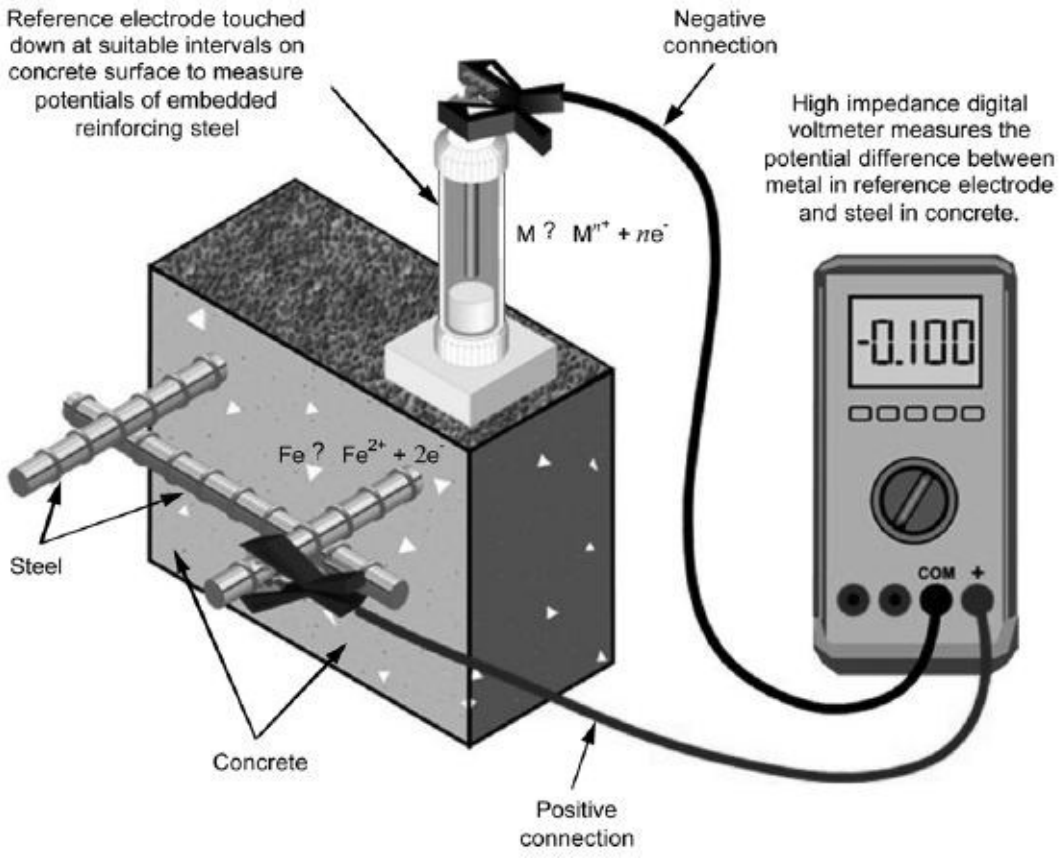

Figure 2-6: Schematic illustration of half-cell potential measurement on the surface of reinforced concrete. (ASTM C876 – 09).

ASTM C876 states that the more negative the measured surface potential, the greater probability of corrosion: half-cell potential measurements less than -350 mV with

respect to the copper/copper sulfate electrode (CSE) corresponds to a 90% probability. When the measurement is greater than -200 mV (vs. CSE) the probability is less than 10%. When the potential is between -350 mV (CSE) and -200 mV (CSE), the corrosion state of the rebar cannot be predicted.

Despite its widespread application, the interpretation of half-cell potential mapping results continues to be a major challenge for engineers. One of the main reasons for this difficulty is that half-cell potential mapping only provides information to predict the probability of the occurrence of corrosion without giving any insight into the rate (or kinetics) of corrosion. Pour-Ghaz et al. (2009) showed that, for the same corrosion rate, one can measure different potentials at the surface of concrete, corresponding to different values of concrete resistivity, and thus have more than one estimated probability of corrosion for the same actual state of corrosion.

The correlation between the half-cell potentials on the concrete surface and the probability of corrosion on the steel surface are quite sensitive not only to the concrete resistivity, but also to the anode-to-cathode surface area ratio (A/C ratio) and cover thickness. Pour-Ghaz et al. (2009) observed that larger concrete resistivity or larger cover thickness result in weaker correlation between the two potentials, making the interpretation of half-cell data on the concrete surface to predict the probability of corrosion on the steel surface rather difficult.

Half-cell potential measurement is also a function of the type of corrosion. In the case of uniform micro-cell corrosion, in which the A/C ratio is near unity, the potential readings at the surface of concrete are typically close to the potential at the interface of steel and concrete; however, in the case of non- uniform macro-cell corrosion, local or pitting corrosion with a small A/C ratio, the measured potentials at the surface of concrete

can be substantially different from those of the steel/concrete interface. When the average potential at the surface of concrete is a large value (i.e., more positive) the probability of the occurrence of corrosion is low, as per ASTM C-876; however the rate of such corrosion, if it occurs in the form of localized corrosion, can be very high. If the average potential at the surface of concrete is a small value (i.e. more negative), the probability of the corrosion is higher, but such corrosion may proceed more uniformly. Accurate detection of localized corrosion, in which A/C ratio can be small, may not be feasible with half-cell potential measurement method unless supplementary information is provided.

2.3.2 Corrosion rate measurement using polarization resistance techniques

The corrosion rate may be expressed in different ways such as corrosion current density (amount of current passing per unit steel surface area), section loss or rebar diameter reduction over time. Faraday's law expresses the relation between section loss and corrosion current:

$$\frac{\Delta x}{\Delta t} = \frac{M}{zF\rho} \times i_{\text{corr}} \qquad \textit{Eq. 2.6}$$

where Δx is the section loss of steel, Δt is the duration of corrosion, M is the molecular weight of metal (M=56 g/mol for Fe), z is the number of ionic charges (z=2 for Fe), F is Faraday's constant (F=96,480 C/mol or A.s/mol for Fe), ρ is the density of metal (for Fe, ρ = 7.85 g/cm^3) and i_{corr} is the density of corrosion current, which is often expressed in μA/cm^2. As per Eq. 2.6, 1 μA/cm^2 of corrosion current density equals to 11.6 μm/yr of section loss.

First, Bonhoeffer and Jenna (1951) described the polarization resistance as a slope of the polarisation curve. The concept of "polarization resistance" describes the rate of potential change, ΔE, due to an external applied current, Δi, at a potential close to the open circuit potential. Later, Stern and Geary (1957) formulated the relation between the polarization resistance, R_p, and the corrosion current at the open circuit potential as follows:

$$R_p = \frac{B}{I_{corr}} = \frac{\Delta E}{\Delta i}\ ,\ E \to 0 \qquad \textit{Eq. 2.7}$$

where B is a constant value, which relates R_p to I_{corr}. The value of B depends on the anodic and cathodic Tafel (βa and βc) slopes in the linear regions of the Tafel diagram (potential versus i), as illustrated in Figure 2.7, and it can be obtained for most systems from:

$$B = \frac{\left|\beta a.\beta c\right|}{2.303 \cdot (\left|\beta a\right| + \left|\beta c\right|)} \qquad \textit{Eq. 2.8}$$

Based on gravimetric comparisons as per ASTM G1 (1999), Andrade and Gonzalez (1978) have suggested B values of 26 mV for active steel and 52 mV for passive steel. However, these assumptions are not without controversy (Song 2000). Under passive conditions, the anodic Tafel slope approaches to Infinity. Assuming the cathodic Tafel slope for rebar in the passive state is around β_c = 200-230 mV/dec, as a number of researchers have pointed out (Elsener 2005, Garces et al. 2005), Eq. 2.8 yields a value of B of around 100 mV ($B = \beta c$ /2.303). The corrosion rates calculated using this constant would be larger than the one calculated with B = 52 mV, as suggested by Andrade and Gonzalez (1978). Therefore, the 52-mV assumption of B for passive steel may not be an appropriate

value for calculating the corrosion rate of reinforcing steel in the passive state; in fact, it underestimates the corrosion rate.

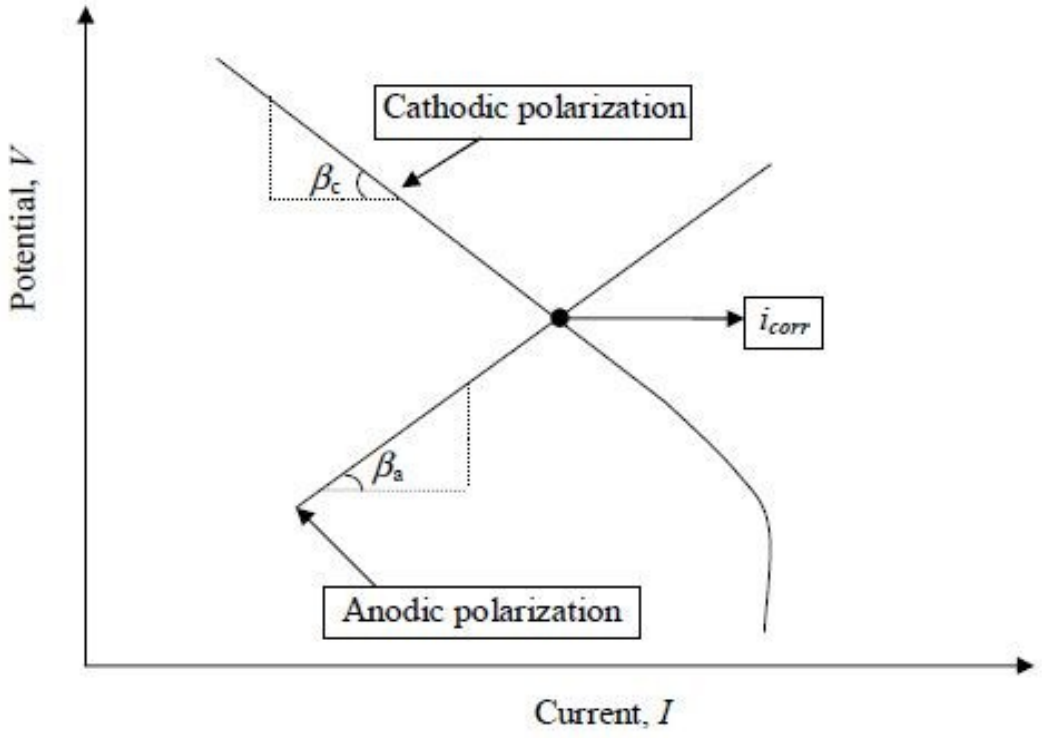

Figure 2-7: Anodic and cathodic polarization curves and corresponding Tafel slopes.

Tafel slopes, partly because of the complex conditions that the concrete pore solution presents and partly due to environmental effects (Ge and Isgor 2007), are quite difficult to estimate. On the other hand, using a reliable value for *B* in Eq. 2.7 is crucial in calculating the corrosion rate of reinforcing steel accurately; therefore, this is one of the main drawbacks of all polarization resistance techniques. The actual polarization resistance, R_p, is the slope of the polarization curve around the corrosion potential when the current, *I*, alters the polarity from negative to positive (Figure 2.8).

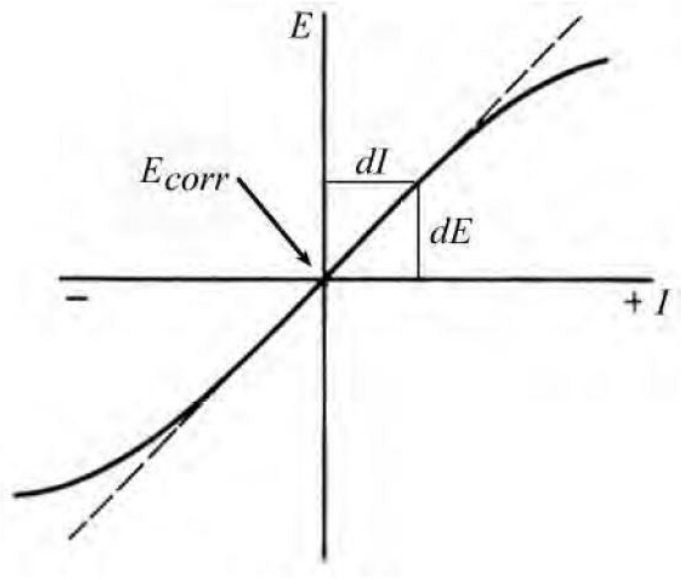

Figure 2-8: Linear relationship between potential drift and current around the open circuit potential, Ecorr (reproduced from Bardal 1994).

There are various techniques for measuring the polarization resistance, such as linear polarization technique, pulse technique and electrochemical impedance spectroscopy (EIS). The linear relation between potential drift and current density (*dE/dI),* as depicted in Figure 2.8, is a requirement for measuring polarization resistance, R_p, in the mentioned techniques. For steel embedded in concrete, this linearity around the corrosion potential has been found to be around 20 mV for non-corroding steel and 50 mV for corroding steel (Andrade 1973, Polder et al. 1993).

A major drawback of this method is that the area of reinforcing steel that is being polarized by the applied potential, *E* is not known with certainty. In order to address this limitation, instruments applying this technique use a "guard ring" to confine the polarization to a specified length of the steel reinforcement. However, the effectiveness of

guard rings in containing the polarized area of the reinforcement is a subject of debate (Flis et al. 1993, Flis et al. 1995, Gepraegs and Hansson 2004).

2.3.3 Linear polarization resistance technique (LPR)

One of the methods of measuring polarization resistance is the linear polarization resistance technique (LPR). The early application of linear polarization technique in reinforced concrete goes back to the 1970`s (Andrade 1973). Later, this technique became popular among researchers as a non-destructive technique to investigate corrosion activity; a number of commercially available devices are based on this technique.

This technique typically uses a three-electrode cell (with or without a guard ring for current confinement) and relies on the identification of the linear portion of the potential drift vs. current relationship around the open-circuit potential. It is generally suggested that the potential sweep should not go beyond ±12 mV on both sides of the open-circuit potential; otherwise, the linearity of the relationship cannot be assured. A typical equipment setup to measure linear polarization resistance is illustrated in Figure 2.9.

The linear relationship between potential drift vs. current can be captured using two approaches (Law et al. 2000):

- Potentiostatic sweep: in which the voltage is increased with a constant sweep rate and the response current is recorded;
- Galvanostatic sweep: in which the current is increased with a constant sweep rate and the response potential is recorded.

As there is an ohmic resistance (concrete resistivity), R_Ω, between the steel and the reference electrode, the applied or recorded potential, ΔE_a, is the sum of the polarizing potential, ΔE_p and the ohmic drop, $I_a \cdot R_\Omega$:

$$\Delta E_{\mathbf{p}} = \Delta E_a - \Delta E_\Omega = \Delta E_a - I_a \cdot R_\Omega \qquad \textit{Eq. 2.9}$$

Hence, it is critical to know the ohmic resistance, R_Ω, in order to calculate the polarization resistance, R_p, accurately.

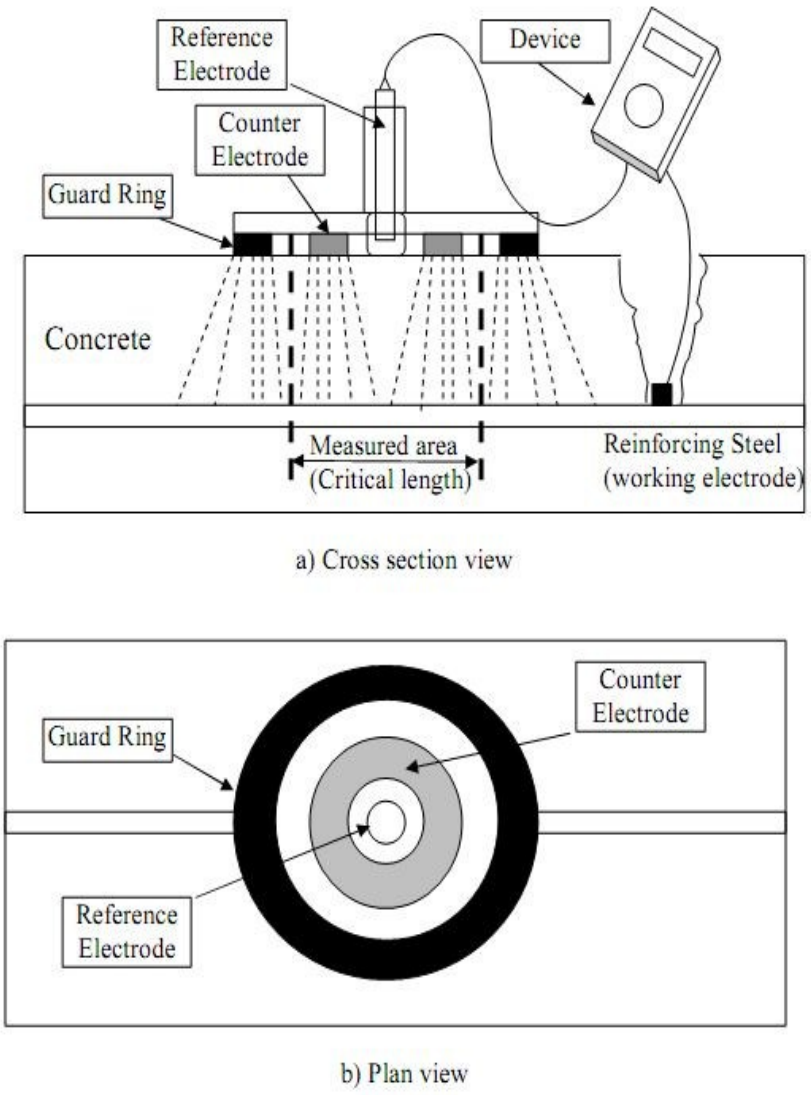

Figure 2-9: Schematic illustration of a polarization resistance probe with current confinement.

GECOR 6 is one of the commercially available instruments to measure corrosion rate according to the linear polarization resistance. This device can be used in concrete testing labs or in the field. This device utilizes galvanostatic linear polarization resistance to measure the polarization resistance, R_p, and has a sensorized guard ring to confine

applied current from counter electrode. GECOR 6 probe consists of two circular stainless-steel rings, the inner one works as a counter electrode (inner diameter, 11 mm; outer diameter, 70 mm), while the other one works as a guard ring (inner diameter, 140 mm; outer diameter, 180 mm).

GECOR 6 probe consists of three $Cu/CuSO_4$ electrodes (Feliu et al. 1990). The electrode located at the center of the probe acts as a reference electrode, and there are two additional auxiliary electrodes, located between the counter electrode and the guard ring which control the counter current. The auxiliary electrodes are at a distance of 45 and 65 mm from the center of the probe. GECOR 6 starts the measurement process by measuring the corrosion potential, E_{corr}, through the three reference electrodes until stability of the difference between the corrosion potential readings is established. After the first step, a trial current pulse is applied to the system by the counter electrode, and the potential response is recorded to calculate the magnitude of optimum current to obtain the polarization resistance. The final step of measurement is to apply a constant current through the counter electrode for 100 seconds; this current changes the potential of the reinforcement in concrete with respect to the time. During the polarization time, a secondary current is applied through the guard ring to keep the potential differences between the auxiliary reference electrodes the same as the ones recorded during the first step (see Figures 2.10 and 2.11).

The obtained polarization resistance, R_p, is corrected for the ohmic potential drop, $I_a \cdot R_\Omega$, and the corrosion rate calculated using Eq. 2.10 by considering a constant value of B equal to 26 mV:

$$i_{corr} = \frac{B}{A \times R_p} \qquad \textit{Eq. 2.10}$$

where i_{corr} is the corrosion rate expressed in μA/cm^2, and A is the confined length of the reinforcement, which needs to be input before any measurement by the operator using Eq. 2.11:

$$A = 3.14 \times 10.5 \times D \qquad \textit{Eq. 2.11}$$

where D is the reinforcement diameter in cm.

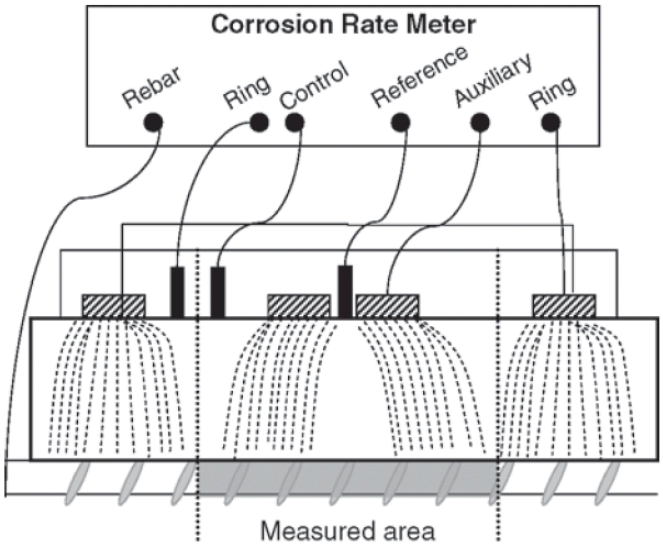

Figure 2-10: Schematic of applied current and guard ring for confinement (Taken from Luping. 2002).

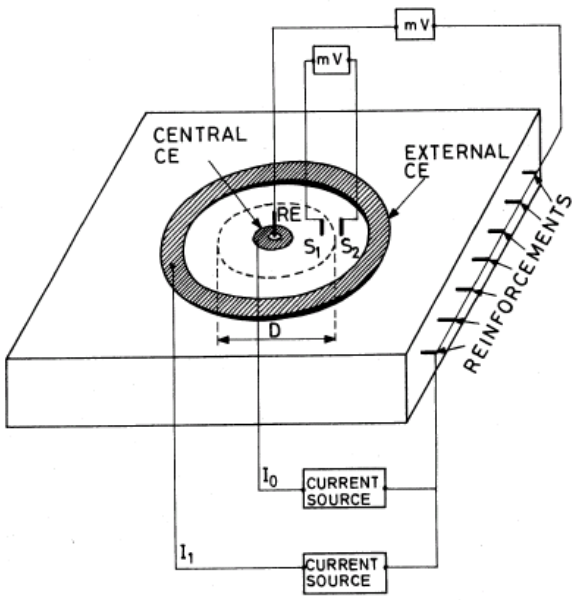

Figure 2-11: Schematic of electrodes arrangement on the GECOR 6 probe (Taken from Feliu et al. 1990).

2.3.4 Galvanostatic pulse technique (GPR)

The main concept of this technique is similar to the LPR technique in terms of the determination of polarization resistance of the reinforcing steel. Basically, an anodic current pulse is galvanostatically applied to the rebar from the counter electrode placed on the surface of concrete (see Figure 2.11). The magnitude of the applied current is normally in the range of 2 to 400 μA, and the duration of pulse is less than 10 s. This small anodic current changes the potential of rebar in concrete (relative to the reference electrode placed on the surface of concrete) with respect to time. In fact, the rebar is polarized in the anodic direction starting from the open-circuit potential. A typical transient response potential is illustrated in Fig. 2.12.

Assuming steel in concrete can be modeled as an equivalent electrical circuit in the form of a Randles Circuit (Newton and Sykes 1988, Andrade and Alonso 1996) as

illustrated in Figure 2.13, the potential of rebar as a function of time can be expressed as (Gonzalez 2001):

$$E(t) = I_{app}\left[R_p\left[1-\exp(-t/R_pC_{dl})\right]+R_c\right] \qquad Eq.\ 2.12$$

where I_{app} is the applied current, R_p is the polarization resistance, C_{dl} is the double layer capacitance, and R_c is the concrete resistance. Using nonlinear regression analysis, the polarization resistance, R_p, can be obtained.

The galvanostatic pulse technique instrument generally consists of a disc probe and a portable device that generates a galvanostatic pulse similar to the ones illustrated in Figures 2.9 and 2.10. Access to the rebar is essential for the electrical connection of the instruments that use this technique. The potential is measured by a reference electrode located at the center of probe and the current is applied through a counter electrode placed around the reference electrode. A guard ring is usually used in this type of instrument to confine the current distribution along the rebar. The same amount of current is applied from the guard ring surrounding the main counter electrode to keep the potential difference between them close to zero. Using this type of confinement allows one to polarize a known area of reinforcement.

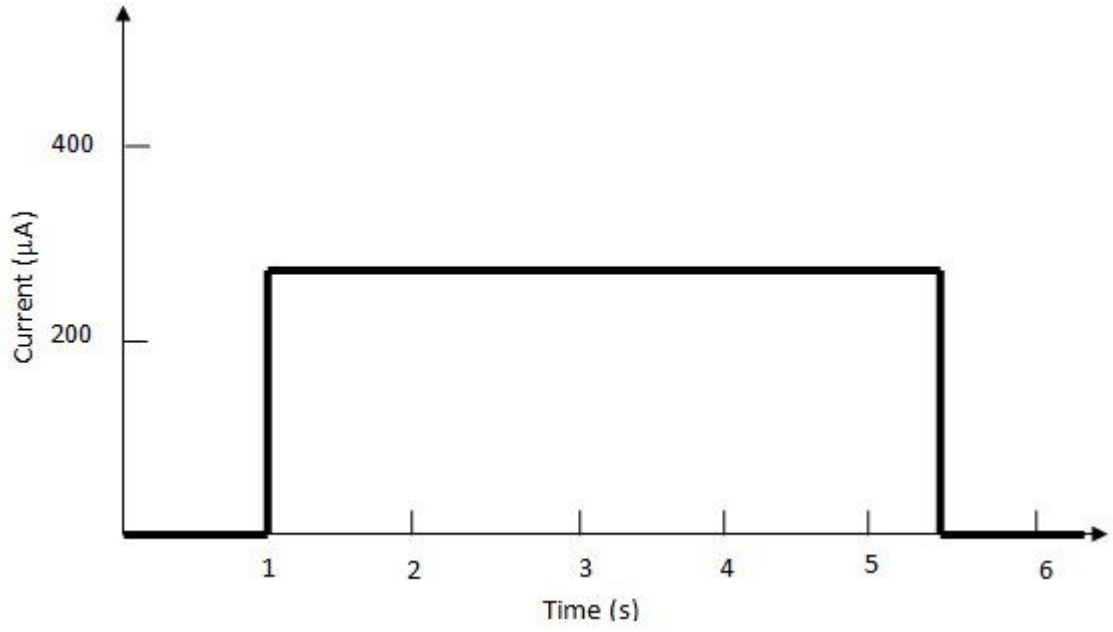

Figure 2-12: A typical current pulse used in galvanostatic pulse technique.

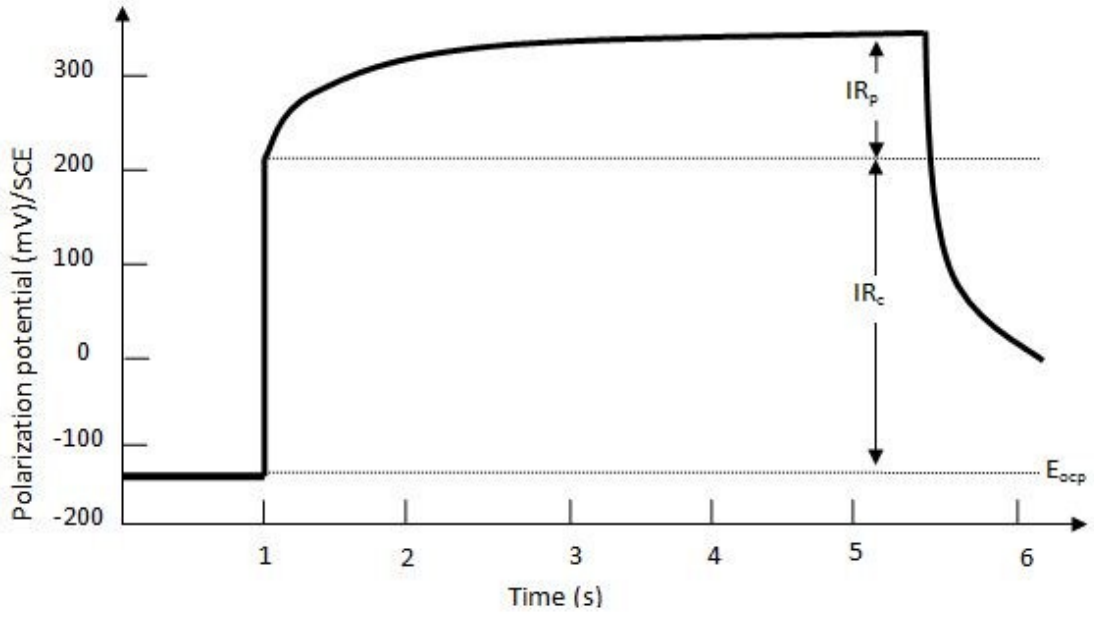

Figure 2-13: A typical potential transient response in galvanostatic pulse technique.

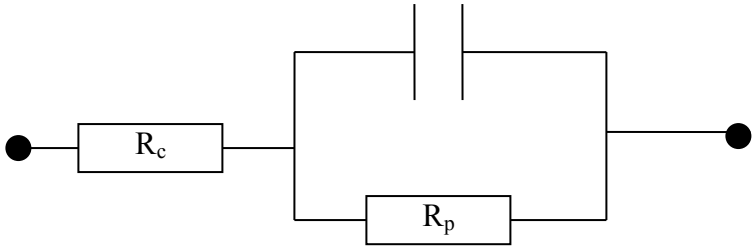

Figure 2-14: Equivalent Randles Circuit representing steel polarization in concrete.

GalvaPulse is one of the commercially available instruments to measure corrosion rate according to the galvanostatic pulse technique. Galvapulse system consists of a probe and a portable device as shown in Figure 2.15. The probe consists of one Ag/AgCl reference electrode and two circular rings, a counter electrode and a guard ring. The corrosion potential is measured by the reference electrode located at the center of the probe before applying a galvanostatic current through the counter electrode. Afterwards a short time current pulse is applied galvanostically into the system. This applied current can be between 5 to 400 μA, and the measurement duration is normally 5 to 10 seconds, but it can be set up to 75 seconds. The reinforcement is polarized in the anodic direction and then compared to its free corrosion potential. The change in electrochemical potential (relative to the reference electrode placed on the surface of concrete) is recorded as a function of the polarization time. A typical potential transient response is depicted in Figure 2.12. Another current is applied through the guard ring to confine the current applied from the counter electrode (current confinement); however, the measurement can be made with or without the use of the guard ring. After calculating the polarization resistance, R_p, the corrosion rate can be estimated using Eqs. 2.10 and 2.11, as in the case of LPR technique.

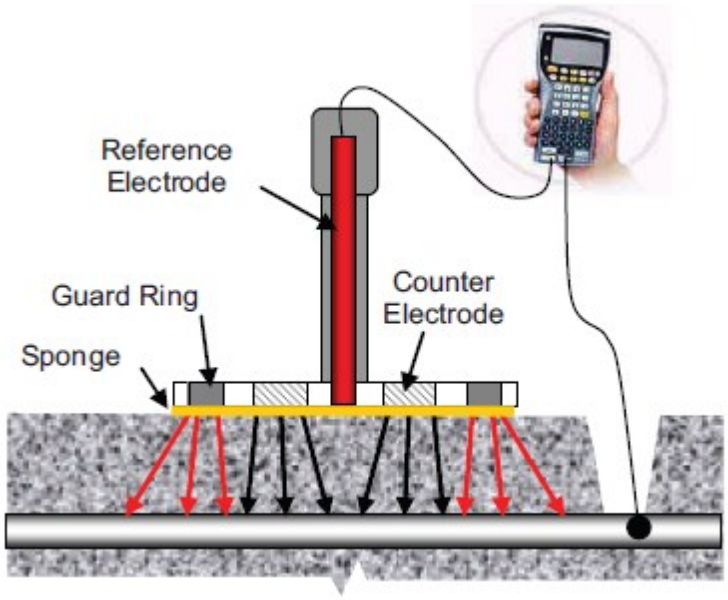

Figure 2-15: Set up of the GalvaPulse instrument (taken from GalvaPulse manual).

2.3.5 Electrochemical impedance spectroscopy (EIS)

AC impedance technique is one of the most powerful electrochemical techniques to determine corrosion rate of reinforcement (Andrade et al. 1984, John 1981). In this technique, a small AC potential is applied to the rebar and concrete system and the response current is measured, respectively. The impedance (Z), which is the ratio of applied potential (ΔE) to measure current (i), is calculated such that:

$$Z = \frac{\Delta E}{i} \qquad \textit{Eq. 2.13}$$

This measurement can be carried out at different AC frequencies, and as a result, a spectrum of impedance as a function of frequency is obtained. The impedance (Z) is a

complex number which can be decomposed in real and imaginary parts at each frequency. Considering the Randles Circuit, introduced in Figure 2.14, as an equivalent electrical circuit representing the electrochemical cell, the polarization resistance of the reinforcement (R_p) and the concrete resistance (R_c) can be calculated by curve-fitting of the data to the following equation:

$$Z = R_{\Omega} + \frac{R_p}{1 + j\varpi R_p C_{dl}} \qquad Eq.\ 2.14$$

where ϖ is the angular frequency (ϖ = 2π*f*), ***j*** is imaginary unit of $\sqrt{-1}$, and *Z* is the ohmic drop or concrete resistance, R_{Ω} at high frequency, while at very low frequency *Z* is equal to $R_{\Omega} + R_p$. The Randles equivalent circuit model is widely used to study the corrosion and calculation of the polarization resistance (Berke and Hicks 1990, Feliu et al. 1998, Li and Sagues 2001, Nmai 2004, Trabanelli et al. 2005, Choi et al. 2006, Ghods 2010).

It should be noted that the measurements that need to be carried out at different frequencies can be quite time consuming, especially at low frequencies; therefore, the on-site application of the EIS technique has practical limitations. In order to decrease the measurement time, most AC impedance instruments, which are designed for field applications only measure the impedance at two points: at very high frequency and very low frequency. Based on Eq. 2.14, the higher frequency estimates concrete resistance (i.e., R_c as the second term in the equation approaches to zero), and the lower frequency determines the sum of concrete resistance and polarization resistance (i.e., $R_p + R_c$). The difference between these two measurements indicates the polarization resistance of rebar (R_p). The minimum frequency which is practical in the field is around 0.01 Hz. At frequencies lower than this quantity, the test would be very time-consuming and it is not

practical. Regarding this limitation, some errors that are not avoidable in field measurements might also be involved. For the high frequency readings, the measurement time is not a problem and frequencies above 10^3 Hz are generally sufficient.

2.3.6 Electrical resistivity of concrete

Electrical resistivity of concrete is an indicator for corrosion vulnerability of steel embedded in concrete (NEA/CSNI 2002). Figure 2.16 by Rodriguez et al. (1994) illustrates this relationship clearly. The relationship between the severity of corrosion and the concrete resistivity has been studied by a number of researchers (Langford & Broomfield 1987, Browne et al.1983 and Millard & Gower 1992) and is summarized in Table 2.2.

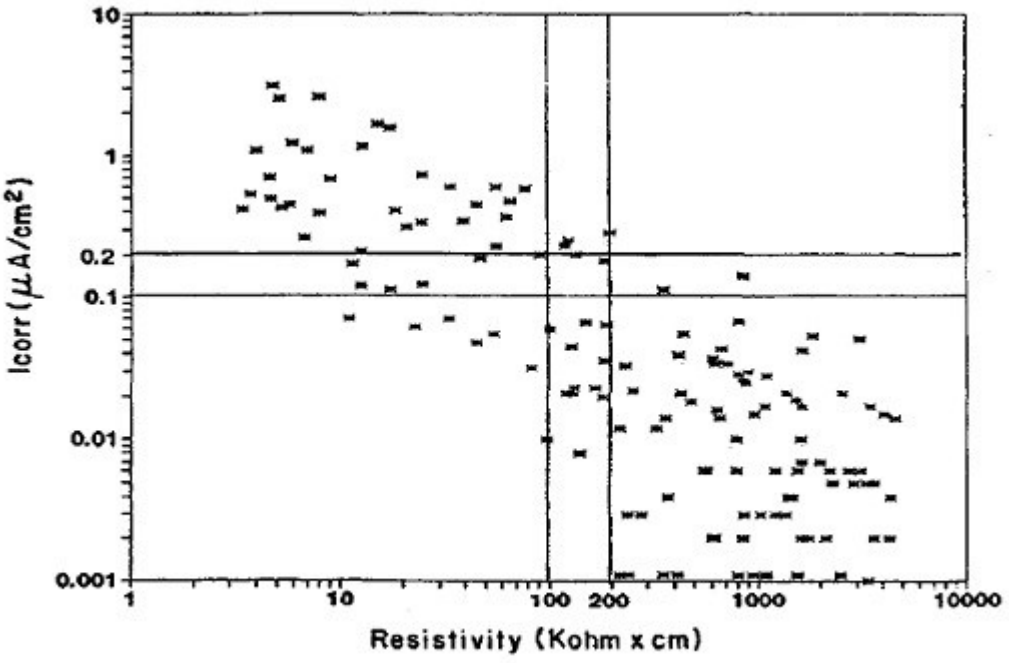

Figure 2-16: Relation between I_{corr} and concrete resistivity obtained from examination on a great number of real structures (Rodriguez et al. 1994).

Concrete resistivity can be obtained by measuring its electrical resistance and multiplying it by a geometrical conversion factor. There are different measurement methods for measuring the concrete resistivity: two-point (two probes) or four-point (four probes) methods, which are also known as the Wenner probe method, and the Disk method (one-point method).

Table 2-2: The relationship between the concrete resistivity and severity of corrosion.

Concrete resistivity (*Ω.m*)	**Severity of corrosion**
>200	Low corrosion rate
100-200	Low to moderate corrosion rate
50-100	High corrosion rate
<50	Very high corrosion rate

In the four-point resistivity method (Wenner probe), there is no need to make a direct contact with the reinforcement. The device consists of four equally spaced point electrodes. The resistivity is obtained by direct contact of the electrodes on the surface (as illustrated in Figure 2.17). The two outer electrodes apply alternating current into the specimen, and the resulting potential drop in the system is measured by two inner electrodes. The resistivity is then calculated from the measured resistance using Eq. 2.15.

$$\rho_c = 2\pi a R_m \qquad \textit{Eq. 2.15}$$

where ρ_c is the resistivity of concrete (Ω-m, Ω-cm or Ω-mm) a is the distance between the electrodes (m, cm or mm), and R_m is the resistance from the four-point measurement (Ω).

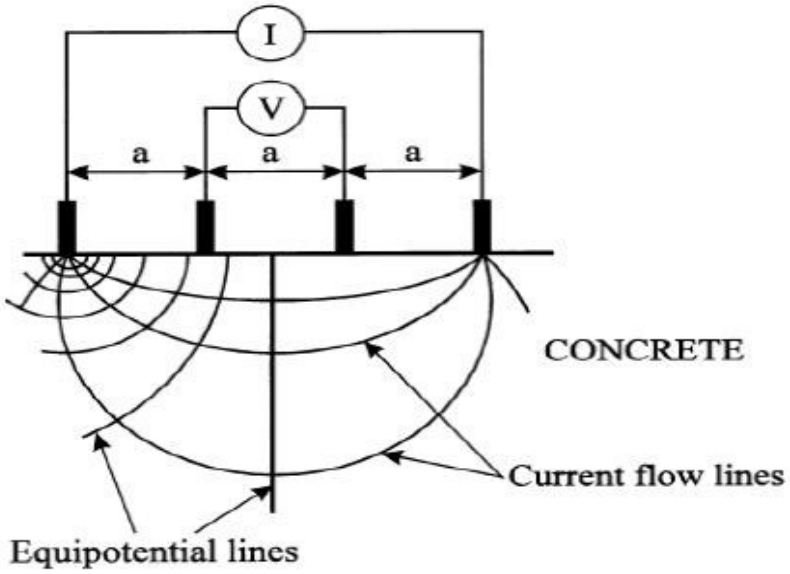

Figure 2-17: Setup of four-point electrode for measurement of concrete resistivity (Gowers and Millard, 1999).

2.4 Selected experimental studies using existing detection and measurement techniques of steel corrosion in concrete

Hamid et al. (1988) have conducted an experimental research to investigate the efficiency of the linear polarization resistance technique to measure corrosion rate of the concrete steel reinforcement. In this study three sets of reinforced concrete specimens, with various water to cement ratio (0.4, 0.5, and 0.7), were immersed in the solution of 5 percent NaCl for about 2 years. After removing the samples from the solution two series of test were conducted: first, the polarization resistance is measured by using potential scan (potentiostaic sweep), then the samples were tested for the Tafel slope. Then the corrosion rate is calculated using the β and the polarization resistance (R_p). After electrochemical measurements the concrete samples were broken to measure the metal mass loss. The

corrosion rate measurement by electrochemical technique showed that the higher the water to cement ratio, the higher the corrosion rate. The comparison of the results shows lower corrosion rate obtained by the mass loss technique, but the authors concluded that the metal mass loss technique is not appropriate to determine the accuracy of the electrochemical technique due to: (1) metal loss determination will not show significant differences in a short time and in environment which is not very corrosive, (2) metal loss determine the average corrosion rate for the whole exposure time while electrochemical techniques define instantaneous corrosion rate. The findings of this study support the significant role of concrete quality (such as w/c ratio) in starting and rate of corrosion in reinforced concrete structures as the corrosion rates in specimens with better quality (i.e. lower w/c ratio) were significantly lower. They concluded that the electrochemical techniques can be used quickly to determine the instantaneous corrosion rate of reinforcement in concrete.

Alonso et al. (1988) carried out an experimental study to investigate the relationship between concrete resistivity and corrosion rate of the reinforcing steel. Figure 2.18 shows the effect of the concrete resistivity on the corrosion process.

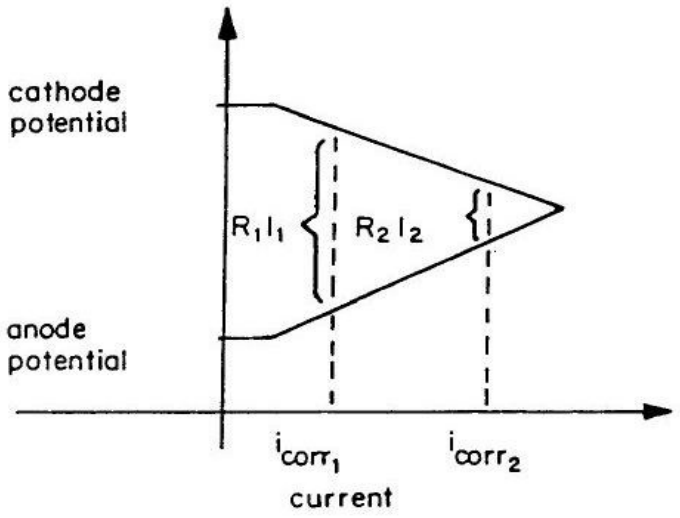

Figure 2-18: Effect of the concrete resistivity on corrosion process (Alonso et al. 1988).

When the concrete resistivity is high (R_1 in the Fig. 2.18) the rate of the corrosion is lower, on the other hand when concrete resistivity is low (R_1 in the Fig. 2.18) the rate of corrosion is higher. From correlation analysis of the result distribution, they found that there is a good relationship between corrosion rate and the concrete resistivity. They expressed that in active corrosion the maximum rate of corrosion seems to be controlled by electrical resistivity of concrete. The authors found a value for the ohmic resistance (5-10 $\times 10^4$ Ω) as a limit for corrosion rate, below which rebar corrosion could be significantly high. They concluded that when corrosion is in progress the mortar resistivity which is a factor of controlling corrosion rate was influenced by the relative humidity.

Lamberte et al. (1991) carried out a study by electrochemical monitoring of steel embedded in concrete. They cast a series of reinforced concrete slabs; the surfaces of these specimens were exposed to the 5 % sodium chloride solution for the 2 years. The corrosion potentials, E_{corr}, and the polarization resistances, R_p, of the steel bars monitored by means of a microprocessor controlled corrosion measurement system. The metal mass losses determined from electrochemical measurements and the results were compared with mass

loss obtained gravimetrically. The results showed convincing evidence of the reliability of the I_{corr} measurements (see Figure 2.19). It should be noted that the polarization resistance was monitored during the exposure, and the average corrosion rate was calculated and then compared with the destructive mass loss test – hence they overcame the problem faced by Hamid et al. (1988).

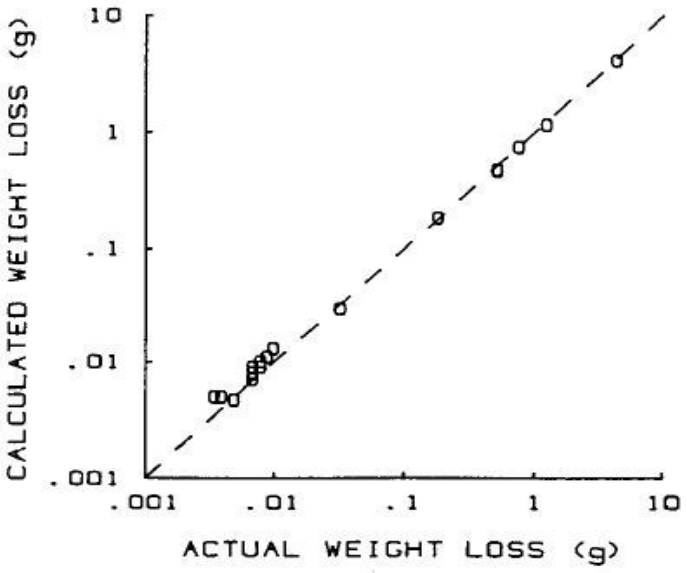

Figure 2-19: Relation between the metal mass losses obtained by the electrochemical monitoring and gravimetrically (Lamberte et al. 1991).

Cigna et al. (1993) conducted a study using corrosion potential, electrical resistivity, and polarization resistance techniques to study the corrosion behaviour of reinforcement embedded in different concrete mixes. They found better results by the measurements of R_p, and calculating the corrosion rate utilizing Stern-Geary equation. The tests showed strong dependency of corrosion potential to environmental conditions, but it was also noted that corrosion potentials are not necessarily good indicators of the corrosion state of the embedded rebar. They concluded that the corrosion rate obtained from the

linear polarization resistance technique over a period of time has shown a reliable indication about whether extensive corrosion is taking place.

Alberto (1993) reviewed the techniques which are used for characterizing the corrosion extent of reinforcement. These techniques included electrochemical (e.g. linear polarization, galvanostatric pulse, EIS, etc.) and non-electrochemical techniques (e.g. sounding, direct examination, etc). The author summarized the results of the review as follows: (1) non-electrochemical techniques are not able to detect corrosion unless the corrosion stage is at an advance stage; (2) electrochemical techniques could provide useful information regarding to the corrosion activity, but they are sensitive and complex. Alberto (1993) also noted that although half-cell potential mapping is one the most applied techniques in the field there are some disadvantages related to this technique. It was shown that the actual potential distribution on an external concrete surface is different from the potential obtained in the concrete which is immediately in contact with the surface of the steel rebar. Figure 2.20 illustrates the mentioned difference clearly such that the half-cell potential mapping on the concrete surface does not reflect the exact surface condition of the rebars. These observations are in line with the ones made by Pour-Ghaz (2009).

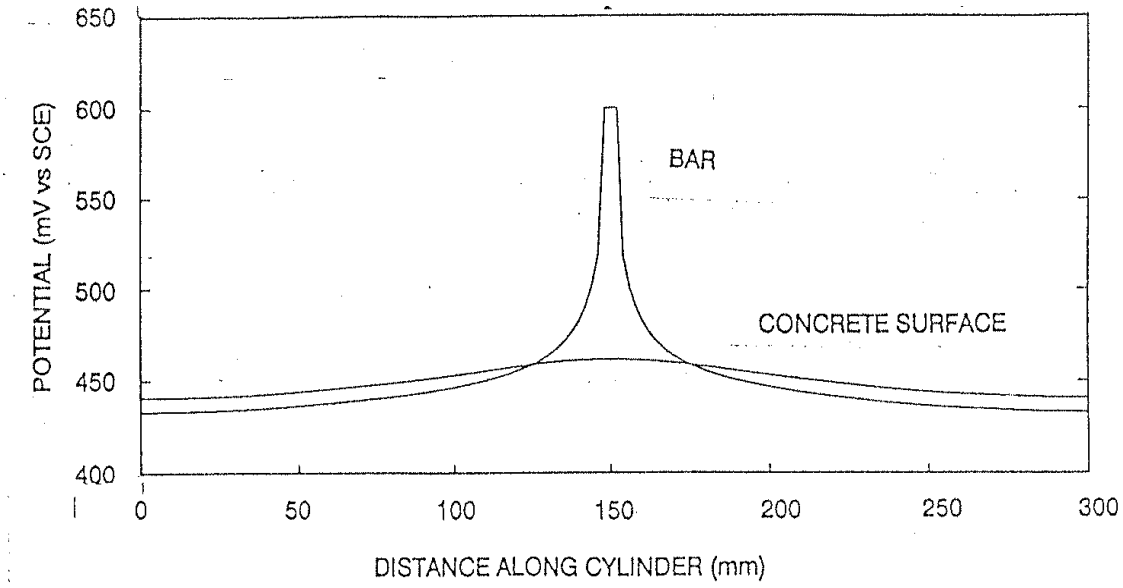

Figure 2-20: Potential distribution for an 11 cm diameter, 30 cm long concrete cylinder containing an axial 1 cm rebar. A 6 mm long ring-shaped region is active at center of the rebar, while the rest is passive (Alberto 1993).

In an effort to find factors influencing corrosion rate of chloride-induced macrocell corrosion, Raupach (1996) studied about 200 concrete specimens having locally separated anodes and cathodes with cell current measurement. The specimens were exposed to cyclic wetting periods using 1% chloride solution to be consistent with the study conducted earlier by Weber (1988). The influences of w/c ratio, crack width (up to 0.5 mm), crack distance, and concrete cover in crack zone were studied by preparing the set up illustrated in Figure 2.21. To evaluate the function of crack distance on corrosion activity, the samples were prepared in a way that three rebars with different distances located on each side of crack. The result achieved by measuring electric current between rebars shown in Figure 2.21. The result of measuring anodic and cathodic current in different locations is given in Figure 2.22. The effect of distance from cracks is obviously seen in this figure: by increasing the distance from cracks the current density of cathodes decreases, as

electrolytic resistance increases. The author concluded that the steel corrosion rate in the crack zone is influenced by the studied parameters (see Figure 2.23): With increasing the concrete cover the steel mass loss due to corrosion decreases considerably. Increasing the w/c ratio also increases mass loss. With increasing crack width (up to 0.5 mm) the corrosion activity increases for a short period, but after two years no clear relationship between crack width and mass loss was observed.

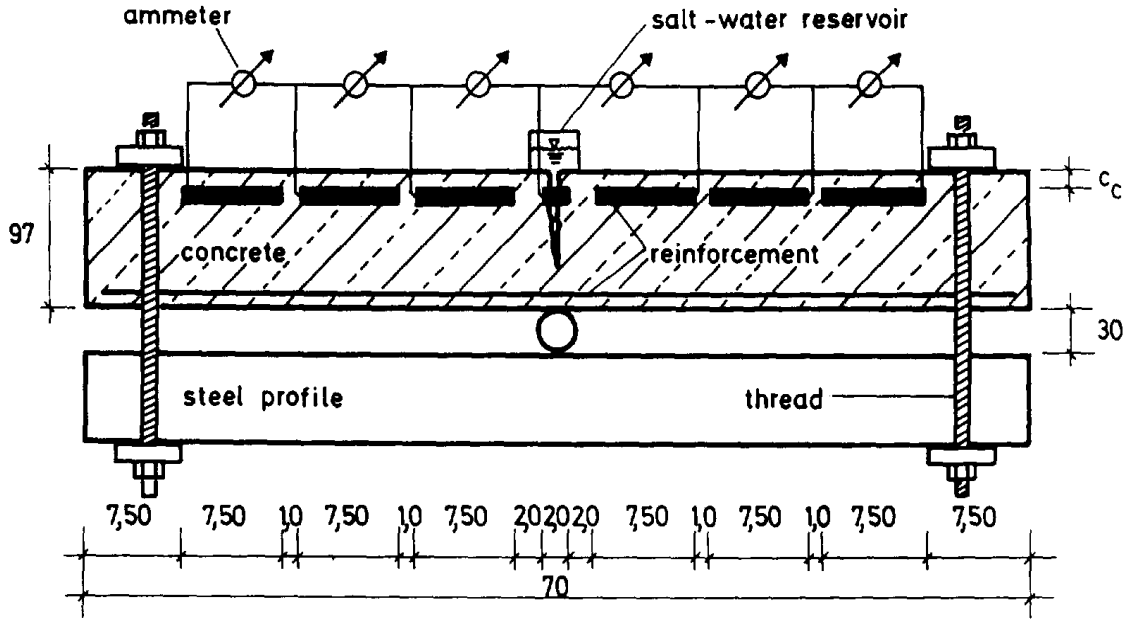

Figure 2-21: Schematic view of test set up for investigation of corrosion mechanism in crack zone (Raupach 1996).

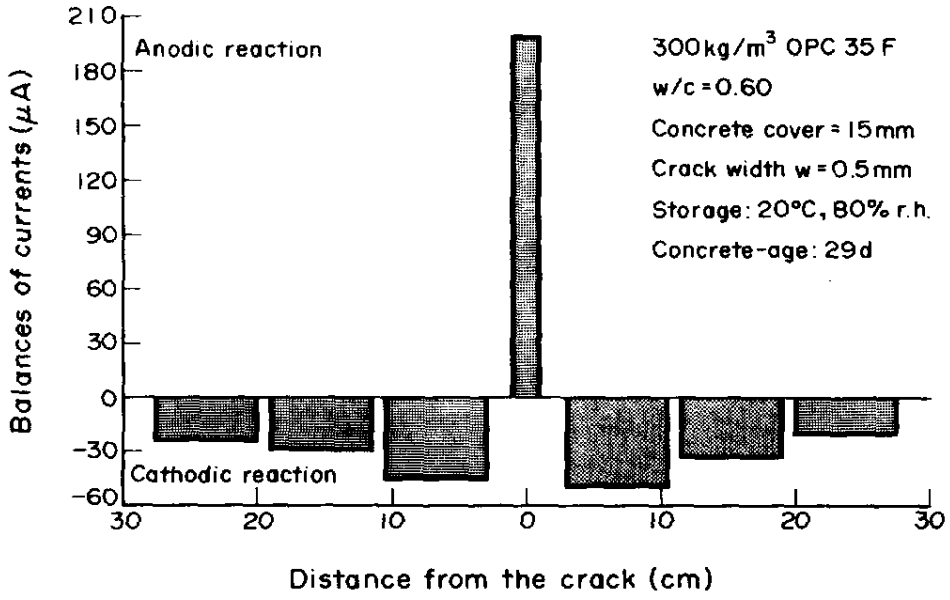

Figure 2-22: Anodic and cathodic currents measurement illustrating the corrosion macrocell current and effect of distance from crack (Raupach 1996).

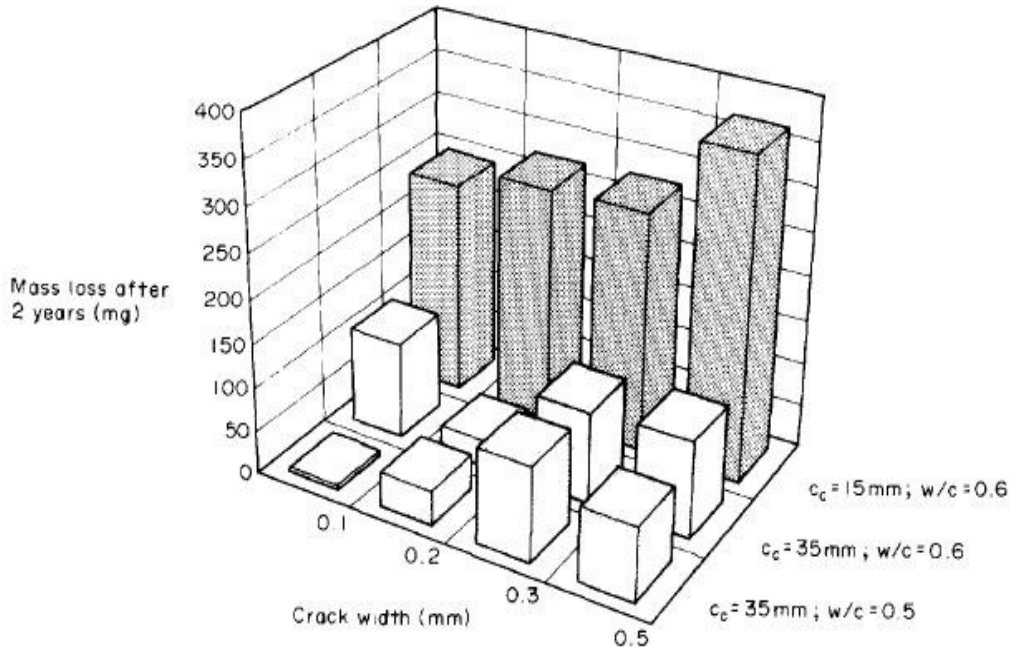

Figure 2-23: Relation between calculated mass loss and crack width, concrete cover (C_c), and concrete water-to-cement ratio (w/c) (Raupach 1996).

Gonzalez et al. (1996a) provided useful information regarding the factors influencing the corrosion in concrete and provided a summary about the methods which are used to monitor corrosion of reinforcement (Gonzalez et al. 1996b). Table 2.3 provides a summary of their study on the corrosion measurement techniques. In their evaluation scheme, they considered control and diagnostic efficiency of the methods such as speed of testing, response to condition variation, level of non-destructiveness, and ability to express the result numerically. As an important conclusion, the authors reported that the lack of knowledge of the area affected by electric signals in on-site measurement (i.e., polarized area of the reinforcement) is the main difficulty related to determination of corrosion kinetics of steel in reinforced concrete structure by means of electrochemical methods.

Table 2-3: Features of the most widely-used methods for monitoring corrosion of reinforcement in concrete structures (Gonzalez et al. 1996-2).

Methods	**Characteristics**					
	Speed of individual measurements	Speed of response to changes	Quantitative information	Non-destructive	Non-disturbing	Measurement parameter
Qualitative visual observation	O	•	•	O	O	Appearance changes
Gravimetric test	•	•	O	•	•	i_{corr} Average
Potential mapping	O	O	•	O	O	Corrosion Potential
LPM (R_p)	O	O	O	O	⊗	i_{corr}
Guard ring	O	O	O	O	•	i_{corr}
Coulostatic method	O	O	O	O	⊗	i_{corr}
Electrochemical choice	⊗	O	⊗	O	O	i_{corr}
EIS	⊗	O	⊗	O	⊗	i_{corr} Mechanisms
Harmonics	⊗	O	O	O	•	i_{corr}

Meaning of the symbols:

O The method possess the listed characteristics in an optimal degree, e.g., the individual measurements is instantaneous

⊗ The method possesses the listed characteristics in a less than fully-satisfactory degree, e.g., the individual measurement is relatively slow.

• The method does not possess at all the listed characteristics, e.g., the individual measurements is very slow.

As stated before concrete resistivity plays significant role in steel corrosion as it controls the ease of migration of the ions through concrete between anode and cathode. Carino (1999) used the results reported by Feliu et al. (1996) and Bungey (1989) to compare the relationships of concrete electrical resistivity and half-cell potential with the corrosion risk. It was observed that after depassivation of steel in concrete there was a better relation between concrete resistivity and corrosion risk in comparison with half-cell potential (see Figures 2.24 and 2.25). This finding is also supported later by Gonzalez et al. (2004). Carino (1999) concluded that due to dissimilarity of the limits for the concrete electrical resistivity (as shown in Table 2.4) there is a need for more studies in this area to achieve a better understanding of the relationship.

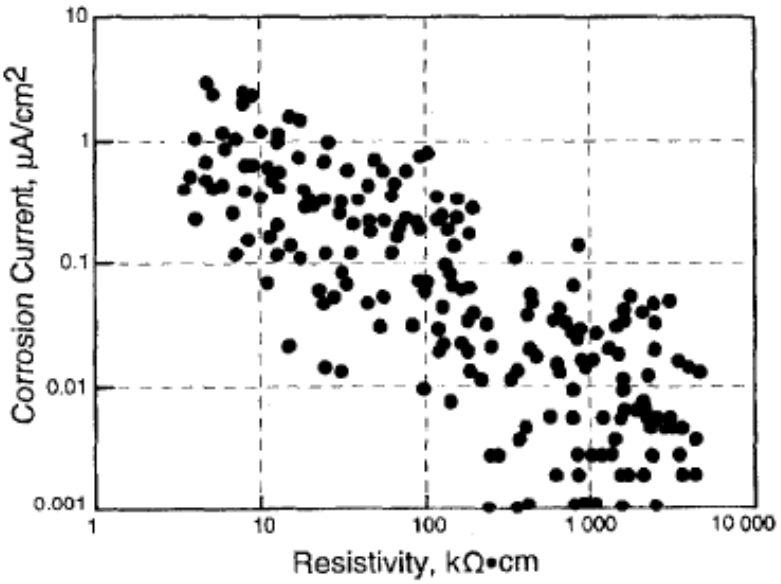

Figure 2-24: Comparison of I_{corr} and resistivity from field measurement (Feliu et al. 1996).

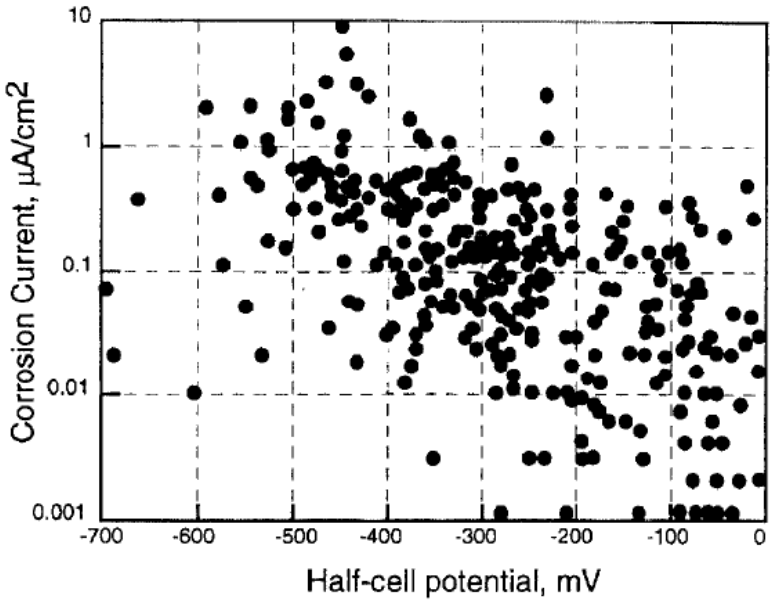

Figure 2-25: Comparison of I_{corr} and Half-cell potential from field measurement (Feliu et al. 1996).

Table 2-4: Comparison of two recommended relationships between concrete resistivity and corrosion risk (reproduced from Carino 1999).

Resistivity (kOhm . cm)	**Corrosion risk**
Feliu et al. 1996	
>100-200	Negligible corrosion,; concrete is too dry
50-100	Low corrosion rate
10-50	Moderate to high corrosion rate when steel is active
<10	Resistivity does not control corrosion
Bungey 1989	
>20	Low
10-20	Low/moderate
5-10	High

Qian et al. (2001) tested concrete slabs that were cut from an old bridge which had been repaired due to corrosion-induced deterioration. The slabs were monitored for about half a year while the relative humidity of the concrete was kept above 90% in order to simulate the in-service environmental conditions. Authors measured half-cell potential, corrosion rate (with LPR technique) and resistivity. Researchers found that the half-cell potential of reinforcements are affected significantly by oxygen concentration at steel-concrete interface. Also the moisture condition at the top layer of concrete has significant influence on the resistivity of the concrete cover. The findings of this research showed that using the guidelines provided by ASTM C867-09 standard for half-cell measurement is not reliable for prediction of corrosion in reinforced concrete. This observation as supported by NEA/CSNI (2002).

Luping (2002) carried out a laboratory investigation to compare the most-widely used corrosion rate measurement devices for reinforced concrete. Four instruments utilizing two types of electrochemical techniques were used (2 LPR and 2 GPR devices). The obtained results were compared with the standard gravimetric mass loss method, ASTM G1. Findings of this research demonstrated that polarization duration has a significant effect on the polarization resistance measurements. The difference in corrosion rate measured by two techniques, the LPR and the GPR, are mainly because of different polarization durations. The corrosion rates obtained by LPR technique are closer to the true mean corrosion rate obtained from mass loss tests, while galvanostatic pulse measurements overestimate it, especially above the passive steel bars. Best results were achieved when the values measured by LPR technique was multiplied by a calibration factor of ~6 (as a pitting factor) for the chloride introduced specimens.

Oh et al. (2005) carried out an experimental research to investigate the ability of thehalf-cell potential mapping technique to detect chloride-induced corrosion. They prepared reinforced concrete samples with various concrete mix designs and chloride content. The half-cell potential was monitored every three days. At the end, the reinforcement was extracted to determine the corroded area. The concrete pore solution was also analyzed. Oh et al. (2005) found a linear relationship between the amount of chloride (either represented as total chloride, free chloride or $[Cl^-]/[OH^-]$ ratio) and the half-cell potential measurement (see Figure 2.26). They also showed a relationship between the extent of corroded area and the half-cell potential values (see Figure 2.27). Unlike previous studies (e.g. by Qian et al. 2001), these findings support the efficiency of the half-cell potential measurement in reinforced concrete structures.

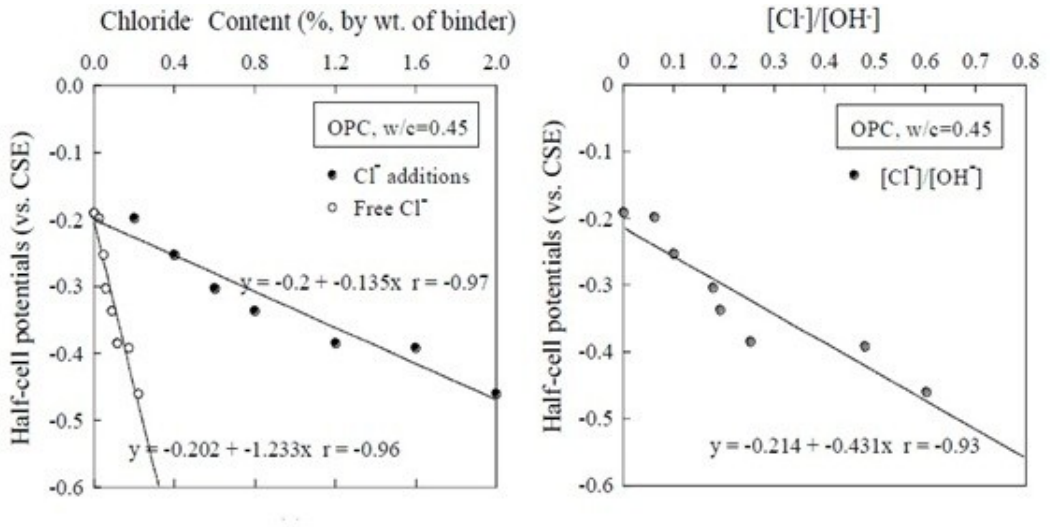

Figure 2-26: Relationship between half-cell potential and the concrete chloride content (Oh et al. 2005).

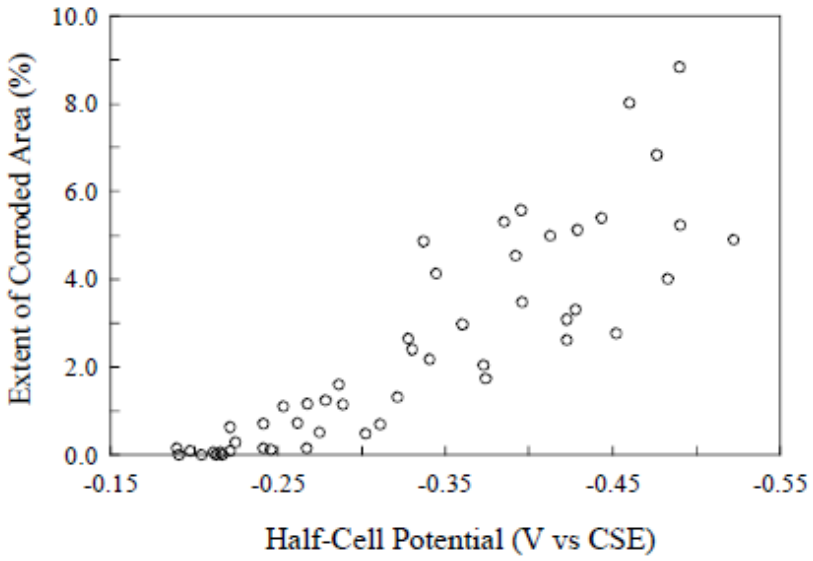

Figure 2-27: Relationship between half-cell potential and extent of corroded area (Oh et al. 2005).

Another controversial result was reported by Nakamura et al. (2008) who studied the practical application of half-cell potential measurements on an existing PC bridge near the coastline of Japan. The researchers used three different reference electrodes for half-cell measurements in summer and winter months: a silver/silver chloride electrode, a lead electrode and a copper/copper sulphate electrode. The values obtained by half-cell potential measurement were compared with chloride content and the corrosion state of steel. The authors concluded that the criteria provided by ASTM 867 are not practically reliable for assessing the corrosion risk.

Nygaard et al. (2010) compared the linear polarization resistance technique with the galvanostatic pulse techniques to measure corrosion activity in reinforced concrete. The experiment was conducted in series of the samples which were contained active and passive rebars. The result of this research showed that in the measurement above the passive reinforcement, both devices overestimated the actual corrosion rates as the

instruments were not able to confine the spread-out of the counter-electrode current. For reinforcement with localized corrosion, none of the instruments was able to locate the actively corroding area due to self-confinement effect which is illustrated in Figure 2.28. They concluded that using an empirical pitting factor is a solution to the mentioned problem.

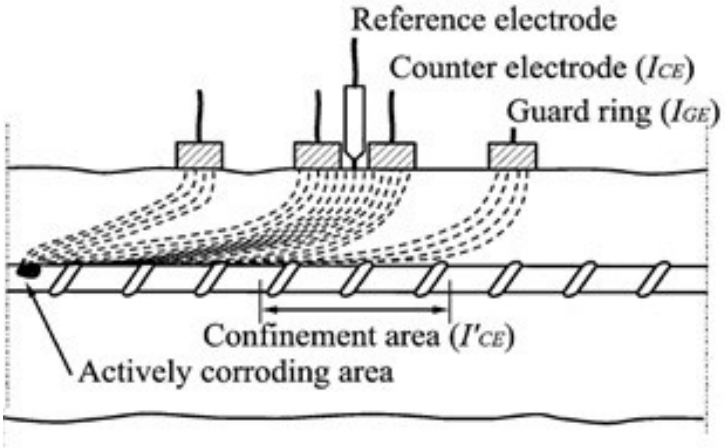

Figure 2-28: Schematic illustration of self-confinement: the current flows into the active area irrespective of the location of instrument on the surface of concrete (Nygaard et al. 2010).

2.5 Summary

The theoretical and literature review presented in this chapter provided the following main gaps that form the basis of the current investigation:

- The existing studies are mostly carried out on laboratory-scale reinforced concrete specimens that did not have realistic reinforcement detailing.

- Those studies carried out in existing reinforced concrete structures, the temperature and humidity were not under the control.
- Most of the specimens were not loaded under service conditions; therefore, a systematic study on the effect of loading conditions and cracking was not carried out.
- There is significant inconsistency between the results of different corrosion measurement techniques, but these differences have not been systematically investigated in large-scale, realistic and loaded specimens that are in controlled environmental conditions.
- The effects of w/c ratio, saturation and concrete resistivity have been identified as important in the effectiveness of the corrosion detection and measurement techniques, but these differences have not been systematically investigated in large-scale, realistic and loaded specimens that are in controlled environmental conditions.
- There are still many controversial studies about the effectiveness of the half-cell corrosion mapping technique and ASTM C876-09 standard.

3. Experimental: Program

3.1 Introduction

This chapter presents a detailed description of the experimental program carried out in this research to compare different corrosion detection/measurement methods and to investigate the effect of concrete saturation, concrete water-to-cement ratio, and structural loading on chloride-induced corrosion of reinforced concrete slabs. The corrosion detection/measurement techniques investigated in this experimental program include half-cell potential mapping, linear polarization resistance, galvanostatic pulse, and electrochemical impedance spectroscopy. In addition, resistivity of concrete is also monitored because of its strong correlation with steel corrosion rates in concrete. Measurements were taken on loaded reinforced concrete slabs under three concrete saturation conditions (dry, partially-saturated, and saturated).

3.2 Test specimen

The chloride-induced corrosion investigation was performed on a reinforced concrete deck built by Deif (2010) in 2006 (Figure 3.1). This deck has three 0.91 m-width reinforced concrete strips, each with a different water-to-cement ratio: (0.35, 0.4 and 0.5). The three reinforced concrete slabs were reinforced with eight top and eight bottom #10M steel rebars, with a yielding strength of 400 MPa. Clear concrete cover to the top and bottom concrete surfaces is 50 mm and 45 mm, respectively. The cross section of a single concrete slab is illustrated in Figure 3.2.

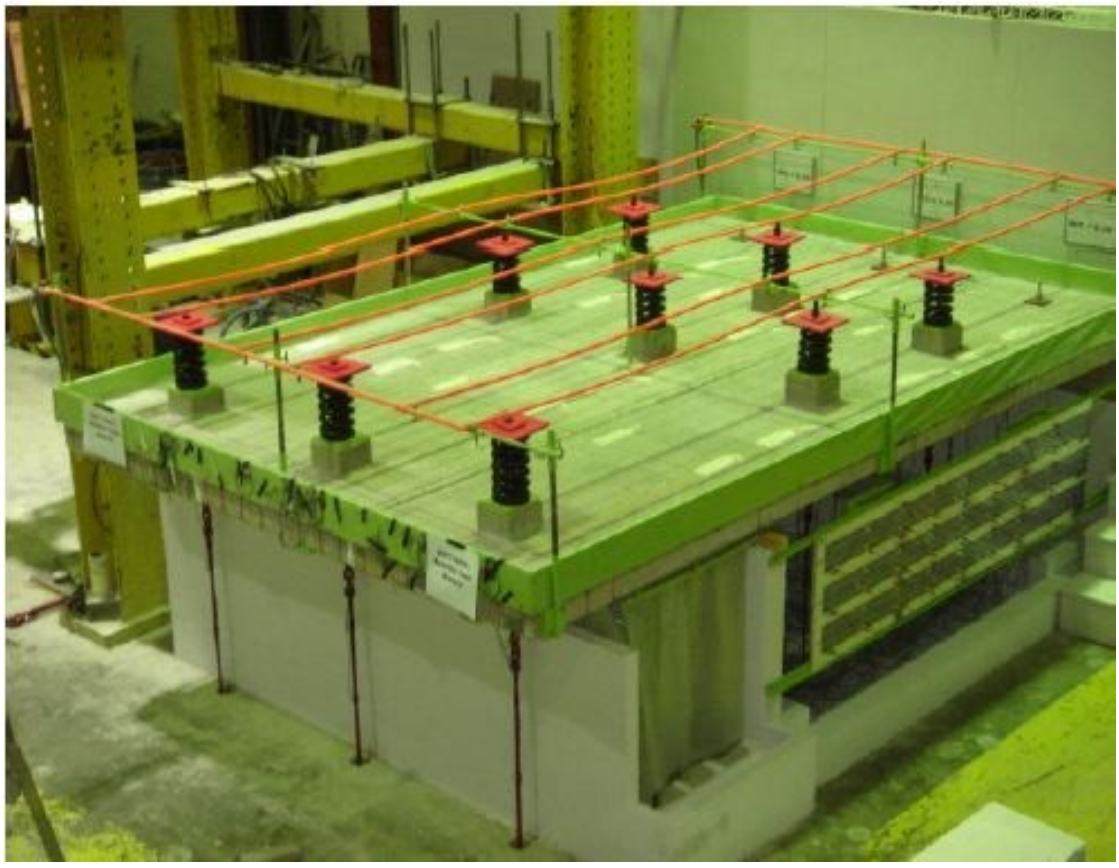

Figure 3-1: Reinforced concrete deck on which measurements were taken (reproduced from Deif 2010).

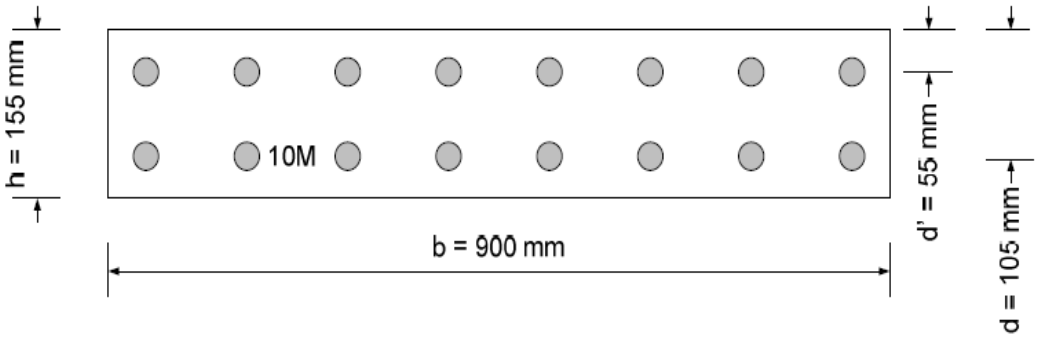

Figure 3-2: Detail of single slab cross section and reinforcement arrangement (reproduced from Deif 2010).

Each slab was simply supported at two locations: at one end and 1.26 meter from the other end, providing a 2.73-meter long span (Figure 3.3). The slabs were loaded by means of three threaded steel bars. In order to distribute the applied axial load across the width of each strip, the slabs were also reinforced along the transverse direction with four steel bars arranged in two layers, two at the top and two at the bottom. A three-dimensional view and a plan view of the reinforcement arrangement are illustrated in Figures 3.4 and 3.5, respectively. Each slab acts independently of the other, and their reinforcements are not connected.

The location of supports and applied loads was designed to induce both positive and negative bending moment regions along the slab, as well as regions of pure bending and a mix of shear and bending. The slab was subjected to 60% of its ultimate moment capacity during the duration of the testing. Details of the applied loads as well as the resulting shear force and bending moment diagrams for a single slab are shown in Figure 3.6.

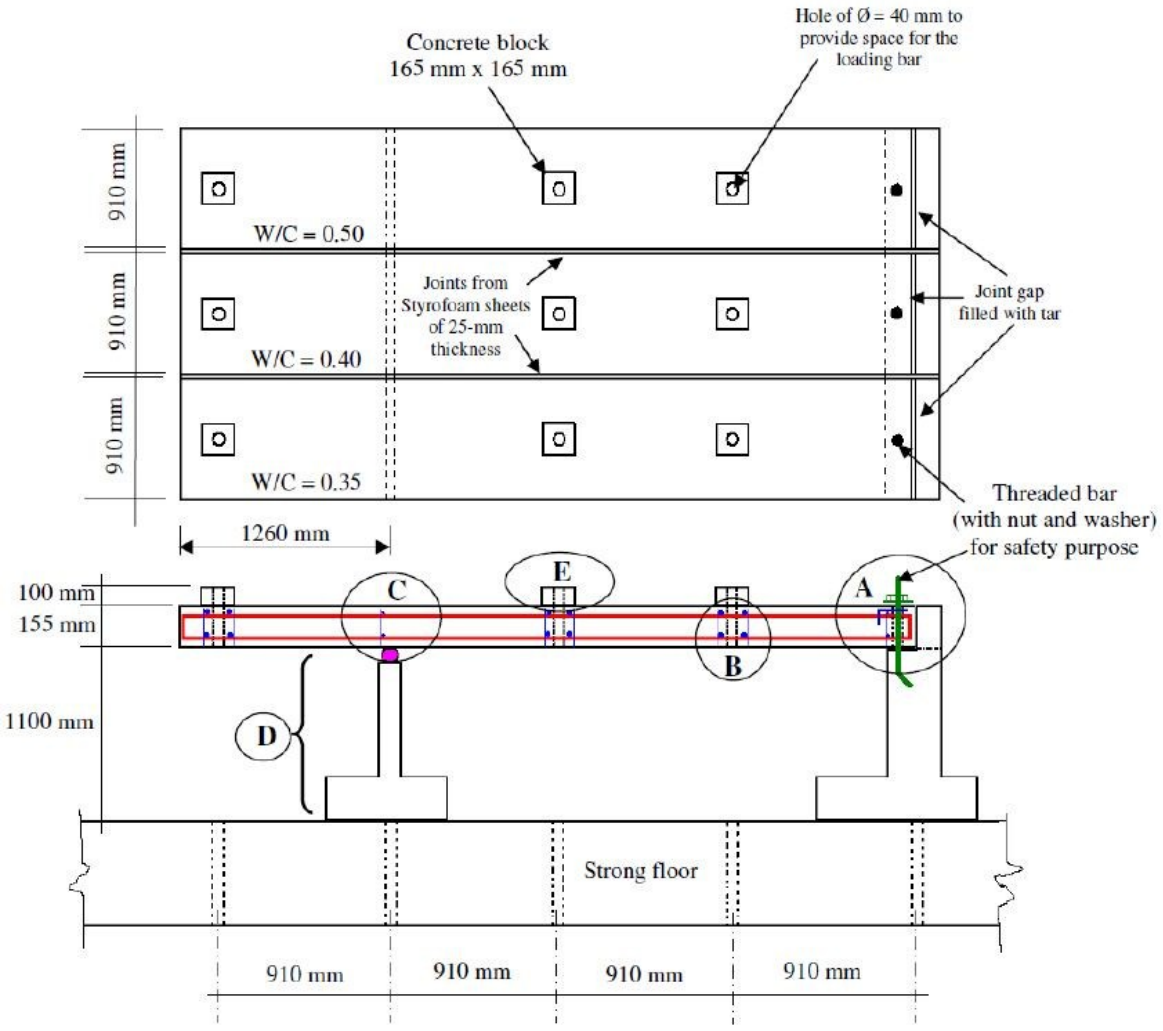

Figure 3-3: Plan and side view of slabs (reproduced from Deif 2010).

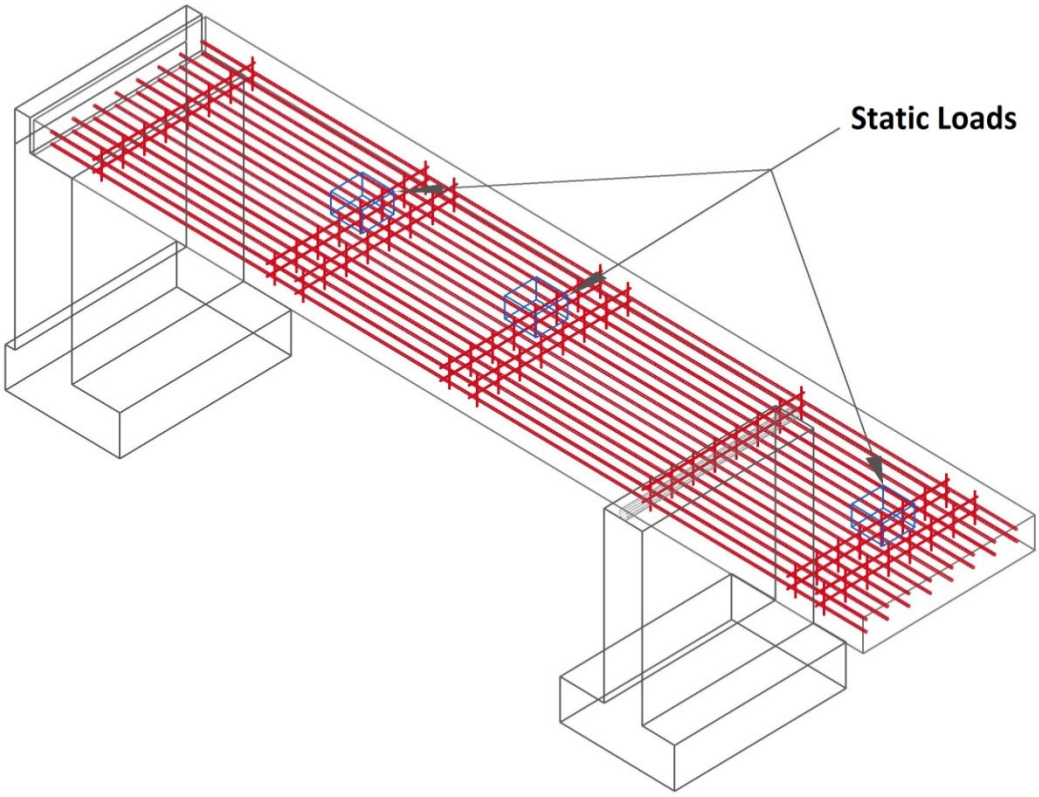

Figure 3-4: Detailed 3D view of a single reinforced concrete slab illustrating the reinforcement arrangement (in red).

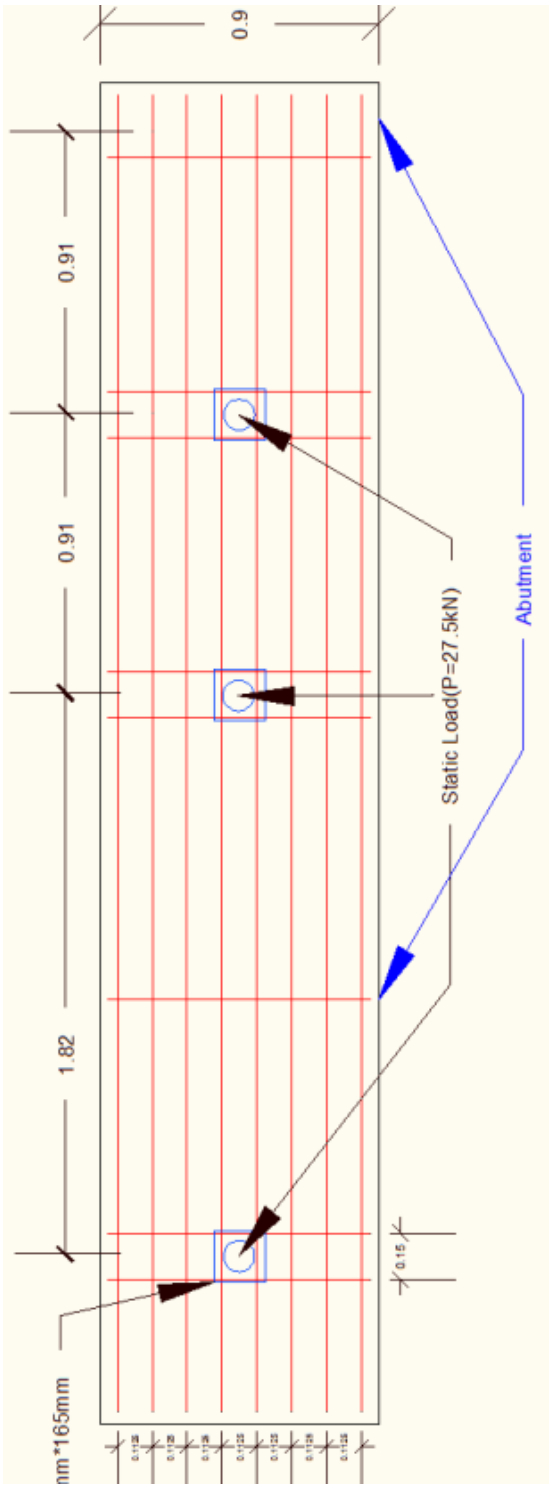

Figure 3-5: Plan view of a single slab.

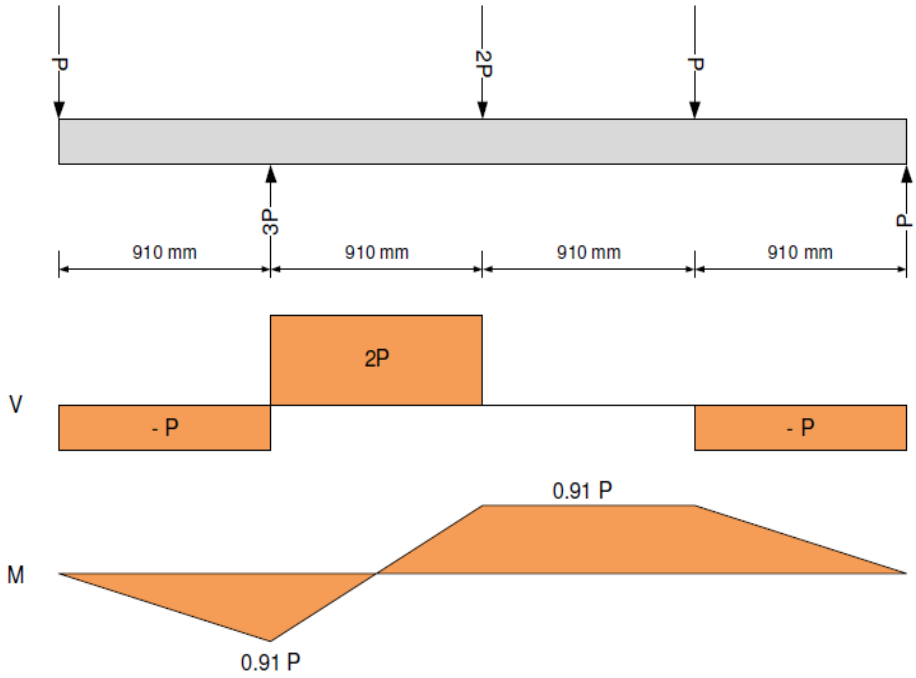

Figure 3-6: Applied loads, shear and bending moment diagram for a single slab, P=27.5 kN (reproduced from Deif 2010).

Concrete mix proportions for each of the concrete strips can be found in Deif (2010). Each concrete strip was cast independently of the others. Loads were first applied to the slabs after 200 days of casting. The concrete compressive strength at 28 days for the concrete with w/c of 0.35, 0.40 and 0.50 were 62.1 MPa, 51.5 MPa and 44.7 MPa, respectively (Deif 2010). The compressive strength at 200 days after casting were 81.0 MPa, 69.4 MPa and 64.5 MPa for the concrete with w/c of 0.35, 0.40 and 0.50, respectively (Deif 2010).The slabs were exposed to de-icing salt and ten wetting/drying cycles to induce corrosion activity prior to the measurements conducted in this research. To simulate chloride exposure condition, regular de-icing salt was spread uniformly all over the deck surface. The slabs were then sprayed with water and allowed to dry for 90 days. This

wetting-drying cycle was repeated ten times. Further details of the construction and exposure of the test specimen are found in Deif (2010).

3.3 Experimental set-Up

3.3.1 Experimental grid

The chloride-induced corrosion activity of the reinforced concrete deck described in the previous section was investigated by measuring half-cell potentials, concrete electrical resistivity, and polarization resistance at several locations on the deck surface. The polarization resistance was measured using different methods: linear polarization resistance (as measured by the GECOR6 instrument), galvanostatic pulse technique (as measured by the GalvaPulse instrument), and electrochemical impedance spectroscopy (as measured by a Gamry potentiostat/frequency response analyzer). All measurements were taken on all three slabs (each of different w/c) three times corresponding to different moisture conditions: dry, partially-saturated and saturated.

Prior to taking any experimental measurement, the actual concrete cover depth was measured using the concrete cover meter (Elcometer 331 Model B. 2010). All three slabs were found to have a top concrete cover of 50±5 mm. The exact location of each reinforcing steel bar was also determined using the cover meter.

As mentioned in section 3.2, each of the slabs has two layers of horizontal reinforcement, and each layer includes 8 rebars. These rebars are distributed across the slab width evenly 11-cm apart. As the top of the slabs were subjected to de-icing salt and several wetting/drying cycles, only the corrosion activity of the top reinforcement layer was investigated. The location of measurement points was partly governed by the size of

the probes of the instruments used. Because the GECOR 6 probe has a diameter of 180 mm, measurements on reinforcing steel bars located at the edges of the slabs were not practical. Therefore, measurements were only taken on the six middle rebars of each slab.

An experimental grid was therefore designed to study the corrosion of the three slabs under various concrete saturation conditions. In order to maintain the saturation level of each slab for all measurements, the location of measurement points was further limited by:

- the length of each GECOR 6 measurement, which takes 3 to 5 minutes.
- the length of one potentiostat measurement to attain the AC impedance spectra, which takes about 30 minutes for each measurement to complete.

Taking into account all of the above, an experimental grid with 240 measurement points was chosen on the top surface of each slab (Figure 3.7). These points are distributed evenly along each of the middle six rebars, 40 points along the length of the slab at a 10-cm interval, and 6 points along the width of the slab at an 11-cm interval (same as the distance between each reinforcing bar). The grid (location) number along the slab was assigned such that grid numbers multiplied by 10 give the distance in cm from the left end of the slabs. Figure 3.7 also illustrates the locations of the abutments, which are located between locations 1-3 and 25 and 30.

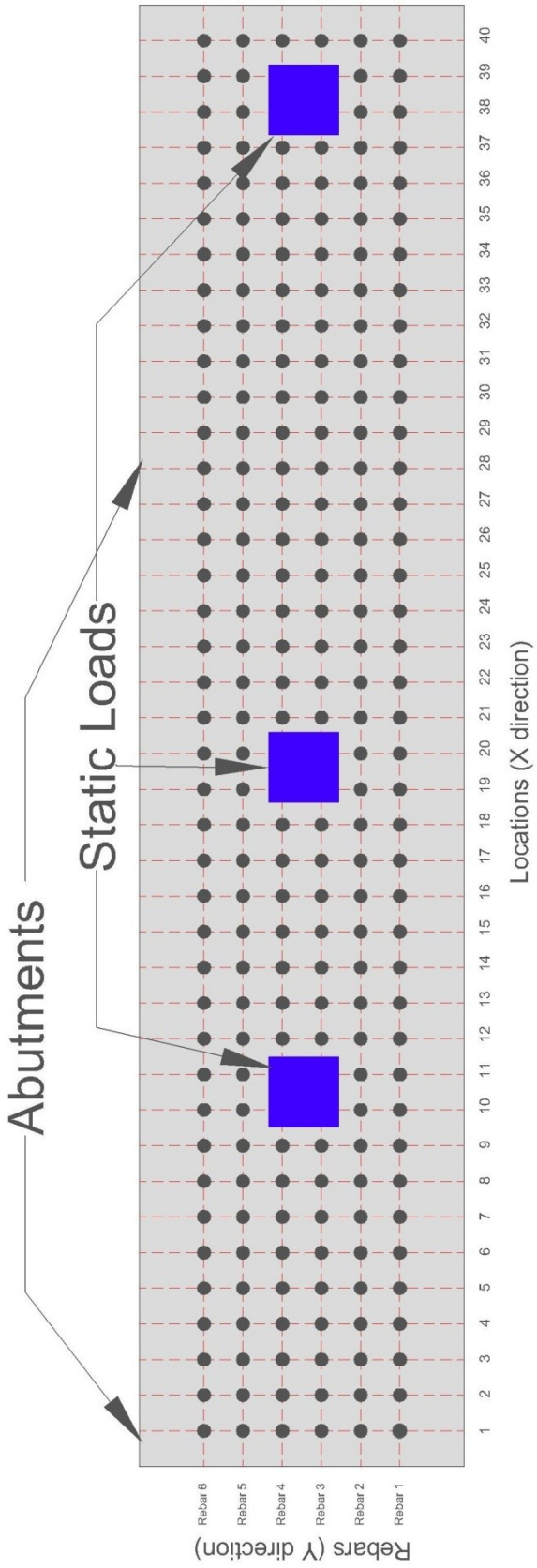

Figure 3-7: Location of measurement points.

3.3.2 Concrete saturation condition

The saturation level of the slabs was monitored through concrete electrical resistivity measurements, which are directly related to the moisture content of concrete. Increasing the moisture content of the concrete decreases its electrical resistivity. The electrical resistivity becomes constant once the concrete has reached saturation. Before applying water on the slabs, the concrete electrical resistivity was measured in the dry condition (i.e. at equilibrium relative humidity of the structural lab) at the specified locations (6 points on each slab). Henceforth, these measurements will be referred to as the measurements in "dry" conditions. These locations were chosen at the side of the slabs, since concrete electrical resistivity measurements could be taken when water was on the top surface of the slab.

For each slab, a series of measurements were carried out at three concrete saturation levels: dry, half partially-saturated and saturated. The first series of experimental measurements were done at the saturated condition. Time limitation was the main challenge to perform all the experimental measurements, as the concrete saturation condition changes with time. In order to optimize the time and measurements, each slab was divided from the other ones by installing a barrier between them (see Figure 3.8). This barrier allowed ponding one slab without affecting the adjacent one. After applying water on the surface of the slabs, the concrete resistivity was measured daily at the reference locations, looking for the saturation condition (see Figure 3.9). Since each of the slabs had a different w/c, the time needed to saturate each of the slabs was not the same. Once one slab would reach the saturated condition, the water could be drained from that slab, while the other slabs remained ponded.

Figure 3-8: Barrier installed between the slabs.

Figure 3-9: Daily monitoring of concrete electrical resistivity at specific locations.

As expected, the concrete electrical resistivity became constant (indicating saturated condition) first in the concrete slab with the highest water-to-cement ratio (slab 1, w/c=0.5). Water was then removed from slab 1, and measurements were carried out on the top surface of that slab. At the end of each working day, the concrete slab was then covered with water again to keep it saturated until all measurements for this moisture condition were completed.

A similar strategy was used to perform measurements on slabs 2 (w/c = 0.4) and 3 (w/c = 0.35). After taking all the measurements at the saturated condition, the slabs were let to dry, and the concrete resistivity was monitored to find the partially-saturated condition. Due to the rapid loss of concrete moisture, taking measurements at the partially-saturated condition was the most critical stage. Therefore, all the measurements were carried out in less than 48 hours on each of the slabs.

More measurements were taken at the saturated condition than other conditions, as water could be applied on the slab at the end of the day, thus maintaining the saturation level. However, the number of measurements which were carried out by the half-cell potential and concrete resistivity techniques was the same in all three of the concrete moisture levels.

Finally, measurements at the dry condition were carried out about 5 months after finishing the tests at the saturated condition. Since the test specimen was in the Structures Lab, there was no significant fluctuation in temperature and relative humidity during the length of this research. The temperature and relative humidity were monitored during all steps of the tests, and the obtained values were almost constant throughout (see Figure 3.10).

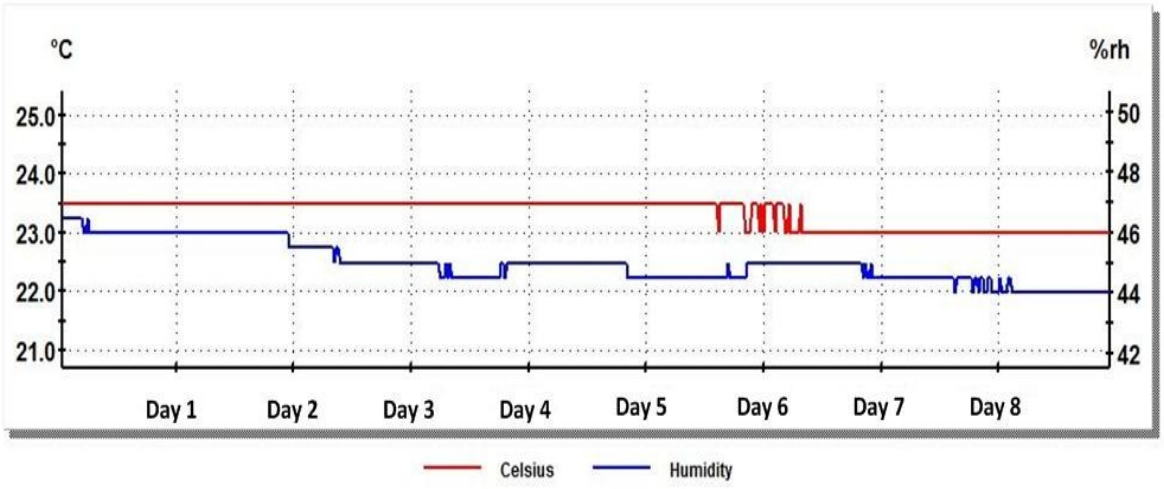

Figure 3-10: Sample of monitoring temperature and relative humidity: red line indicates the temperature while blue line indicates relative humidity.

3.4 Measurements

3.4.1 Half-cell potential mapping

Measuring the half-cell potential on the surface of concrete takes just a few seconds. Half-cell potential readings were therefore recorded on all the 240 measurement points on each slab at each moisture condition.

To measure the half-cell potential, the saturated calomel electrode was selected as the reference electrode (Figure 3.11). Three reference electrodes and two voltmeters were used in this study to assure the accuracy of the measurements. Prior to measuring the half-cell potentials, the accuracy of the reference electrodes and voltmeters was investigated to ensure consistency of the measurements. The electrical connections and wires were also checked to make sure that they did not introduce any errors in the measurements.

As the reference electrodes can easily lose their accuracy as they dry, after each series of measurements, the tip of the reference electrodes were kept wet by storing them in containers of distilled water.

The half-cell potential mapping was performed according to ASTM C876 – 09 (2009). At dry and partially-saturated conditions, the surfaces of the slabs were wet by spraying a water-based solution. This solution was prepared according to the ASTM C876 – 09 (2009), by mixing 95 ml of liquid detergent with 19 l of tap water. Better electrical connection between the wet sponge at the tip of the reference electrode and the concrete was achieved by spraying this solution on the surface.

Figure 3-11: Saturated calomel electrode used as a reference electrode to measure corrosion potential (Fisher Scientific, 2012).

Since an electrical connection to the steel rebar is essential to measure the corrosion potential, two locations at the end of each slab were drilled. After removing the concrete cover at the end side of the concrete slab, two solid electrical connections were made by taping a screw in a hole drilled into the reinforcing bar (see Figure 3.12).

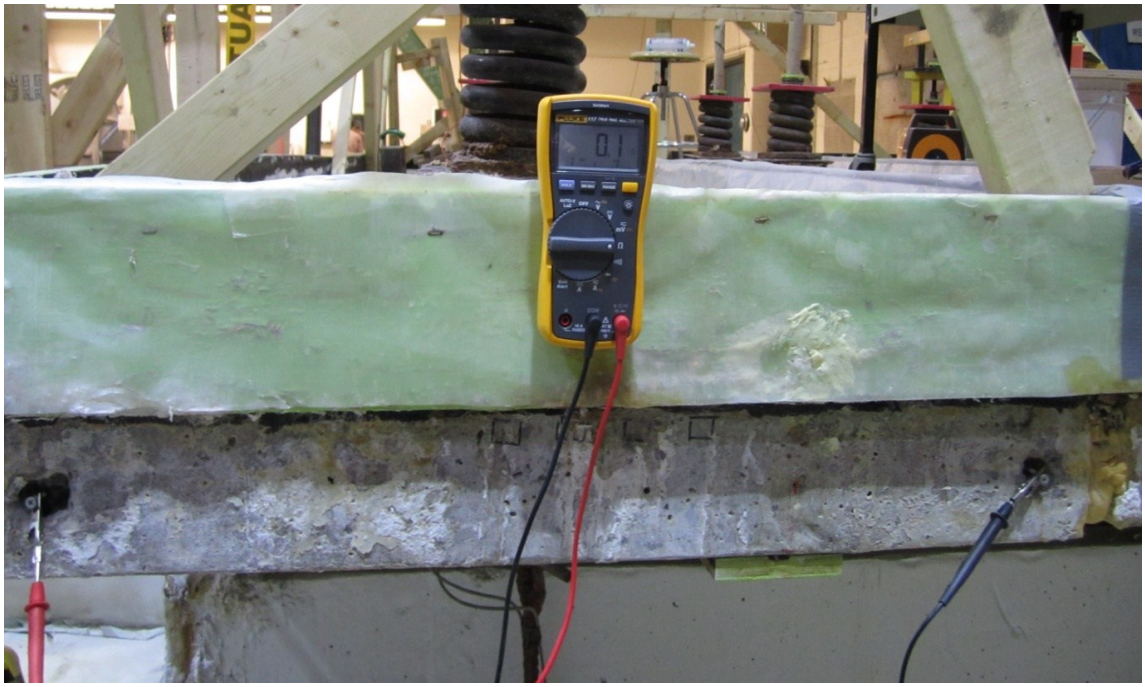

Figure 3-12: The electrical connection of the reinforcement was checked using the multimeter. The electrical resistance between the first and the last rebars was 0.1 Ohm.

3.4.2 Concrete electrical resistivity

The electrical resistivity of the concrete was measured using the Wenner probe. This measurement takes a few seconds to complete on a concrete which is not too dry. In contrast to half-cell potential measurements, an electrical connection to the steel rebars is not necessary. As the concrete resistivity measurement should not be taken directly on top of the rebars, the resistivity was measured on both sides of the reinforcing steel bar, and the average value was taken as the concrete resistivity at that location. By considering the length of the resistivity meter, which is 15 cm, 20 measurement points 20-cm apart were selected along the length of each reinforcing steel bars. Therefore, a total of 140

measurements were taken on each slab at each saturation condition (7 points in the Y direction).

The concrete resistivity could not be measured at the dry condition, since the surface of the concrete slabs did not have the necessary electrical conductivity to complete the measurements. In order to overcome this problem, the same solution used in the half-cell potential measurements was sprayed on the concrete surface to enhance the electrical connection between the probes and the concrete.

3.4.3 Linear polarization resistance technique

Linear polarization resistance (LPR) was measured at different locations on the slabs using the commercially available instrument GECOR 6 (James Instruments, 2010). A detailed description of the operating basis of the GECOR 6 is provided in section 2.3.3. To take a measurement with LPR device, an operator needs to enter the area of a rebar as described in section 2.3.3. Three problems were observed using LPR device: (i) slow measurement; (ii) confinement in some locations, there was a message displaying *"confinement is not fully achieved"* at the end of measurement); and, (iii) error in some locations, as device could not complete the measurements. Because of the LPR device probe size (180 mm) and the slow measurement procedure (10 to 14 measurements per hour), taking measurements at the 240 points on the slab was not possible. Therefore, 20 measurement points 20-cm apart were selected along the length of each reinforcing steel bars. Therefore, a total of 120 measurements were taken on each slab at saturated condition. In partially-saturated and saturated condition 60 measurements were taken. The locations of these points are illustrated in Figure 3.13.

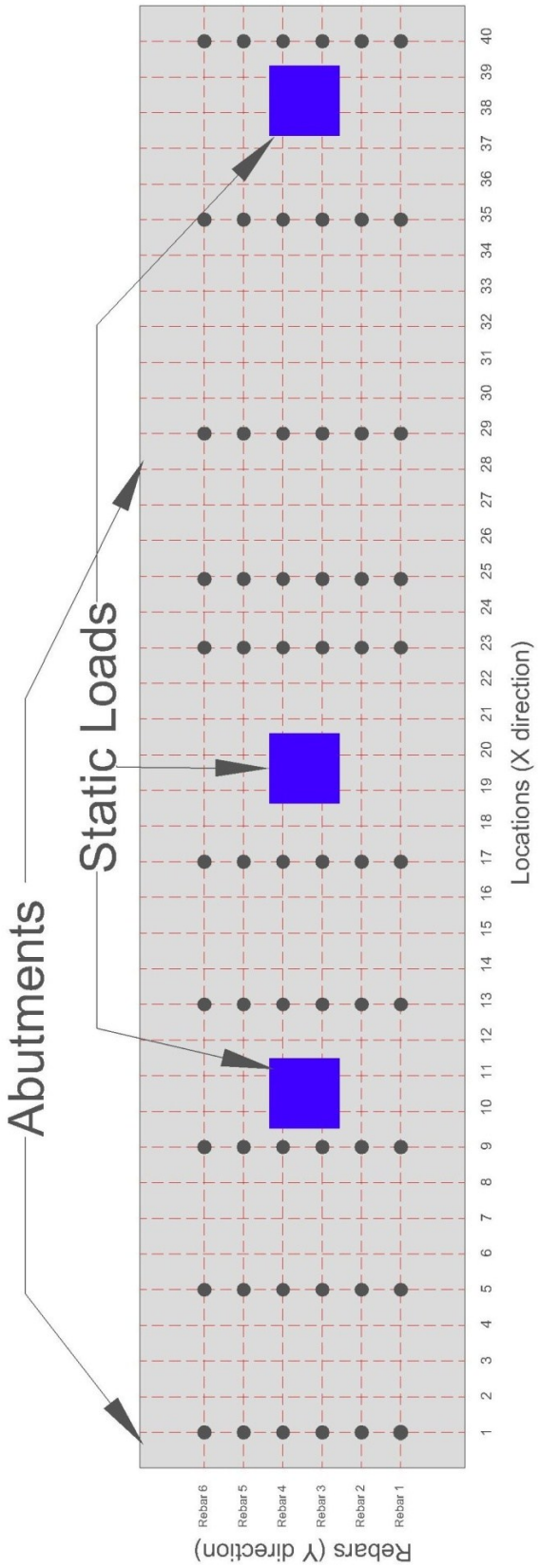

Figure 3-13: Location of measurement with GECOR 6 at partially-saturated and dry conditions.

The LPR device probe has three reservoirs which should be filled by a copper-copper sulphate solution before taking any measurement. Wetted sponges should be placed between the probe and the surface of concrete (see Figure 3.14). A constant pressure on the probe makes a better electrical connection between the probe and the concrete surface. Therefore, a 5-kg weight was put on top of the probe prior to taking each measurement (the weight is not shown in Figure 3.14). A significant high number of error messages were obtained when measurements were taken without this additional pressure on the probe.

Figure 3-14: GECOR 6 instrument and its probe.

3.4.4 Galvanostatic pulse technique

The polarization resistance was also measured by the galvanostatic pulse method (GPR) using the commercially available instrument GalvaPulse (Germann Instrument, 2010). A description of its operation is provided in section 2.3.4 Taking measurements with the GPR technique is fast and easy. Its capability for fast measurements as well as the small size of its probe (100 mm), allowed taking a higher number of measurements in comparison to the LPR instrument. Therefore, 40 measurement points 10-cm apart were selected along the length of each of the reinforcing steel bars. Therefore, a total of 240 measurements were taken on each slab at the saturated condition. In the partially-saturated and saturated condition 120 measurements were taken. The locations of these points are illustrated in Figure 3.15.

The GPR device uses the Ag/AgCl electrode as the reference electrode. This type of electrode is filled with the gel solution and does not require refill prior taking the measurement. To take a measurement with GPR device, the operator needs to enter the cross section area of the reinforcing steel bar, the duration of the galvanostatic pulse and the magnitude of the applied current. The GPR device default values for the current and its duration are 25 μA and 5 s, respectively. In reinforced concrete structures with high corrosion activity, the default values are not suitable, and measurements cannot be obtained. It is suggested in the GPR device manual (Galvapulse-Germann Instruments, 2012) to apply a higher magnitude of current on active areas. Choosing the right magnitude of the current is quite challenging due to given the small region of linearity in the current-potential relationship (~ 20 mV) around the open circuit potential (Gowers and Millard 1993, Andrade et al. 2001). Applying a current to the steel-concrete system polarizes the

steel. Therefore, it is not practical to take frequent measurements on a single location by increasing the current magnitude until an appropriate value of the current is determined.

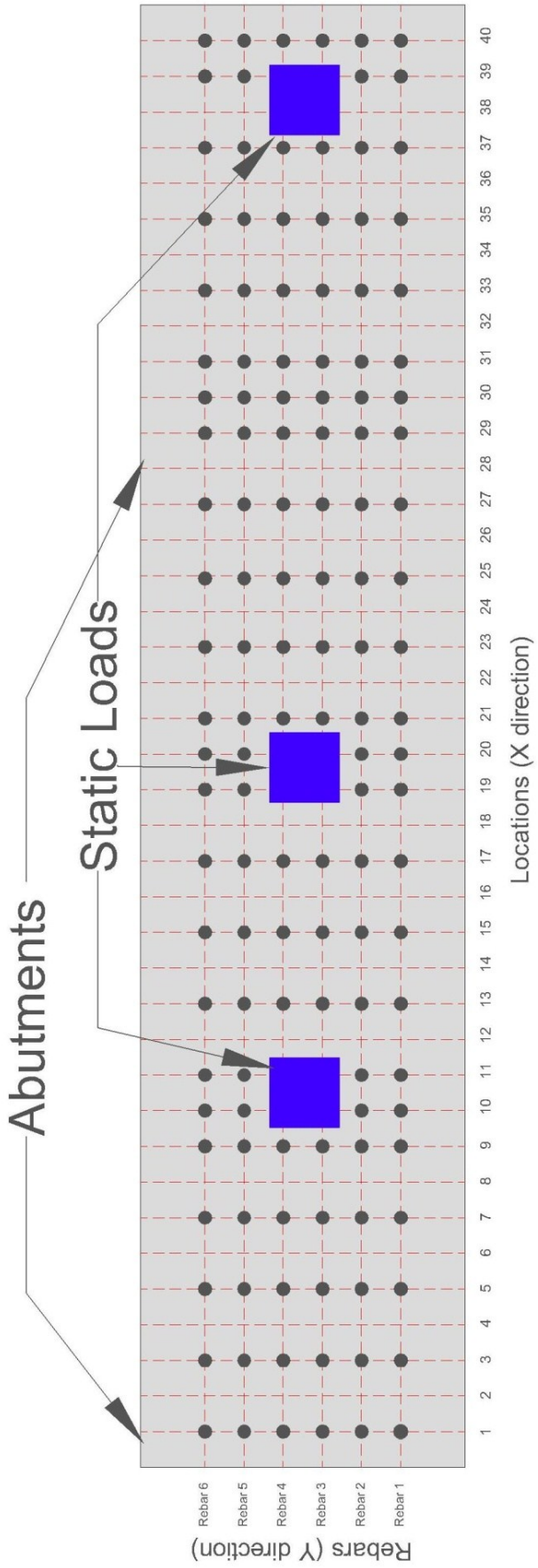

Figure 3-15: Location of measurement with GalvaPulseat partially-saturated and dry conditions.

Prior to the start of measurements in the saturated condition, a series of measurements were taken to evaluate the GPR device capabilities. Taking measurements with the GPR device default values for the current and duration was not successful in 90% of the trial measurements. Therefore, a much higher magnitude of the applied galvanostatic current, up to 400 μA, was used. In the most of trial measurements, a 100-μA current applied for 10 s was enough to obtain readings. So these values were chosen as the new default values for the subsequent GPR device measurement. Figure 3.16 shows the GPR device hand-held instrument and its probe.

Figure 3-16: GalvaPulse instrument and its probe.

3.4.5 Electrochemical impedance spectroscopy (EIS)

A detailed description of the operating basis of the EIS measurement is provided in section 2.3.5.

Performing the test with a potentiostat to obtain AC impedance spectra takes time, and it does need knowledge of EIS. The main difficulty to obtain AC impedance in this research was finding a suitable electrical connection, as the electrical connection between the probe and concrete surface is essential. In other methods, such as linear polarization resistance and galvanostatic pulse technique, using wet sponges provide adequate electrical contact between the probe and the concrete surface. Initial AC impedance measurements were actually done using wet sponges to provide the electrical connection. However, the obtained results did not have the required quality due to the high sensitivity of the EIS technique to the presence of a capacitor and a resistance. The electrical connection must have a very low electrical resistivity itself, otherwise its resistance or probable electrical capacitance will reflect in the results. Furthermore, the electrical characteristics of wet sponges are not clearly known, and they vary depending on the sponge type, water content and the amount of applied pressure. Different types of conductive media were investigated in this research to find a suitable electrical connection with a very low electrical resistance and capacitance.

A novel probe was designed to use the Gamry potentiostat along frequency response analyzer (see Figure 3.17). This probe consists of a saturated calomel reference electrode and a circular stainless steel plate with a hole in the center. The dimension of this probe was chosen to be close to the probes of other instruments (GalvaPulse and GECOR 6).

Taking measurements using the EIS technique at low frequencies is quite time consuming. It takes about 3 hours to obtain the impedance spectra using a frequency range of 0.001 mHz to 1 kHz with 10 data points per decade, while using 0.01 mHz to 1 kHz takes only about 30 minutes. Therefore, the material used as an electrical connector cannot dry during the duration of the measurement. To determine the most suitable conductive media, preliminary tests were conducted on two concrete samples; one had a stainless steel bar embedded in it, and the other one had a corroded steel bar embedded in it. The concrete resistivity of the concrete samples was measured prior to and after taking the EIS measurements using the Wenner probe resistivity meter. The AC impedance results obtained for different types of conductive media were compared and modeled using the Using Gamry Echem Analyst V5.61. The following conclusions were drawn from these preliminary tests:

- The wet sponges are not suitable as electrical connectors since their capacitance and resistance affect the AC impedance spectra.
- Homogeneous conductive media like conductive gels provide better results.
- The viscosity of conductive media is important, due to the long duration of the AC impedance measurement.
- The conductive media should not change the initial resistivity of the concrete resistivity.

By considering all of these findings and selecting a frequency range of 0.01 mHz to 1 kHz with 10 data points per decade, it was concluded that a conductive gel with medium viscosity provided the best result among other materials (e.g. sponges, hair gels, low and high viscosity conductive gels).

Another problem to be overcome when measuring AC impedance at low frequencies was noise in the system interrupting the measurement. Any kind of electrical device can produce some noise. In this research, the fluorescent lamps of the Structures Lab were found to affect the EIS measurements. Therefore, the EIS measurements had to be done while the fluorescent lamps were off in the Lab.

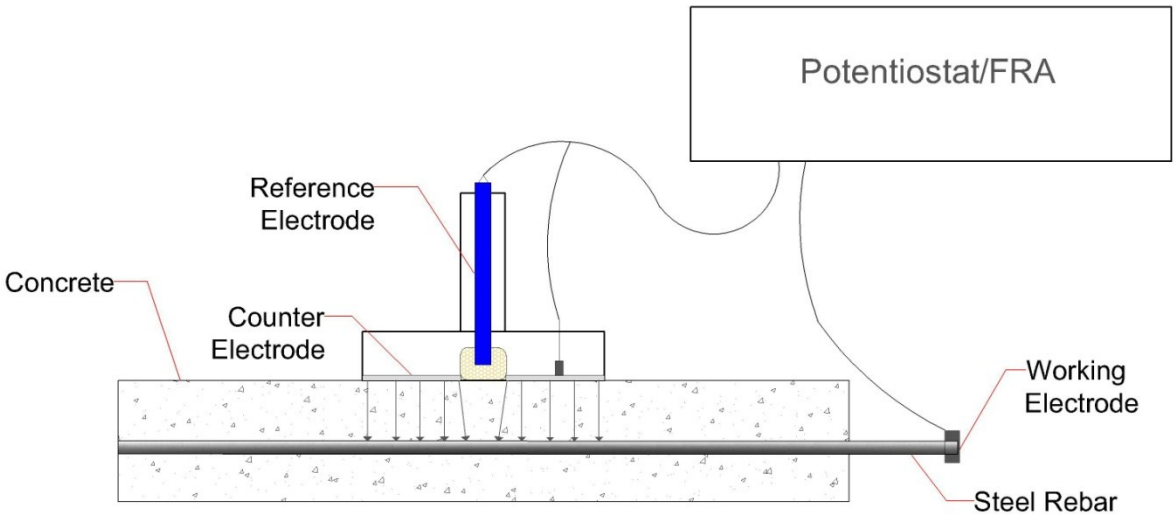

Figure 3-17: Schematic illustration of EIS setup used in this research to obtain polarization resistance.

The magnitude of the applied potential to obtain AC impedance spectra is also important. Two major considerations govern the magnitude of the potential; first, a low applied potential should be used to stay in the linear region of current response, and second, the potential should be powerful enough to allow measurements in dry concrete. Three different levels of applied potential were studied on concrete samples in dry,

partially-saturated and saturated conditions: 10 mV, 20 mV and 40 mV. The results in saturated and partially saturated conditions were almost the same, while in the dry condition, potentials of 10 mV and 20 mV could not provide results of good quality, as the concrete resistivity is quite high in this state. Consequently, an applied voltage of 40 mV was chosen to carry out the subsequent AC impedance tests.

4. Experimental: Results

4.1 Introduction

This chapter focuses on presenting the results of the experimental program described in Chapter 3; the analysis and discussion of the results are carried out in Chapter 5. Specifically, measurements that are critical to monitor corrosion activity in loaded reinforced concrete slabs are reported. These measurements include the mapping of half-cell potentials on concrete surface, resistivity of concrete, corrosion rates and polarization resistance of steel reinforcement. All measurements were carried out for three levels of concrete saturation: saturated, partially saturated and dry.

Polarization resistance data obtained from AC impedance (EIS) are presented in table format because the number of measurement points was limited due to the duration of these tests. All other data (i.e., half-cell potentials, resistivity, and corrosion rates) are presented in contour plots because of the large number of data points that span the two dimensional surface of the slabs. The contour plots were prepared by Golden Surfer software (V.10).

There are different interpolation methods to interpolate the measured data in contour plots; these methods include, but are not limited to, the Kriging method, inverse distance weighing, nearest neighbor interpolation, and triangulation with linear interpolation. A preliminary study, which is not presented here, was carried out to investigate the most appropriate mapping method that represents the data most accurately. As a result of this preliminary study, triangulation with linear interpolation was chosen to prepare the contour plots that present the results.

Figure 3.7 shows the locations of the data points for the measurements. In this figure, and all other contour plots presented in this chapter, the measurement points are identified with the rebar number and the grid (location) number along the slab (e.g. Rebar 1 - Location 7). All the measurements taken on each data point are given in the Appendix.

4.2 Results

4.2.1 Polarization resistance using AC impedance (EIS)

A sample EIS scan is illustrated in Figure 4.1 as Bode plot and 4.2 as Nyquist plot. Each EIS scan as illustrated in Figure 4.1 and 4.2 takes about 30 minutes to complete; therefore, the number of measurements points were limited to the one shown in Table 4.1. The locations were selected from different regions of the slabs considering loading conditions (e.g. zero moment, positive moment, negative moment). All EIS scans were carried out using Gamry PC4/300 Potentiostat/Galvanosatat/ZRA; the details are presented in Chapter 3.

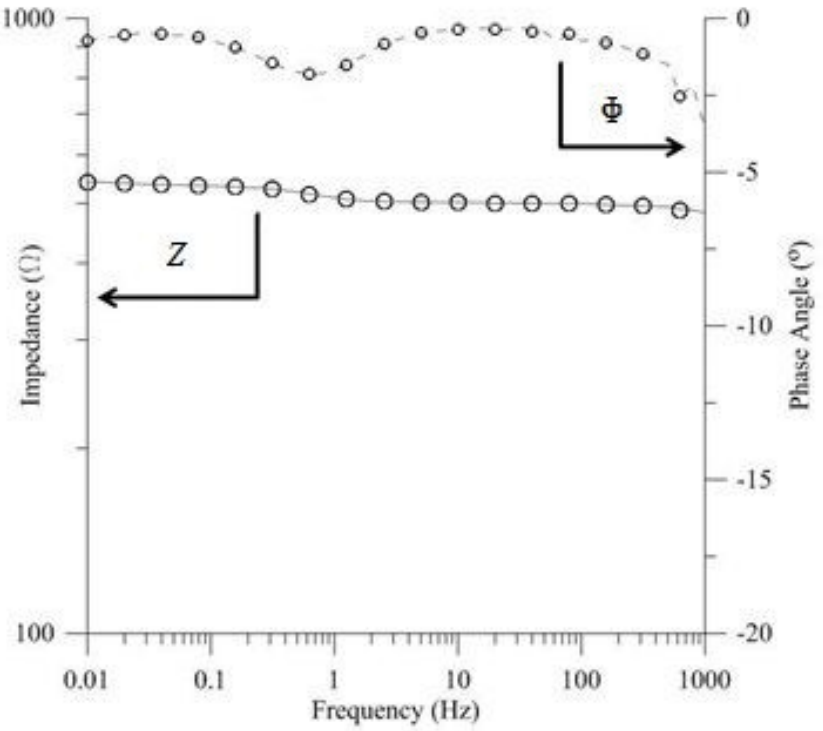

Figure 4-1: Bode plot obtained by EIS scan on slab 3 above rebar 3 location 15 in saturated condition.

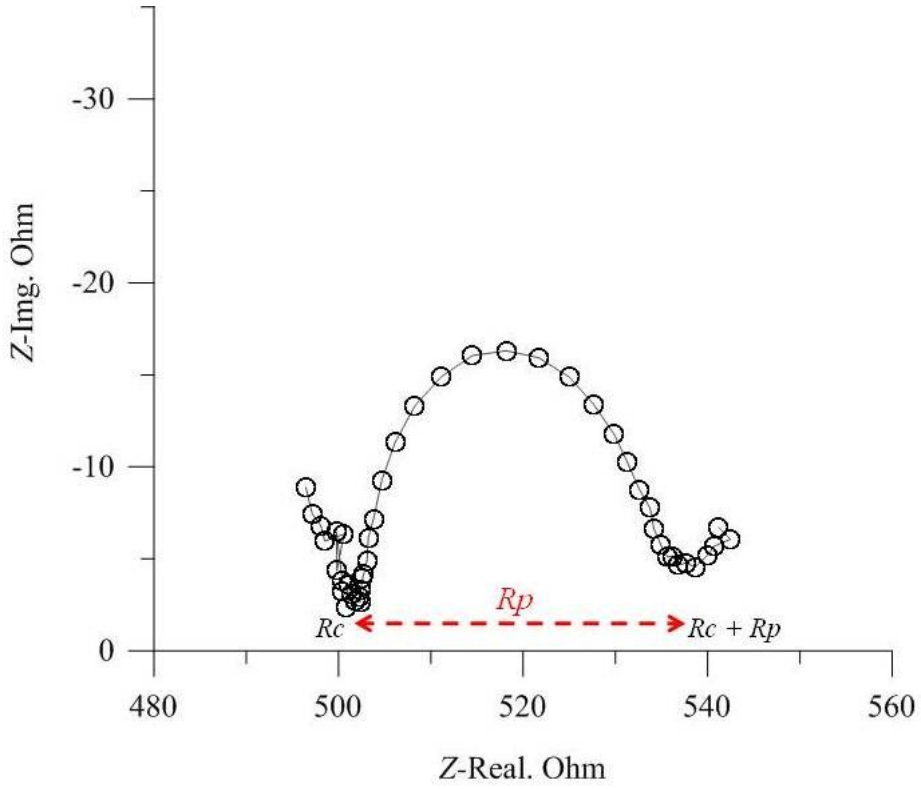

Figure 4-2: Nyquist plot obtained by EIS scan on slab 3 above rebar 3 location 15 in saturated condition and schematic illustration of extracting the polarization resistance, R_p.

The obtained data from EIS scans were fitted to an equivalent electrical circuit model to obtain polarization resistance, R_p. The modelling of the EIS results to equivalent electrical circuit was done by using Gamry Echem Analyst V5.61 software and Randles electrical circuit model. Tables 4.2-4.4 provide the polarization resistance measurements obtained from EIS scans using Randles circuit model for all slabs at different concrete saturation conditions.

Table 4-1: Location of EIS measurements.

Slab 1 (w/c=0.35)	**Slab 2 (w/c=0.4)**	**Slab 4 (w/c=0.5)**
Rebar 1 - Location 7	Rebar 1 - Location 15	Rebar 1 - Location 13
Rebar 1 - Location 13	Rebar 1 - Location 27	Rebar 1 - Location 31
Rebar 1 - Location 21	Rebar 1 - Location 31	Rebar 2 - Location 1
Rebar 2 - Location 5	Rebar 2 - Location 25	Rebar 2 - Location 13
Rebar 2 - Location 17	Rebar 2 - Location 40	Rebar 3 - Location 15
Rebar 2 - Location 27	Rebar 3 - Location 7	Rebar 3- Location 27
Rebar 2 - Location 40	Rebar 3 - Location 13	Rebar 3 - Location 40
Rebar 4 - Location 17	Rebar 5 - Location 5	Rebar 4 - Location 13
Rebar 5 - Location 7	Rebar 5 - Location 40	Rebar 4- Location 29
Rebar 5 - Location 25	Rebar 6 - Location 1	Rebar 5 - Location 5
Rebar 5 - Location 40	Rebar 6 - Location 17	Rebar 6 - Location 15
Rebar 6 - Location 15	Rebar 6 - Location 27	Rebar 6 - Location 19
Rebar 6 - Location 29	Rebar 6 - Location 40	Rebar 6 - Location 35
		Rebar 6 - Location 40

Table 4-2: Polarization resistance from AC impedance measurements using Randles circuit model for the slab 1 (w/c=0.35) at different concrete saturation conditions.

Measurement Location	Polarization Resistance (Ω)		
	Dry	Partially Saturated	Saturated
Rebar 1 - Location 7	178.7	26.9	47.0
Rebar 1 - Location 13	109.6	41.2	24.4
Rebar 1 - Location 21	79.21	33.5	42.07
Rebar 2 - Location 5	210.9	69.1	78.2
Rebar 2 - Location 17	390.5	20.9	34.0
Rebar 2 - Location 27	118.7	15.4	31.4
Rebar 2 - Location 40	167.5	32	54.1
Rebar 4 - Location 17	98.7	32	45.0
Rebar 5 - Location 7	166	44	81.7
Rebar 5 - Location 25	38	32.7	73.5
Rebar 5 - Location 40	348.5	37.1	61.0
Rebar 6 - Location 15	149	17.5	50.4
Rebar 6 - Location 29	238.2	51.2	84.3

Table 4-3: Polarization resistance from AC impedance measurements using Randles circuit model for the slab 2 (w/c=0.40) at different concrete saturation conditions.

Measurement Location	Polarization Resistance (Ω)		
	Dry	Partially Saturated	Saturated
Rebar 1 - Location 15	185.7	112.6	65.6
Rebar 1 - Location 27	151.9	23.9	31.5
Rebar 1 - Location 31	105	22.1	21.6
Rebar 2 - Location 25	210.1	76.3	68.5
Rebar 2 - Location 40	227.7	96.6	60.0
Rebar 3 - Location 7	180	54.3	59.8
Rebar 3 - Location 13	129	50.6	47.9
Rebar 5 - Location 5	580	142.5	73.8
Rebar 5 - Location 40	310.1	84	147.0
Rebar 6 - Location 1	202.2	84	61.5
Rebar 6 - Location 17	207	46	58.2
Rebar 6 - Location 27	165	77.6	49.8
Rebar 6 - Location 40	335.1	39	48.3

Table 4-4: Polarization resistance from AC impedance measurements using Randles circuit model for the slab 3 (w/c=0.50) at different concrete saturation conditions.

Measurement Location	Polarization Resistance (Ω)		
	Dry	Partially Saturated	Saturated
Rebar 1 - Location 13	82.6	30	47.8
Rebar 1 - Location 31	31.9	24	15.2
Rebar 2 - Location 1	103.8	48.9	46.7
Rebar 2 - Location 13	49.1	24.7	35.7
Rebar 3 - Location 15	127.6	25.6	33.5
Rebar 3- Location 27	45.1	32.1	32.5
Rebar 3 - Location 40	44.9	28.7	64.2
Rebar 4 - Location 13	140.2	19.3	52.4
Rebar 4- Location 29	87.3	34.2	34.5
Rebar 5 - Location 5	289.9	58.5	42.1
Rebar 6 - Location 15	178.9	68.7	28.4
Rebar 6 - Location 19	298.6	54.1	88.0
Rebar 6 - Location 35	100.2	32.3	44.6
Rebar 6 - Location 40	322.2	40.3	49.1

4.2.2 Half-cell potential mapping

Figures 4.3-4.5 illustrate the half-cell potential measurement of three slabs (w/c = 0.35, 0.40, 0.5) in dry, partially saturated and saturated conditions, respectively. The potential contour interval is chosen to be 50 mV to meet the ASTM C-867-09 standard that requires a maximum of 100 mV contour interval. Darker colours in the contour plots represent more negative half-cell potentials (i.e. zones of higher corrosion probability) measured with respect to saturated calomel electrode (SCE).

4.2.3 Concrete resistivity

Figures 4.6-4.8 illustrate the concrete resistivity measurements (using Wenner probe) of three slabs (w/c = 0.35, 0.40, 0.5) in dry, partially saturated and saturated conditions, respectively. All resistivity measurements are presented in KOhm.cm.

4.2.4 Corrosion rate by Galvapulse

Figures 4.9-4.11 illustrate the corrosion rate measurements (using Galvapulse) of three slabs (w/c = 0.35, 0.40, 0.5) in dry, partially saturated and saturated conditions, respectively. All the results are presented in $\mu A/cm^2$.

4.2.5 Corrosion rate by GECOR 6

Figures 4.12-4.14 illustrate the corrosion rate measurements (using GECOR 6) of three slabs (w/c = 0.35, 0.40, 0.5) in dry, partially saturated and saturated conditions, respectively. All the results are presented in $\mu A/cm^2$.

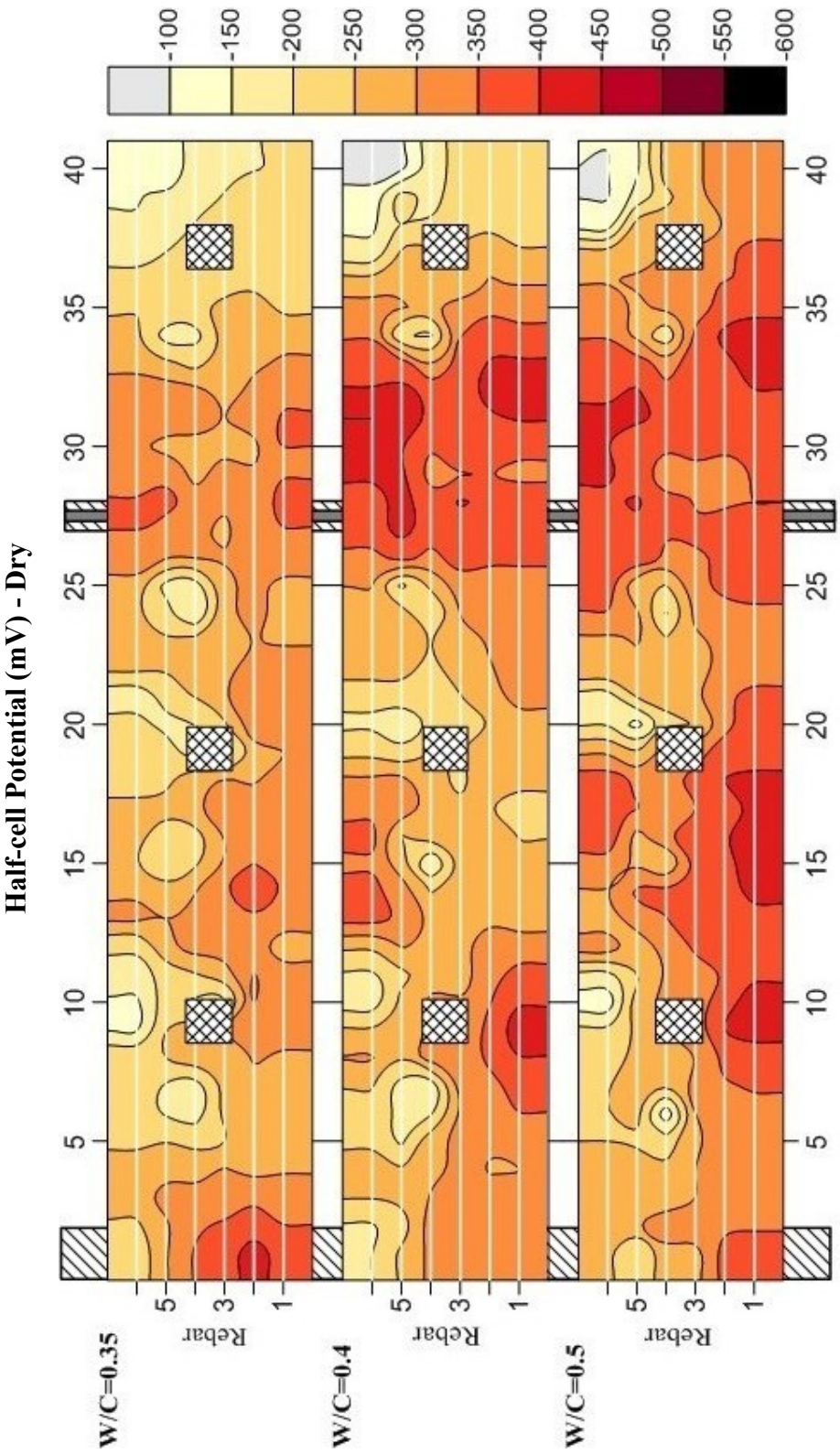

Figure 4-3: Contour maps of the half-cell potential measurements of the Slab 1 (W/C=0.35), Slab 2 (W/C=0.40) and Slab 3 (W/C=0.5) in dry condition.

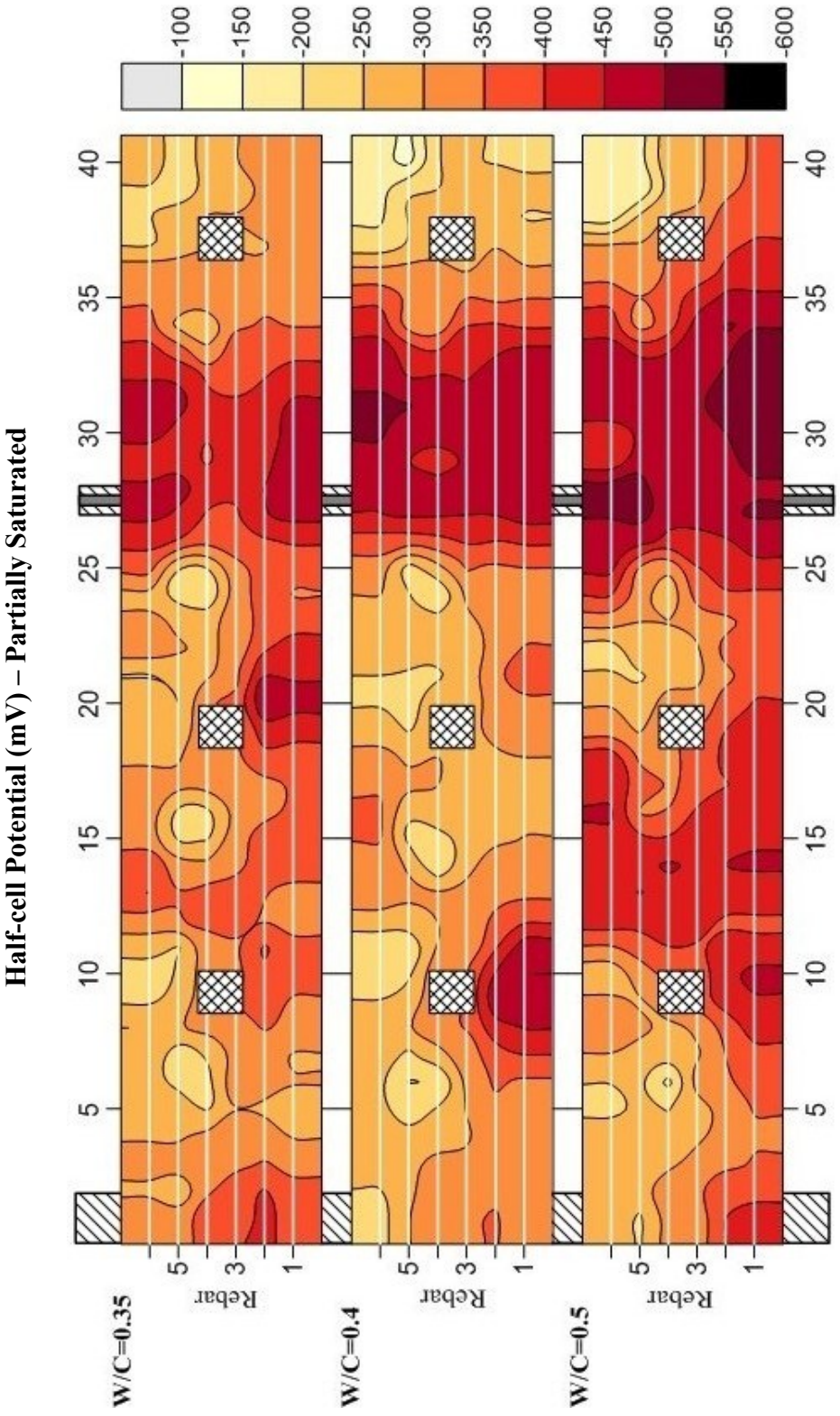

Figure 4-4: Contour maps of the half-cell potential measurements of the Slab 1 (W/C=0.35), Slab 2 (W/C=0.40) and Slab 3 (W/C=0.5) in partially-saturated condition.

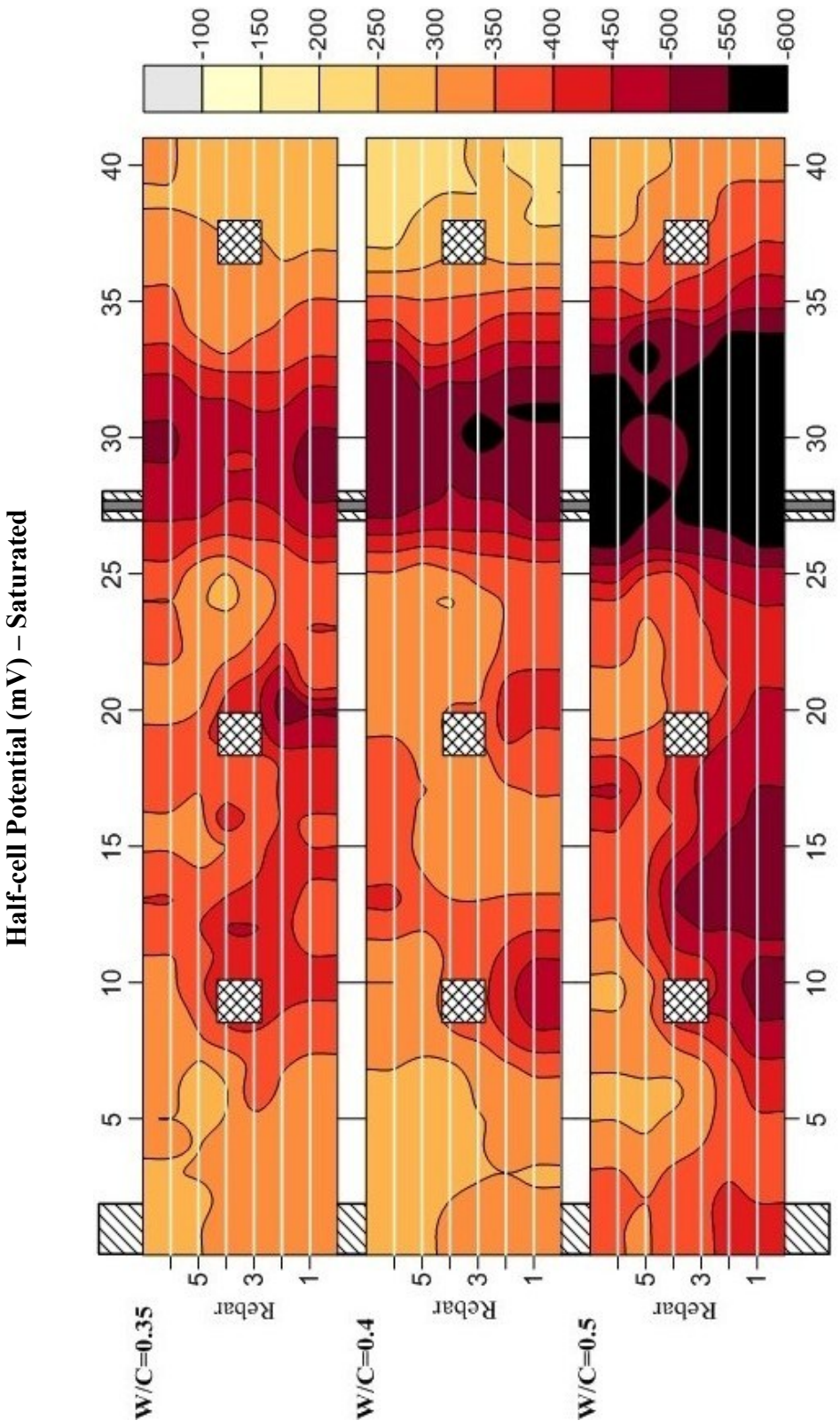

Figure 4-5: Contour maps of the half-cell potential measurements of the Slab 1 (W/C=0.35), Slab 2 (W/C=0.40) and Slab 3 (W/C=0.5) in saturated condition.

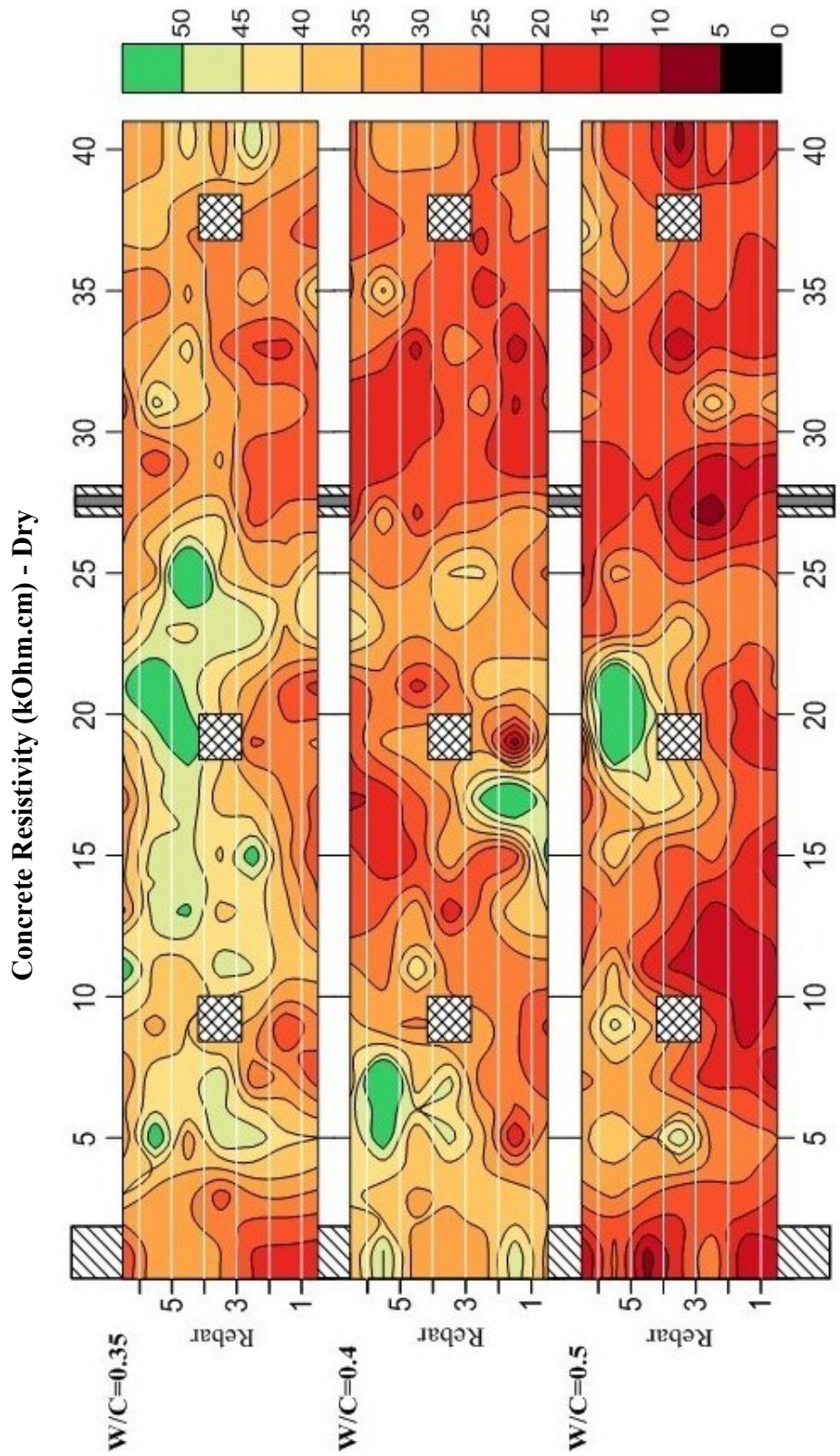

Figure 4-6: Contour maps of the concrete resistivity measurements of the Slab 1 (W/C=0.35), Slab 2 (W/C=0.40) and lab 3 (W/C=0.5) in dry condition.

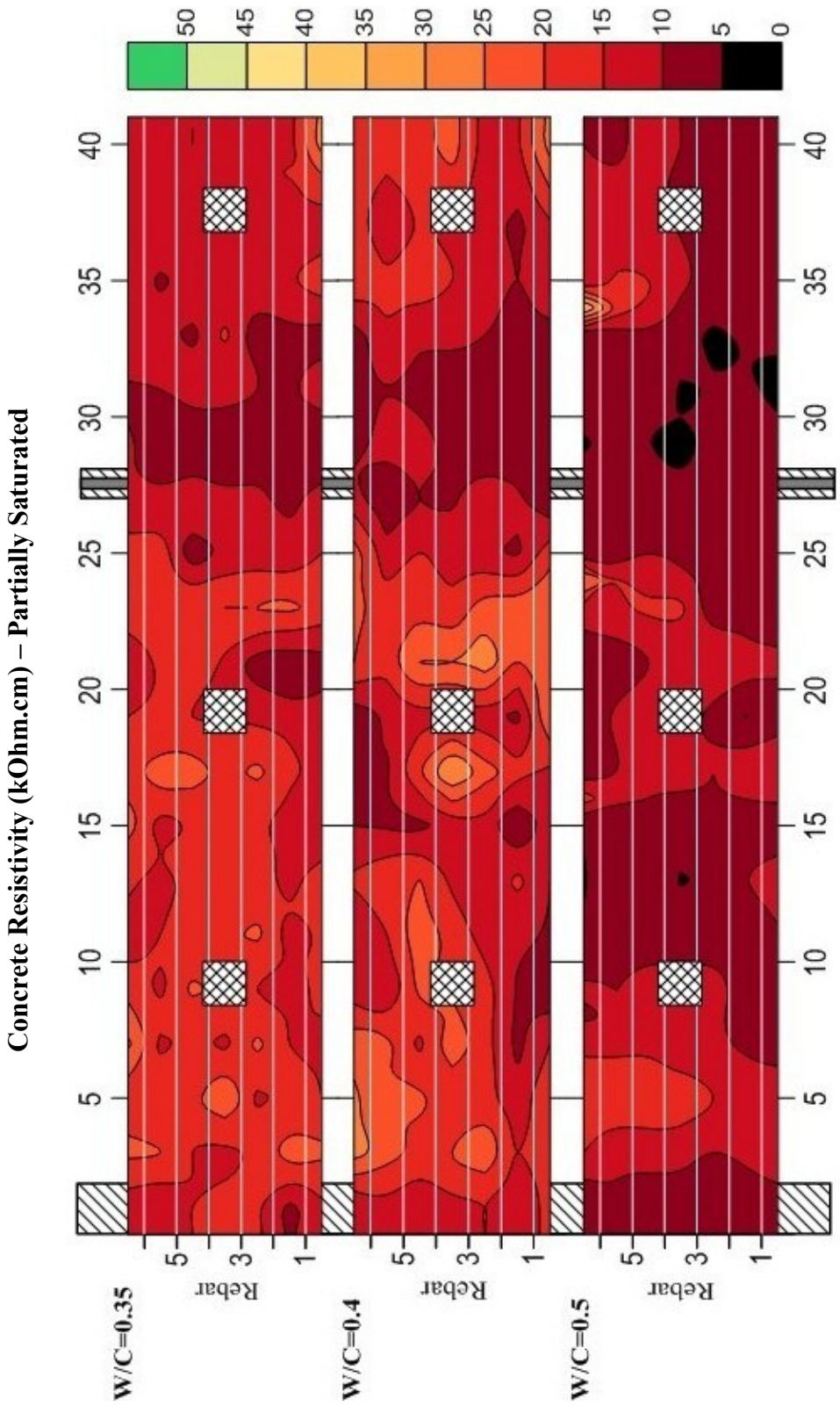

Figure 4-7: Contour maps of the concrete resistivity measurements of the Slab 1 (W/C=0.35), Slab 2 (W/C=0.40) and Slab 3 (W/C=0.5) in partially-saturated condition.

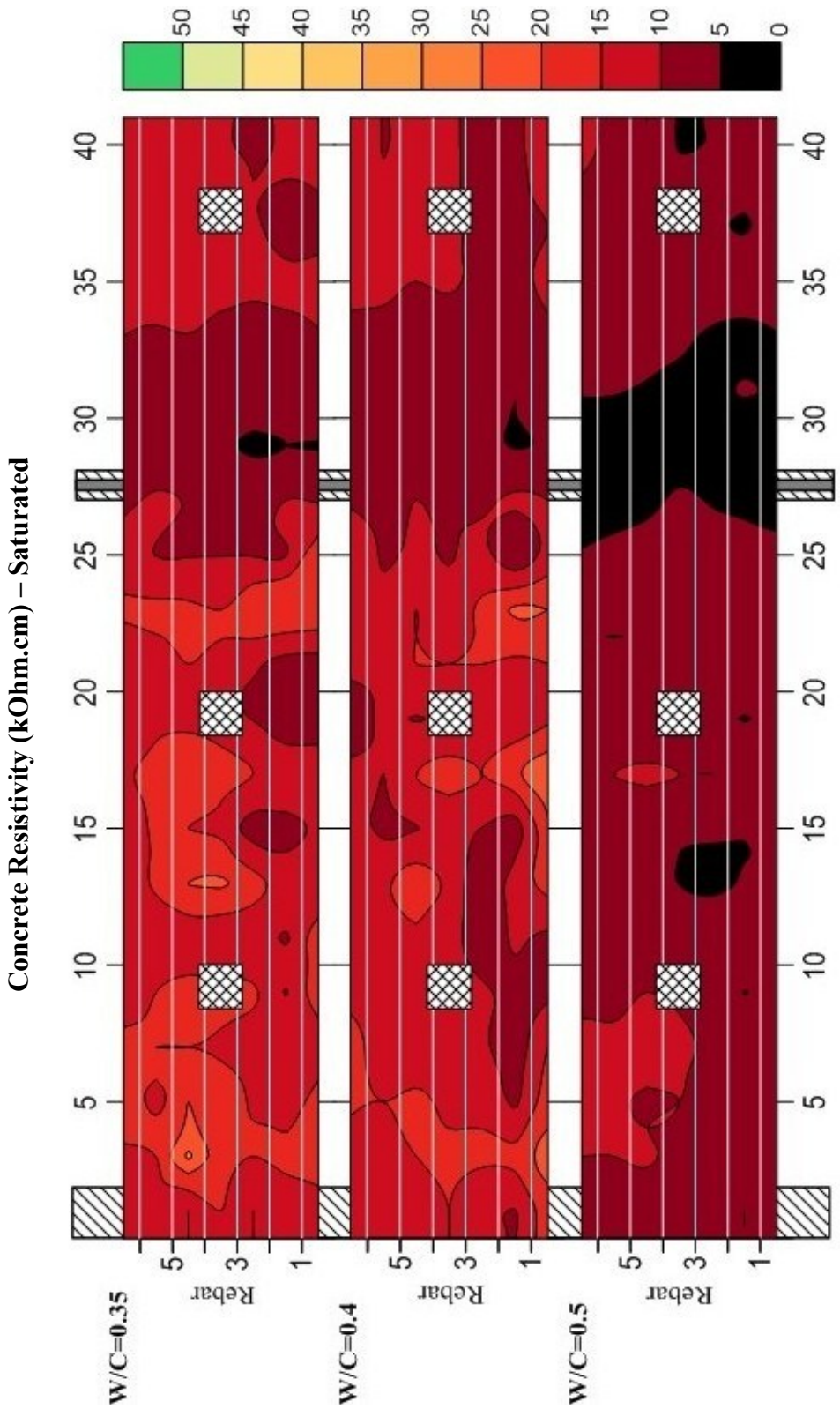

Figure 4-8: Contour maps of the concrete resistivity measurements of the Slab 1 (W/C=0.35), Slab 2 (W/C=0.40) and Slab 3 (W/C=0.5) in saturated condition.

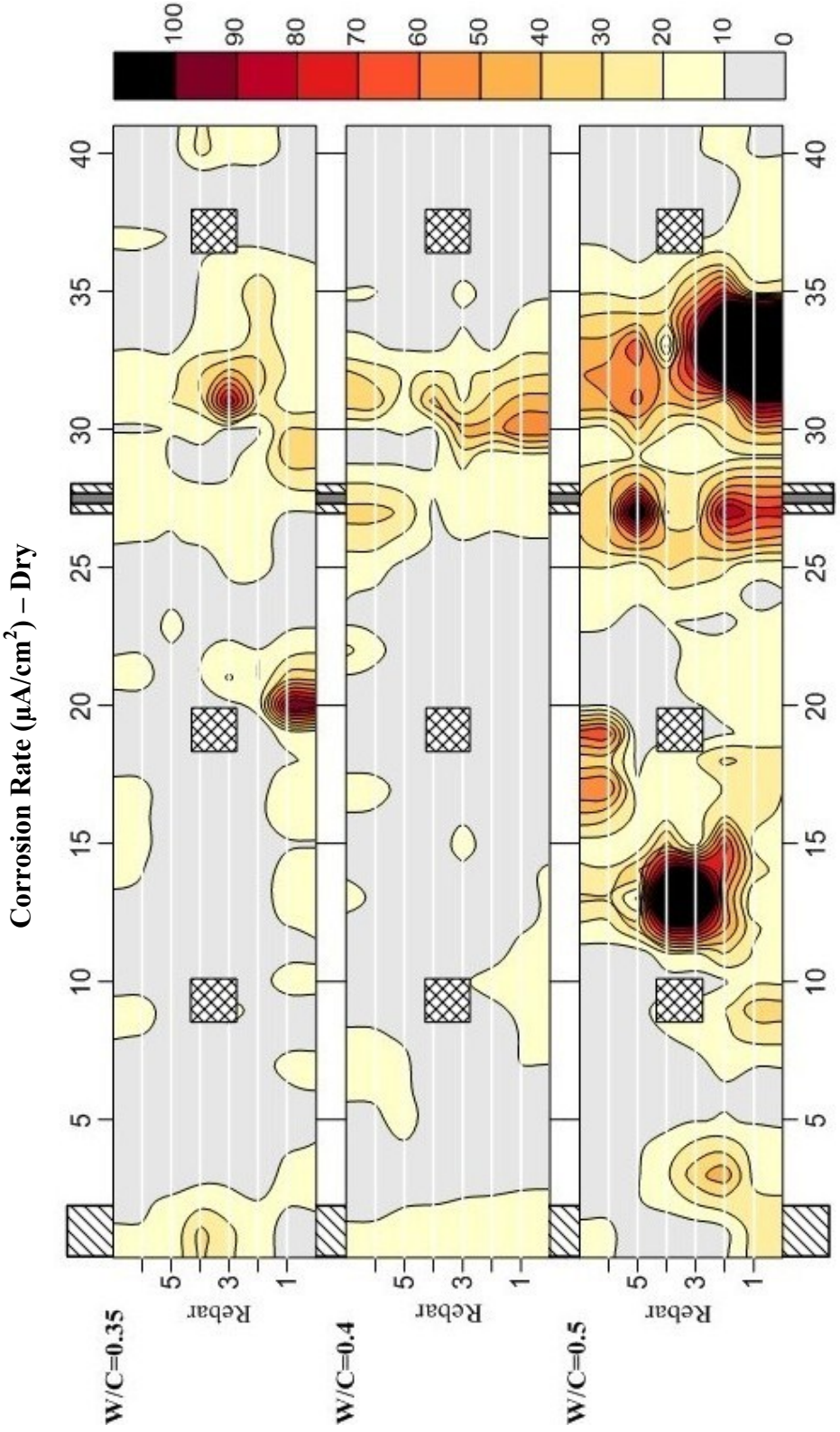

Figure 4-9: Contour maps of the corrosion rate measurements of the Slab 1 (W/C=0.35), Slab 2 (W/C=0.40) and Slab 3 (W/C=0.5) in dry condition, measured by GalvaPulse.

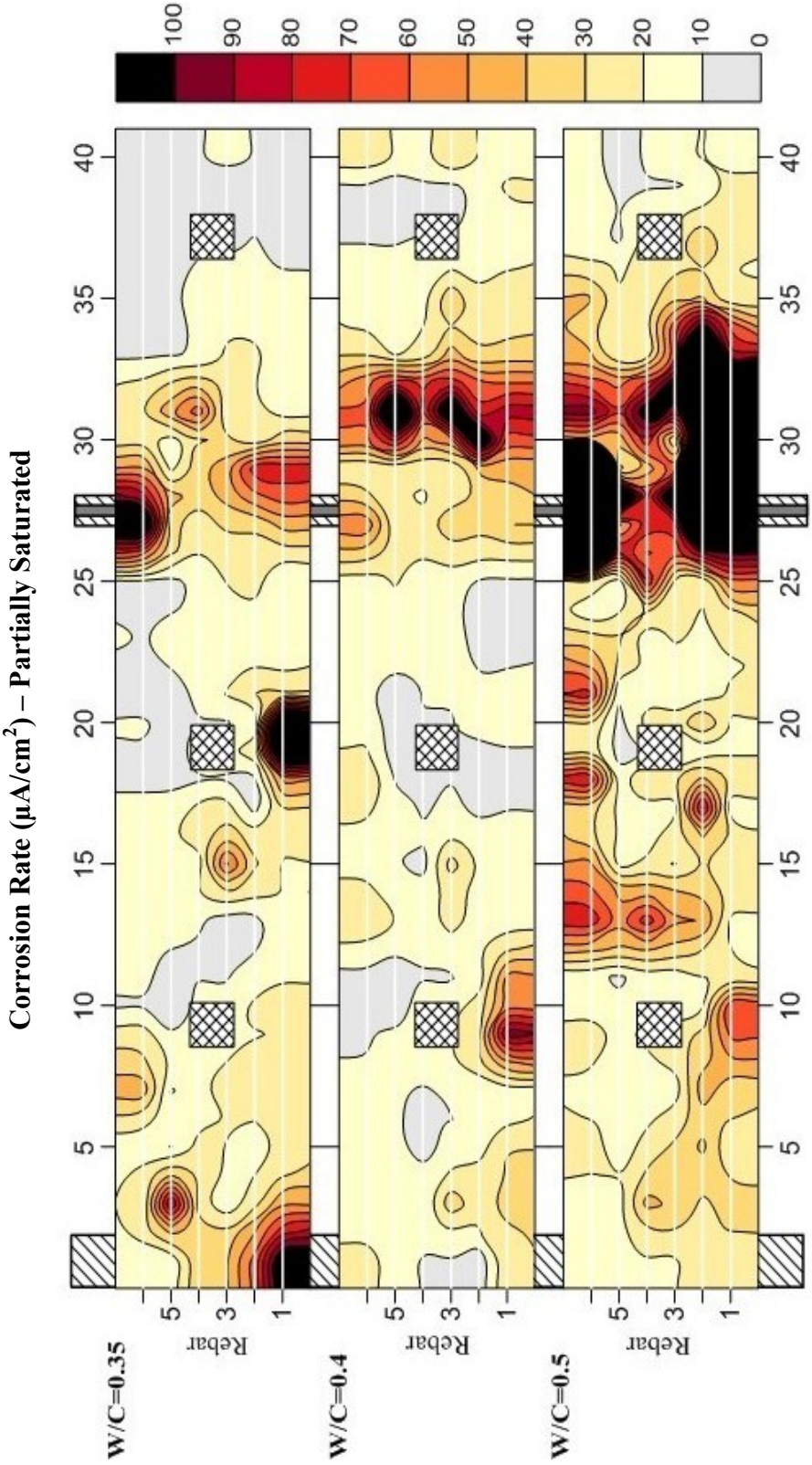

Figure 4-10: Contour maps of the corrosion rate measurements of the Slab 1 (W/C=0.35), Slab 2 (W/C=0.40) and Slab 3 (W/C=0.5) in partially saturated condition, measured by GalvaPulse.

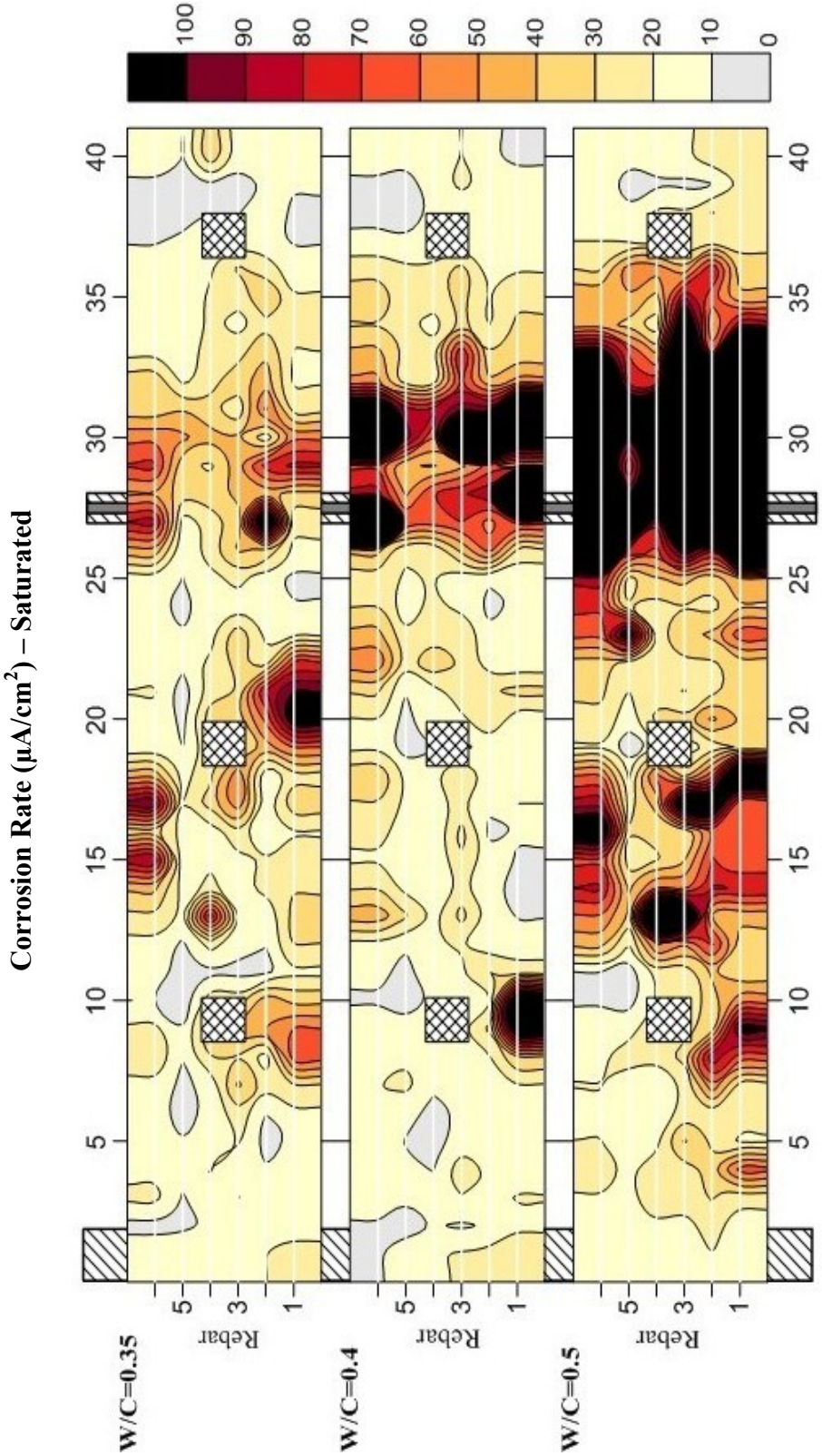

Figure 4-11: Contour maps of the corrosion rate measurements of the Slab 1 (W/C=0.35), Slab 2 (W/C=0.40) and Slab 3 (W/C=0.5) in saturated condition, measured by GalvaPulse.

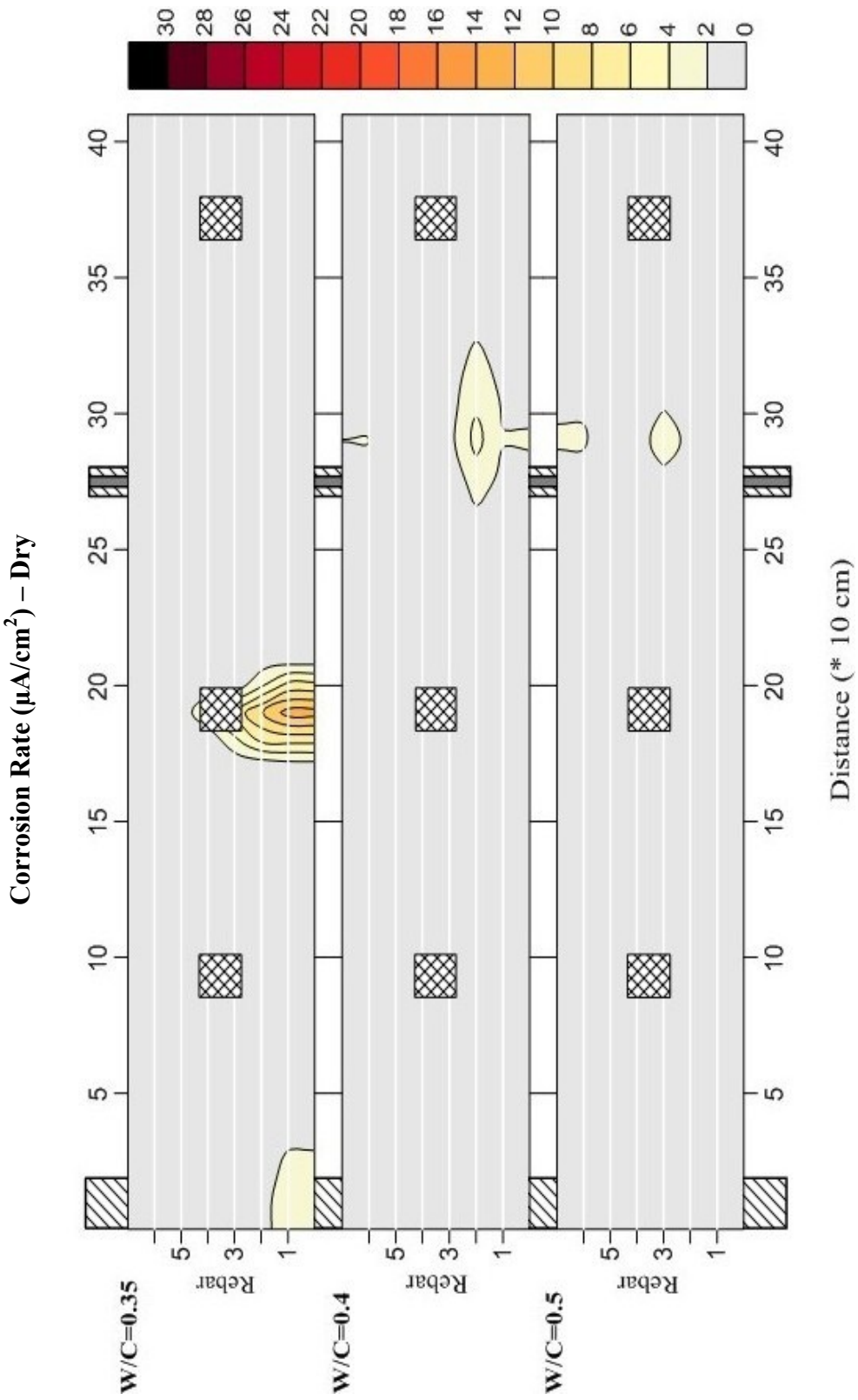

Figure 4-12: Contour maps of the corrosion rate measurements of the Slab 1 (W/C=0.35), Slab 2 (W/C=0.40) and Slab 3 (W/C=0.5) in dry condition, measured by GECOR 6.

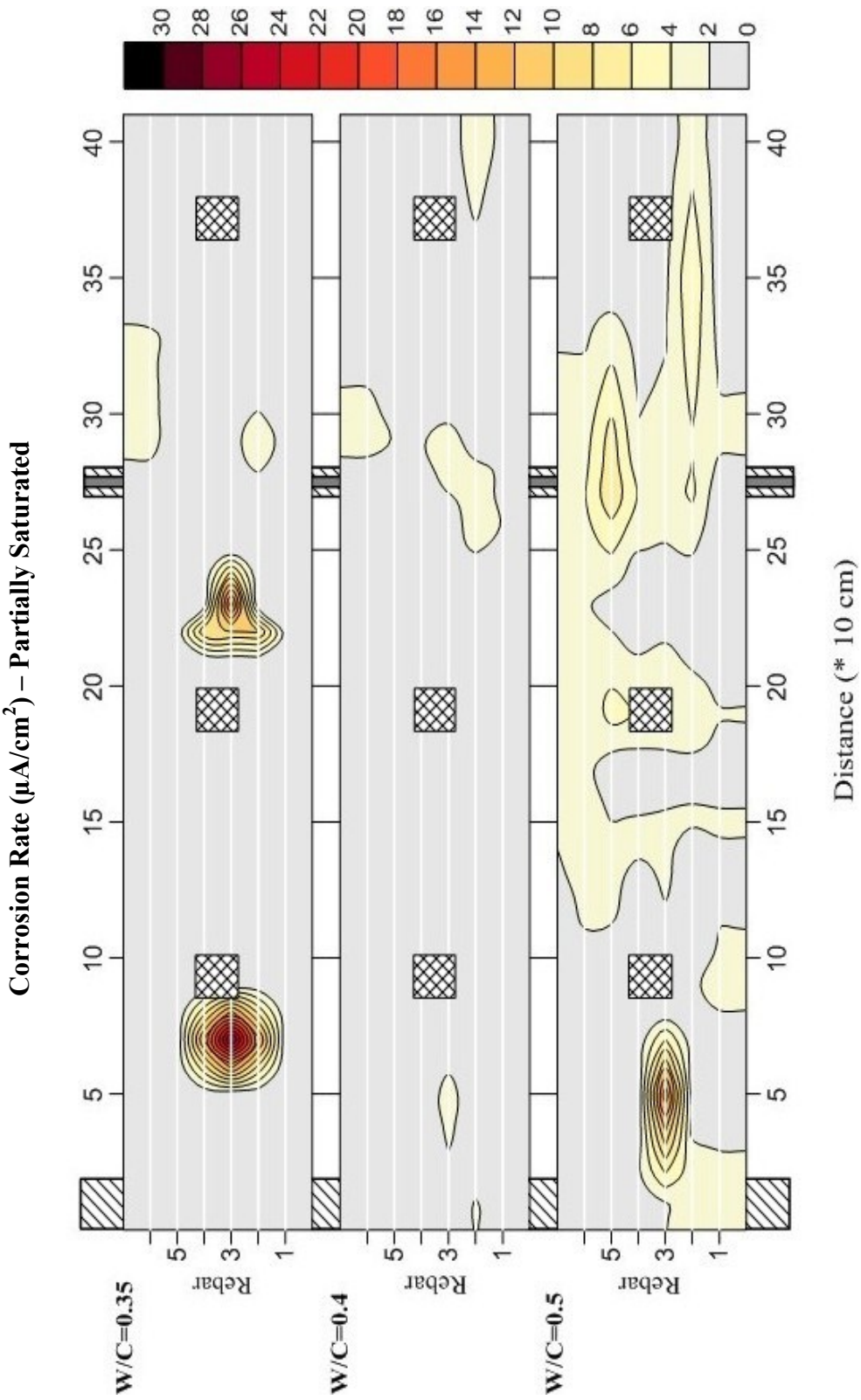

Figure 4-13: Contour maps of the corrosion rate measurements of the Slab 1 (W/C=0.35), Slab 2 (W/C=0.40) and Slab 3 (W/C=0.5) in partially saturated condition, measured by GECOR 6.

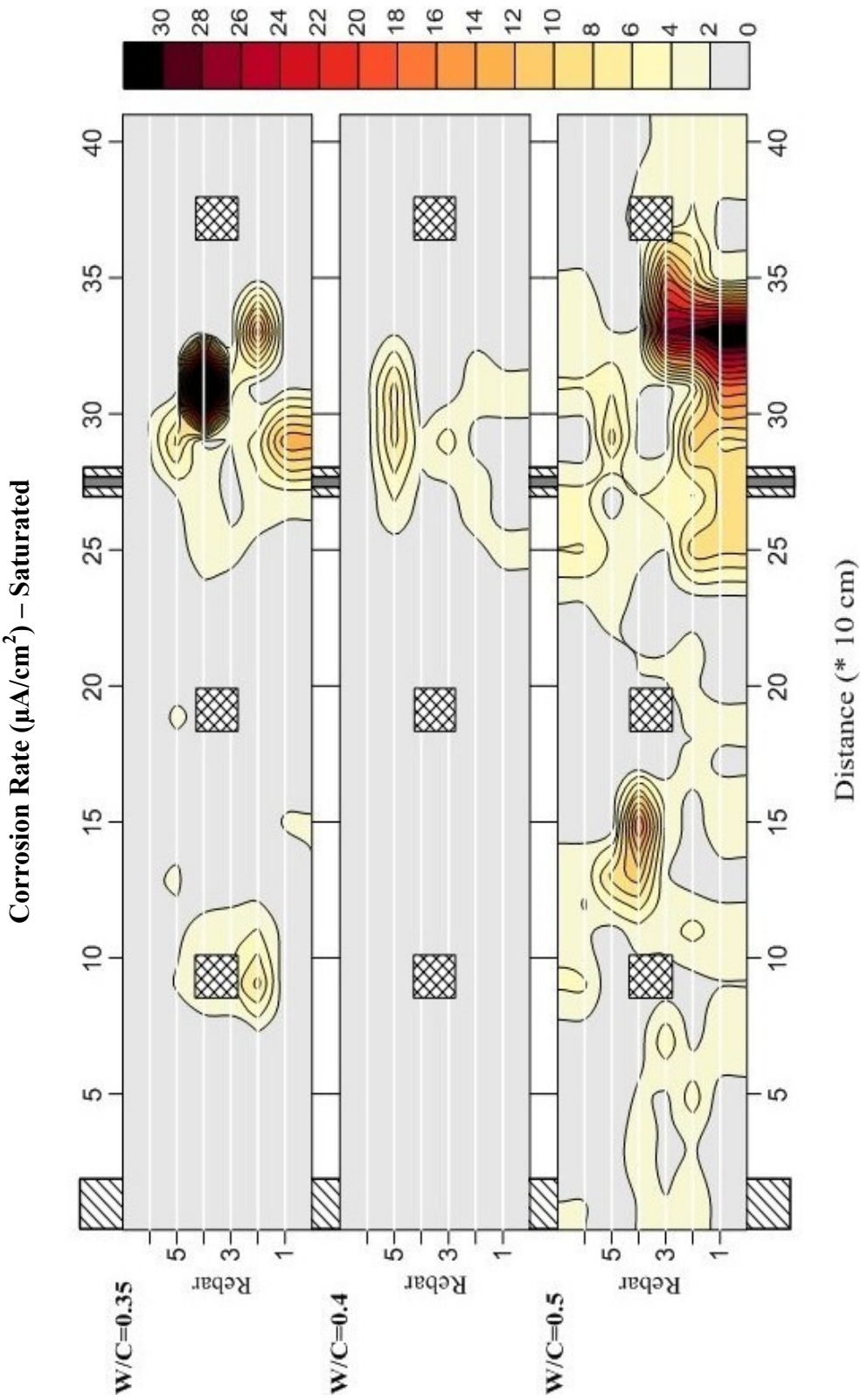

Figure 4-14: Contour maps of the corrosion rate measurements of the Slab 1 (W/C=0.35), Slab 2 (W/C=0.40) and Slab 3 (W/C=0.5) in saturated condition, measured by GECOR 6.

5. Experimental: Analysis and Discussion

5.1 Introduction

The experimental results presented in Chapter 4 are analyzed and discussed in this chapter. The relation among values of polarization resistance obtained by the different techniques is investigated as a function of four testing parameters: concrete electrical resistivity, water-to-cement ratio, concrete saturation condition, and applied structural loading. Furthermore, the relationship between concrete resistivity and polarization resistance is studied for different concrete saturation levels and applied loading conditions. Finally, the correspondence between half-cell potentials and polarization resistance is explored to investigate the criteria provided by ASTM C876-09.

5.2 Polarization resistance

This section investigates the correlation in the results obtained from different polarization resistance techniques (LPR, GPR and EIS). This relationship is studied as a function of four different parameters: concrete resistivity, water-to-cement ratio, concrete saturation condition, and applied structural loading.

5.2.1 LPR technique vs. EIS technique

In this section the polarization resistances measured by the LPR and the EIS techniques are compared to each other. As mentioned in Chapter 2, the LPR device used in this study does not give the polarization resistance value directly. Instead, it provides the corrosion rate i_{corr}, which is calculated according to Eq. 2.10. The polarization resistance, normalized with the LPR probe size, $R_p \times A$, is thus calculated from Eq. 5.1:

$$R_p \times A = \frac{B}{i_{corr}} \qquad \textit{Eq. 5.1}$$

where i_{corr} is the corrosion rate expressed in μA/cm^2, B is equal to 26 mV, and A is the surface area of the rebar under the probe (i.e., $A = \pi D \times 10.5 = 37$ cm^2, with the rebar diameter D = 11.3 mm). For AC impedance measurements, the polarization resistance is normalized with the EIS probe size using Eq. 5.2:

$$R_p \times A = R_p \times \left(\pi D \times 2R\right) \qquad \textit{Eq. 5.2}$$

where A is the surface area of the rebar under the EIS probe, D is the diameter of the rebar (11.3 mm), and R is the radius of the EIS probe, which is 5 cm in this study. Taking these values into account, the polarization resistance is multiplied by 35 cm^2 to make it independent of probe size.

The polarization resistance values obtained by the LPR and the EIS techniques are shown in Figure 5.1. The polarization resistance measured by the LPR technique is always higher than the one obtained by the EIS technique, with some locations displaying a difference by a factor of 100. Based on these results, the LPR technique underestimates the

corrosion rate in comparison with the EIS technique. Generally, these techniques are not correlated well.

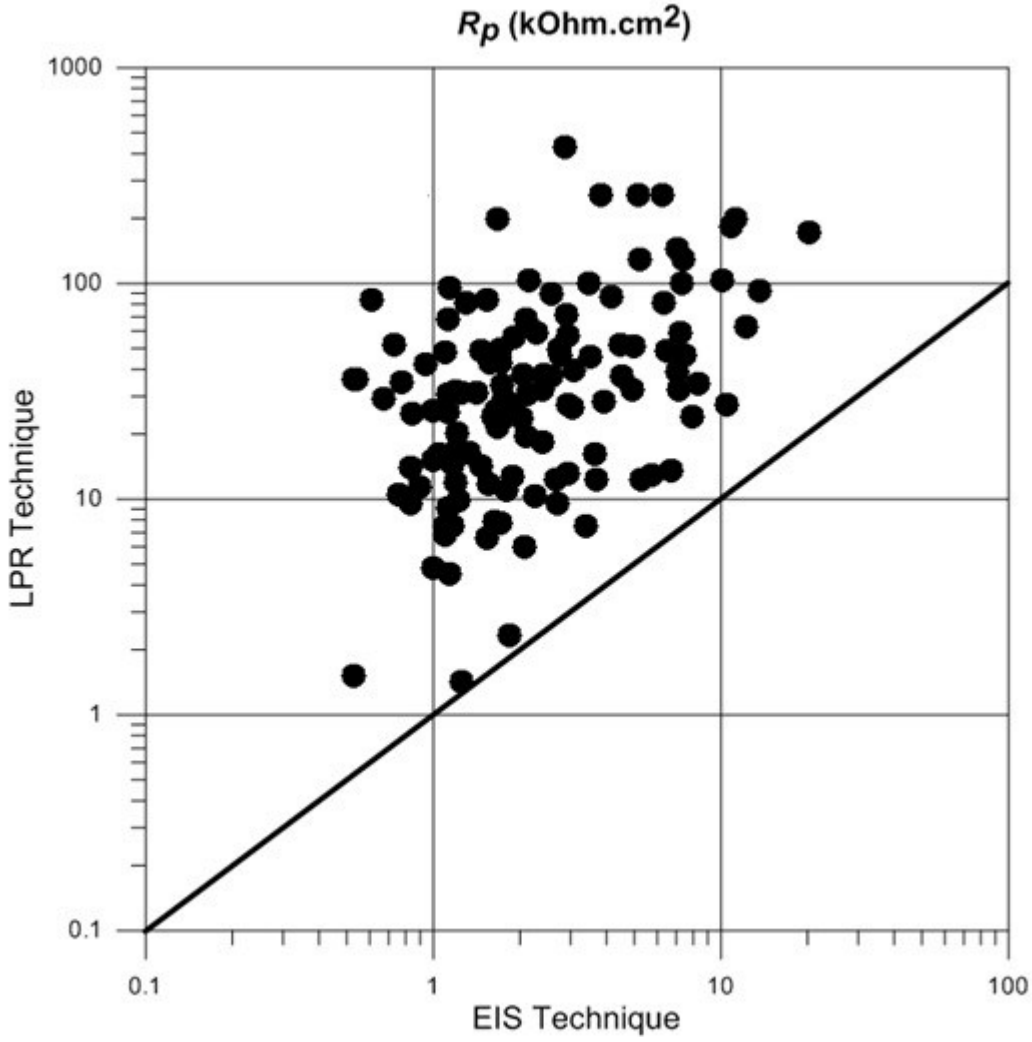

Figure 5-1: Correlation between polarization resistance values measured by LPR and EIS techniques.

The polarization resistance obtained by the LPR and EIS techniques as a function of the concrete electrical resistivity is shown in Figure 5.2. The data pairs presented in Figure 5.1 are color coded according to the corresponding concrete electrical resistivity. To determine the effect of concrete resistivity on the correlation between LPR and EIS values,

the data are divided into three intervals: (i) locations in which the concrete resistivity is smaller than 10 kOhm.cm (red); (ii) locations in which the concrete resistivity ranges between 10 kOhm.cm and 20 kOhm.cm (blue); and, (iii) locations in which the concrete resistivity is larger than 20 kOhm.cm (green). Note that the data illustrated in Figure 5.2 includes all the measurements collected at the three concrete saturation conditions.

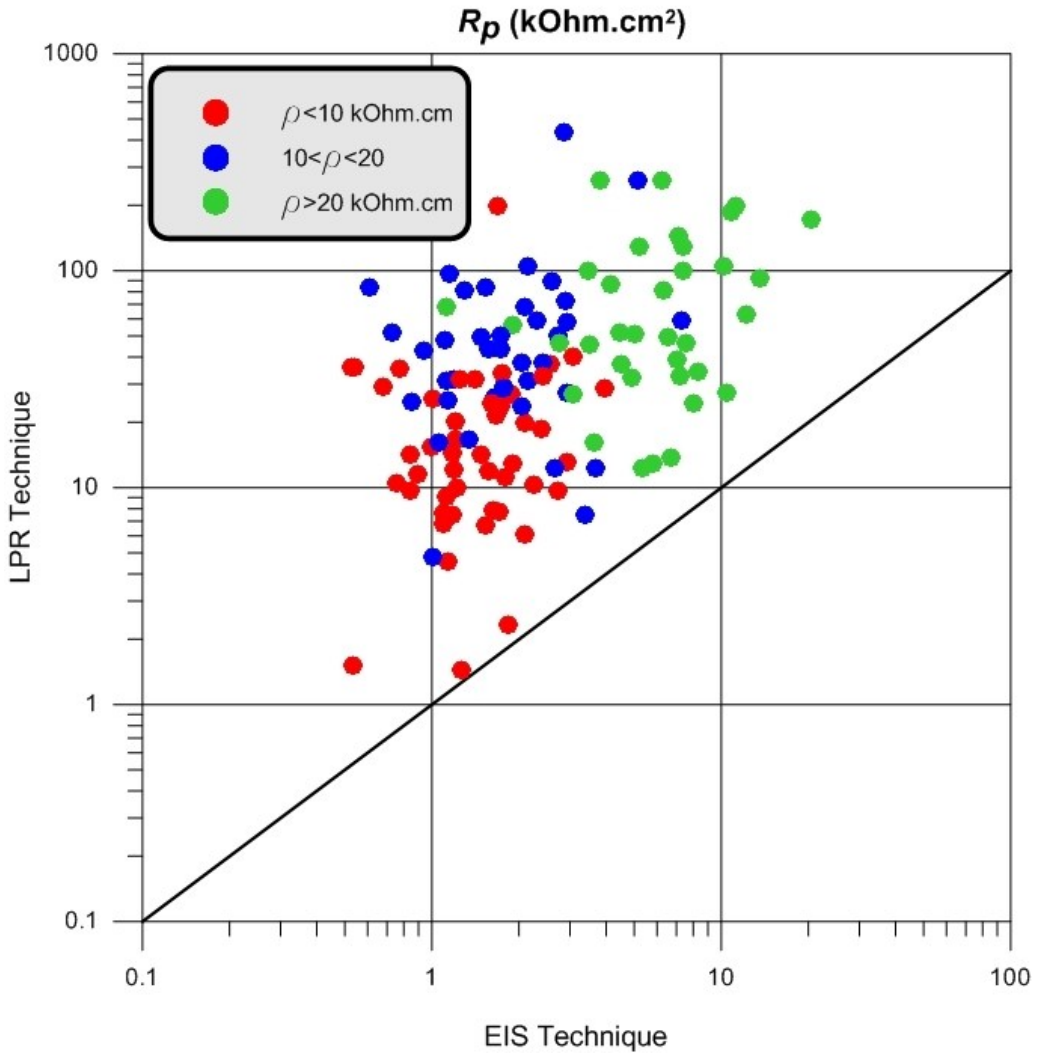

Figure 5-2: Polarization resistance obtained by the LPR technique versus the EIS technique as a function of the concrete electrical resistivity.

Generally, when the concrete resistivity is high, the polarization resistance obtained from both methods is also high, and when the resistivity is low the polarization resistance is low as well. The same observation has been reported by Feliu et al. (1996). Although the corrosion current density can only be obtained from polarization resistance measurements, low/high values of polarization resistance and concrete resistivity are respectively associated to high/low corrosion rates. In the locations where the concrete electrical resistivity is high (i.e., ρ > 20 kOhm.cm), the polarization resistance results from LPR and EIS techniques correlate better (Figure 5.3), while in the locations where the electrical resistivity is lower, the results are more scattered (higher mean μ and standard deviation).

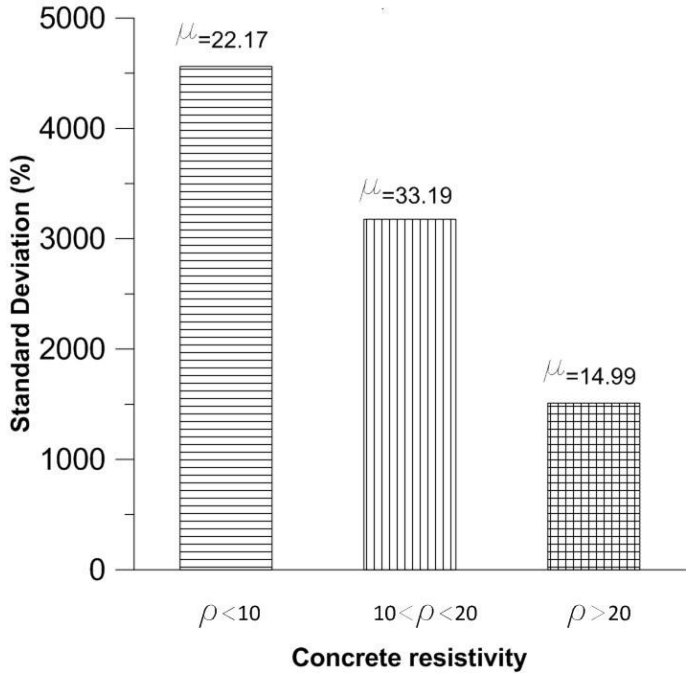

Figure 5-3: Mean and standard deviation of the ratio of LPR to EIS polarization resistances as a function of the concrete electrical resistivity.

The polarization resistance values obtained by the LPR and EIS techniques as a function of the concrete water-to-cement ratio are shown in Figure 5.4. The data

corresponding to different water-to-cement ratios are colour coded as follows: green for slab 1 (w/c = 0.35), blue for slab 2 (w/c = 0.4), and red for slab 3 (w/c = 0.5). The data illustrated in Figure 5.4 include all measurements taken at the three concrete saturation levels.

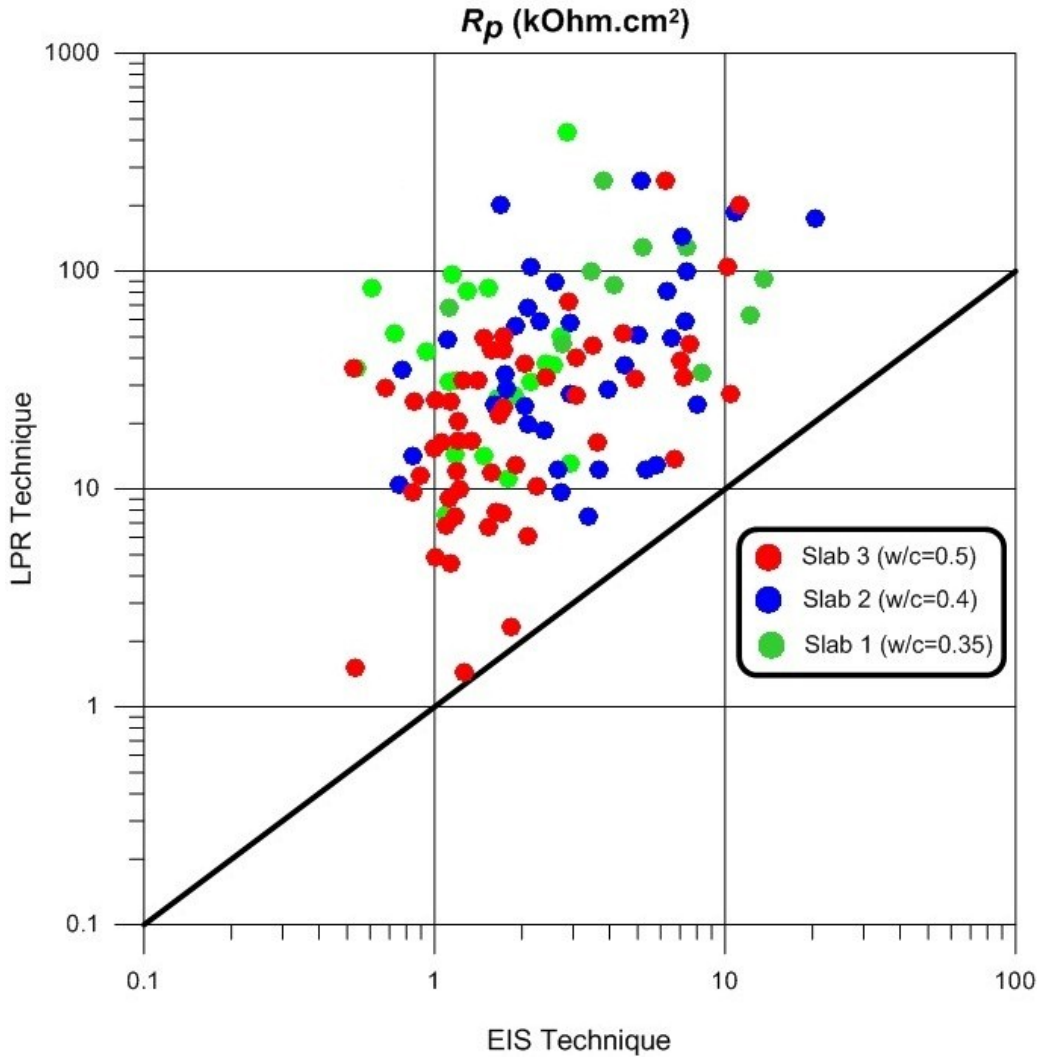

Figure 5-4: Polarization resistance obtained by the LPR technique versus the EIS technique as a function of the concrete water-to-cement ratio.

The concrete water-to-cement ratio does not provide any clear information on the correlation between the polarization resistances measured by these two techniques. In

general, corrosion activity is indirectly related to concrete water-to-cement ratio as this parameter is indicative of the associated permeability properties. Figure 5.4 indicates that a larger proportion of measurements associated to low polarization resistance values correspond to slab 3 with w/c = 0.5 and thus lower concrete quality. This observation is in agreement with the results presented by Raupach (1996). Furthermore, values associated with higher w/c display less scatter in the data than those associated with a lower w/c (Figure 5.5).

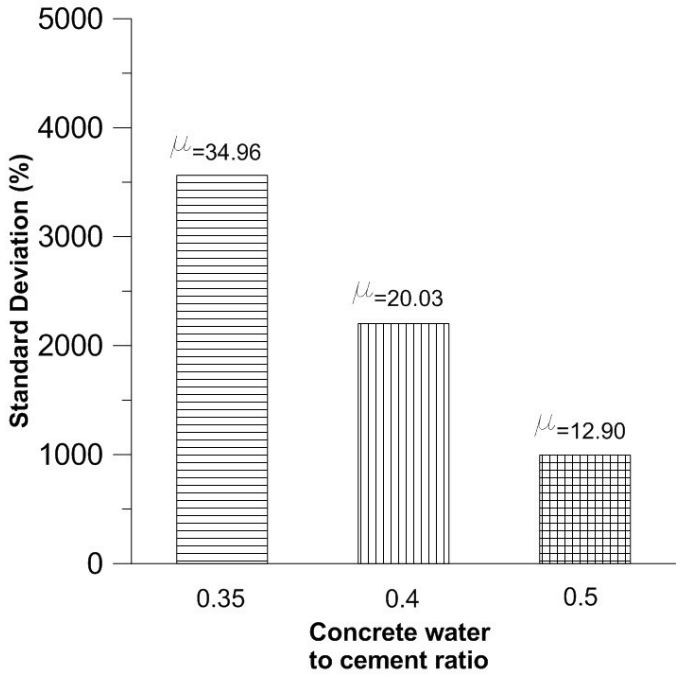

Figure 5-5: Mean and standard deviation of the ratio of LPR to EIS polarization resistances as a function of the concrete water-to-cement ratio.

The polarization resistance values obtained by the LPR and EIS techniques as a function of the concrete saturation condition are shown in Figure 5.6. The results are colour coded to differentiate the concrete saturation level; green, blue and red symbols represent data collected in dry, partially saturated, and saturated conditions, respectively.

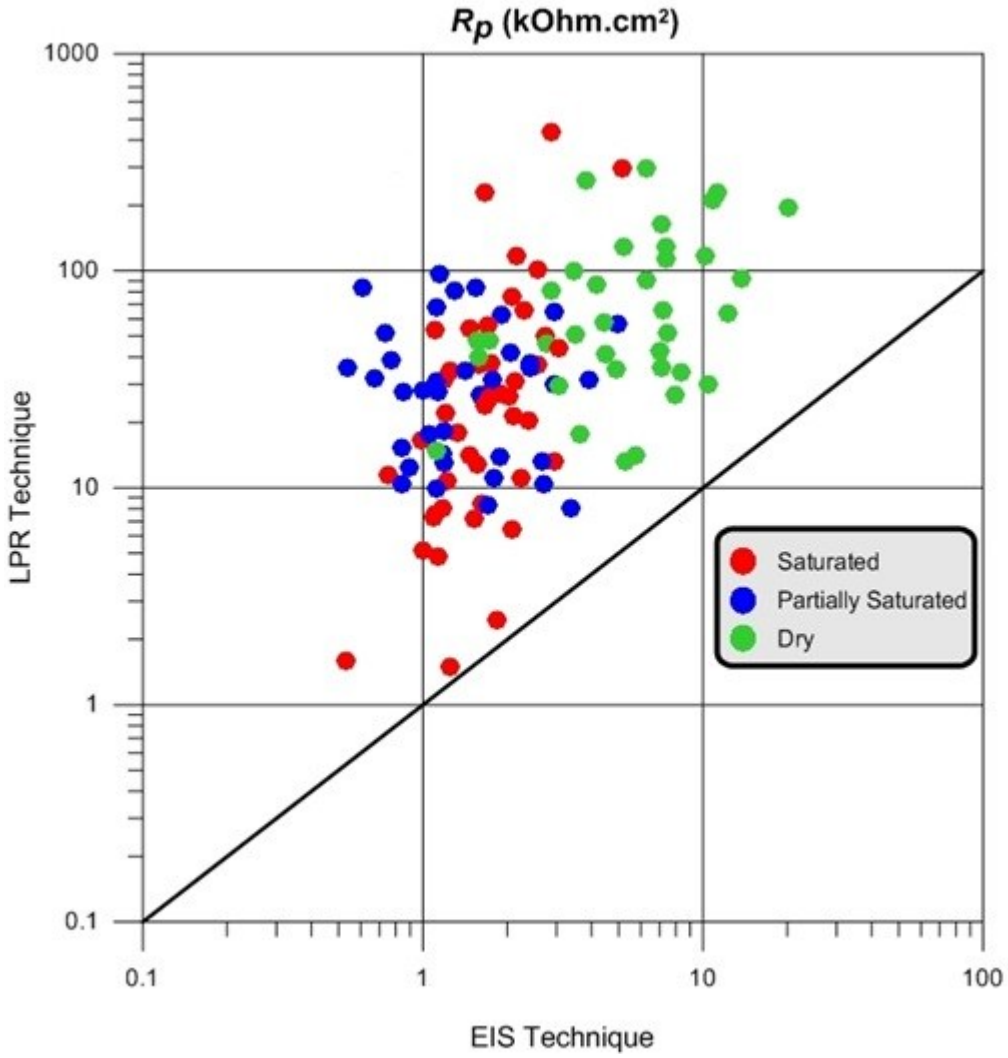

Figure 5-6: Polarization resistance obtained by the LPR technique versus the EIS technique as a function of the concrete saturation condition.

It is observed from Figure 5.6 that lower values of polarization resistance are associated to higher moisture contents. Furthermore, the correlation between the polarization resistance measurements changes for partially-saturated and saturated concrete (blue and red symbols, respectively). The concrete saturation level affects the measurement of the polarization resistance which alter correlation between these techniques.

In saturated and partially-saturated conditions, the data collected by the LPR technique ranges from almost 1 to 100 kOhm.cm^2, whereas the range of data obtained by the EIS technique varies from 0.7 to 5 kOhm.cm^2.

Figure 5.7 indicates that the correlation between these two techniques is almost similar in partially-saturated and saturated conditions. However, there is better correlation of the data for dry conditions (lower mean and standard deviation values).

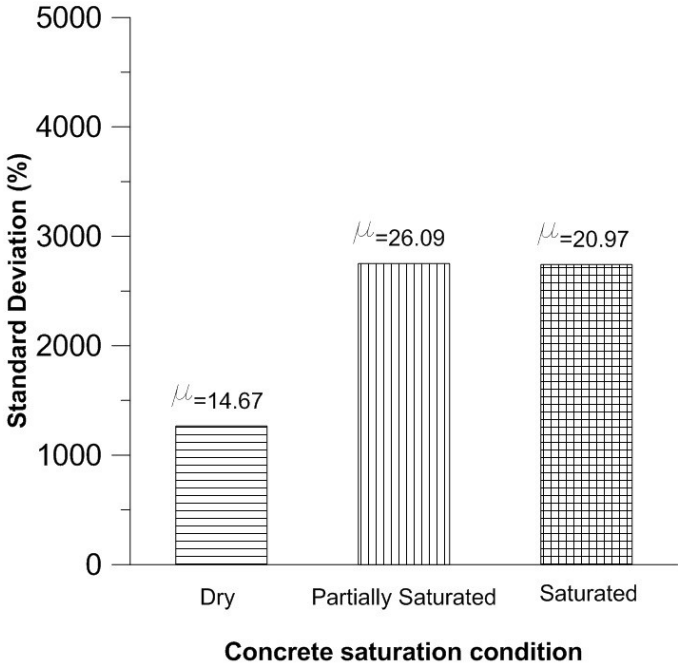

Figure 5-7: Mean and standard deviation of the ratio of LPR to EIS polarization resistances as a function of the concrete saturation condition.

The polarization resistance values obtained by the LPR and EIS techniques as a function of the applied bending moment along each slab are shown in Figure 5.8. To study the effect of applied bending moment (Figure 3.6) on the correlation between the polarization resistance measurements from the LPR and EIS techniques, the results are categorized into four structural zones based on the applied bending moment:

- Zone 1: portion of the slab sustaining a positive moment that is less than the cracking moment ($+M < M_{cr}$);
- Zone 2: portion of the slab sustaining a positive moment that is higher than the cracking moment ($+M > M_{cr}$);
- Zone 3: portion of the slab sustaining a negative moment that is higher than the cracking moment ($-M > M_{cr}$);
- Zone 4: portion of the slab that does not sustain load ($M = 0$);

The calculated cracking moments are 19.5 kN·m, 18.0 kN·m, and 17.4 kN·m for slab 1 (w/c = 0.35), slab 2 (w/c = 0.4), and slab 3 (w/c = 0.5), respectively (Deif 2010). Since these regions have different surface area, the number of measurement points located in each zone is different.

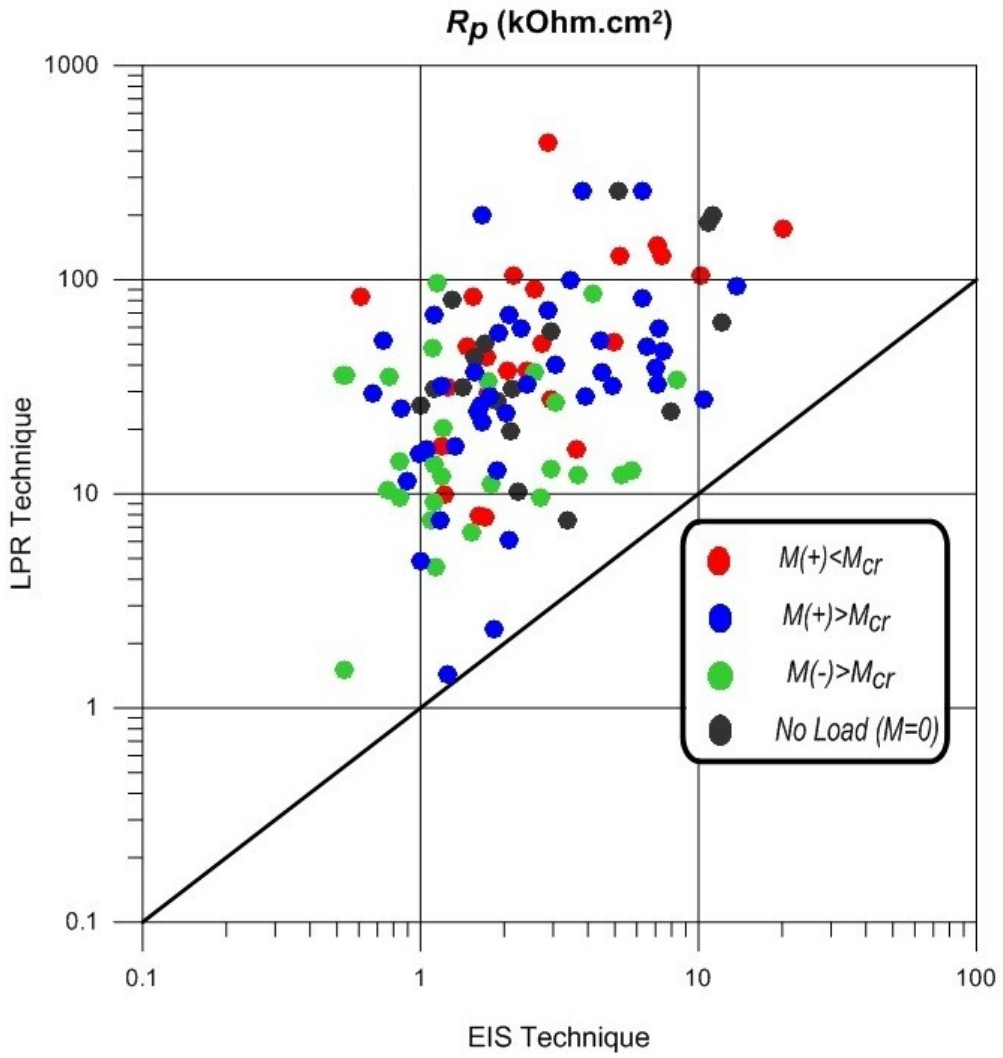

Figure 5-8: Polarization resistance obtained by the LPR technique versus the EIS technique as a function of applied bending moment.

In general, the applied bending moment does not provide any information on the correlation between the measurements from both techniques. However, a large proportion of data points collected on zone 3 (green data points), which corresponds to the region sustaining a negative moment higher than the cracking moment ($-M > M_{cr}$), shows lower polarization resistance than other regions, indicating that the corrosion activity in this zone is higher than the other zones. This could be due to the presence of flexural cracks on the

top surface of the concrete slab. These cracks facilitate the ingress of chloride, water and oxygen into the concrete. It is interesting to note that the region with higher scatter in the measurements is that associated with positive bending moment below the cracking value (Figure 5.9).

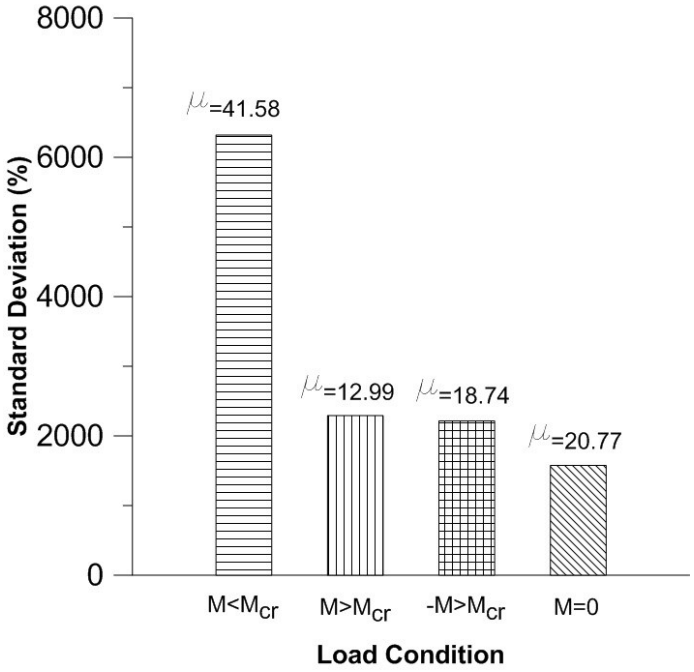

Figure 5-9: Mean and standard deviation of the ratio of LPR to EIS polarization resistances as a function of applied bending moment.

Summarizing, the range of the polarization resistance values measured by the LPR technique is between 1 to 500 kOhm.cm^2, whereas the range of the values measured by the EIS technique is between 0.6 to 20 kOhm.cm^2. Regardless of the concrete electrical resistivity, the concrete water-to-cement ratio, the concrete saturation condition, and the applied bending moment, the polarization resistance measured by the LPR technique is quite higher than the one measured by the EIS technique. Calculated corrosion rates from

these values are therefore underestimated in comparison with those obtained by the EIS technique.

5.2.2 GPR technique vs. EIS technique

In this section, the polarization resistance values measured by the GPR and the EIS techniques are compared to each other. The results are analyzed taking into the account the same parameters used in the previous section: the concrete electrical resistivity, the concrete water-to-cement ratio, the concrete saturation condition, and the applied bending moment.

Similar to the LPR device, the GPR device used in this study does not give the polarization resistance directly. The polarization resistance is calculated from Eq. 5.1 by entering the corrosion rate i_{corr} provided by the GPR device. Here the surface area of the rebar under the probe is $A = 24$ cm^2; note that the probe of the GPR device is smaller than that of the LPR device.

The polarization resistance values obtained by the GPR and the EIS techniques are shown in Figure 5.10. The polarization resistance measured by the GPR technique is in general lower than that obtained from the EIS technique. The GPR measurements R_p^{GPR} are correlated to those from EIS R_p^{EIS} through a linear regression analysis of the data as shown in Figure 5.10, i.e.,

$$R_p^{GPR} = 0.387 R_p^{EIS} \qquad \textit{Eq. 5.3}$$

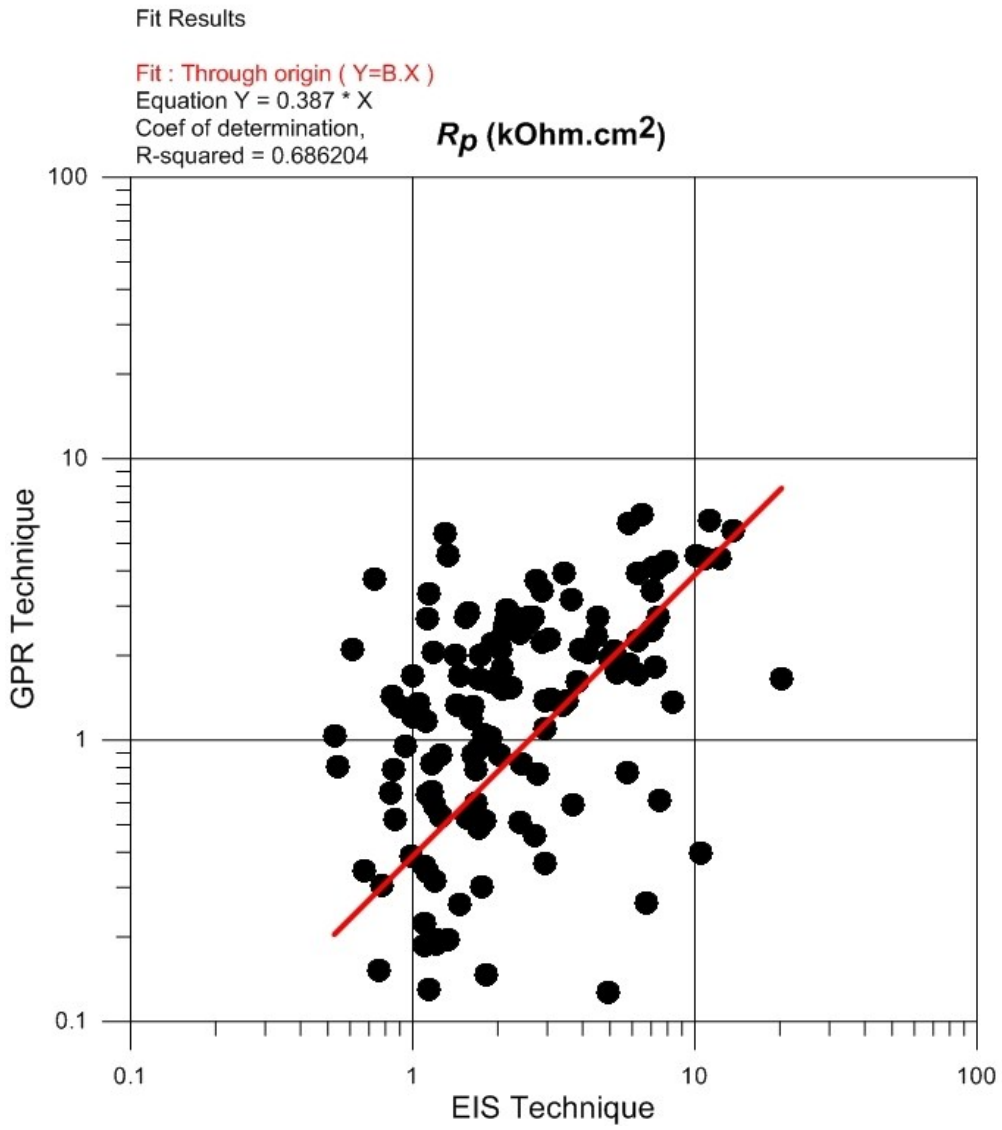

Figure 5-10: Polarization resistance obtained by the GPR technique versus the EIS technique.

The polarization resistance values obtained by the GPR and the EIS techniques as a function of the concrete electrical resistivity are shown in Figure 5.11. The values are colour coded according to the concrete electrical resistivity measured at the same locations, and they include all the measurements collected in various concrete saturation conditions. Figure 5.11 shows that as the concrete resistivity increases (from red to blue to green

points), so does the polarization resistance obtained from both techniques. In the locations where the concrete electrical resistivity is between 10 to 20 kOhm·cm (blue symbols), the results seems to be more scattered in comparison with the locations where the electrical resistivity is within the lower or higher bounds (Figure 5.12).

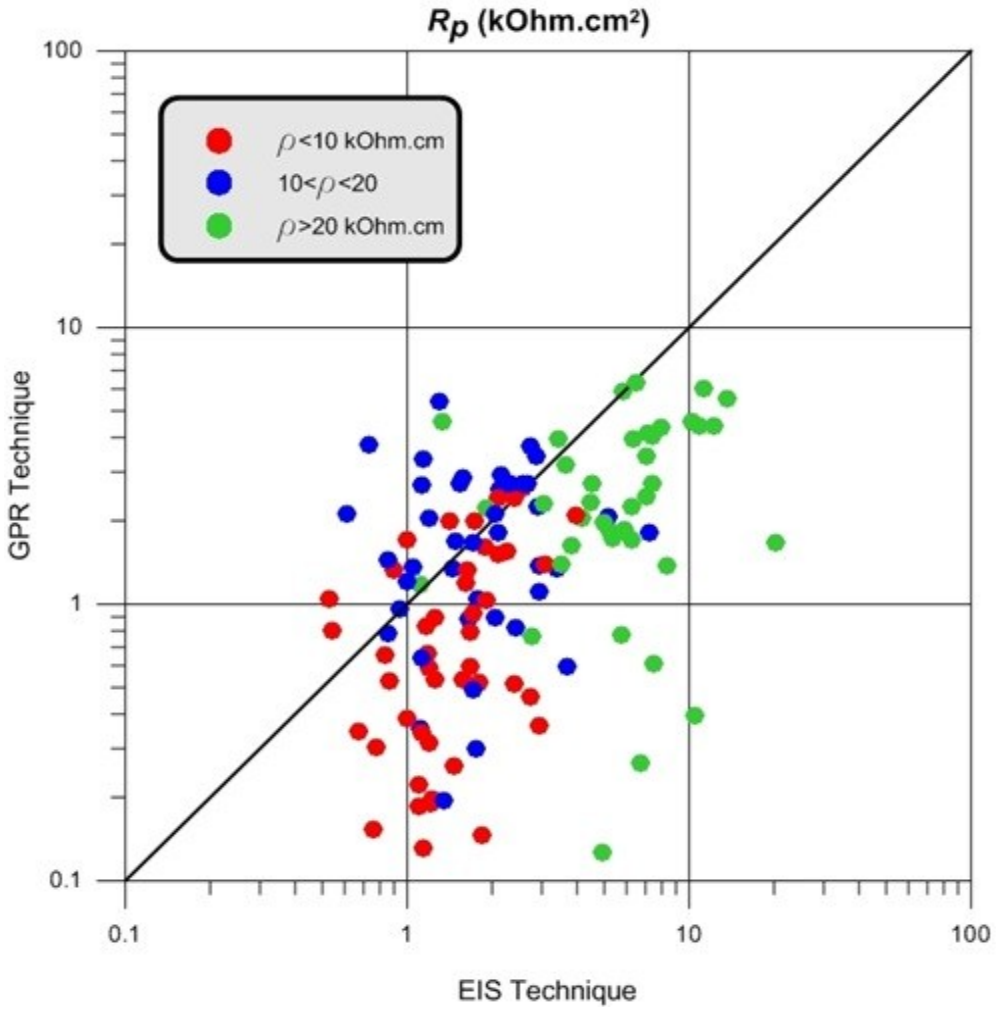

Figure 5-11: Polarization resistance obtained by the GPR technique versus the EIS technique as a function of the concrete electrical resistivity.

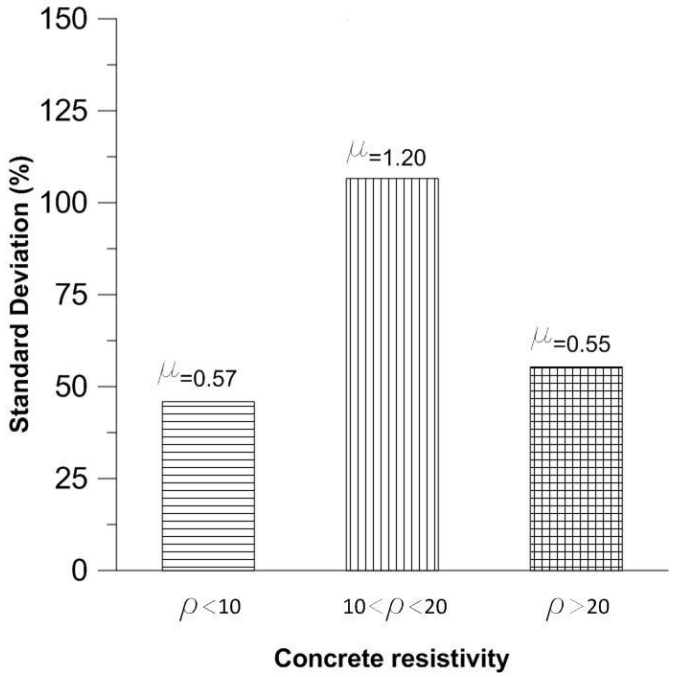

Figure 5-12: Mean and standard deviation of the ratio of GPR to EIS polarization resistances as a function of the concrete electrical resistivity.

The polarization resistance values obtained by the GPR and EIS techniques as a function of the concrete water-to-cement ratio are shown in Figure 5.13. As observed previously, the concrete water-to-cement ratio does not seem to provide any information on the correlation between the GPR and EIS techniques. Likewise, the slab with lower water-to-cement ratio (w/c = 0.35) displays higher scatter in the data (Figure 5.14).

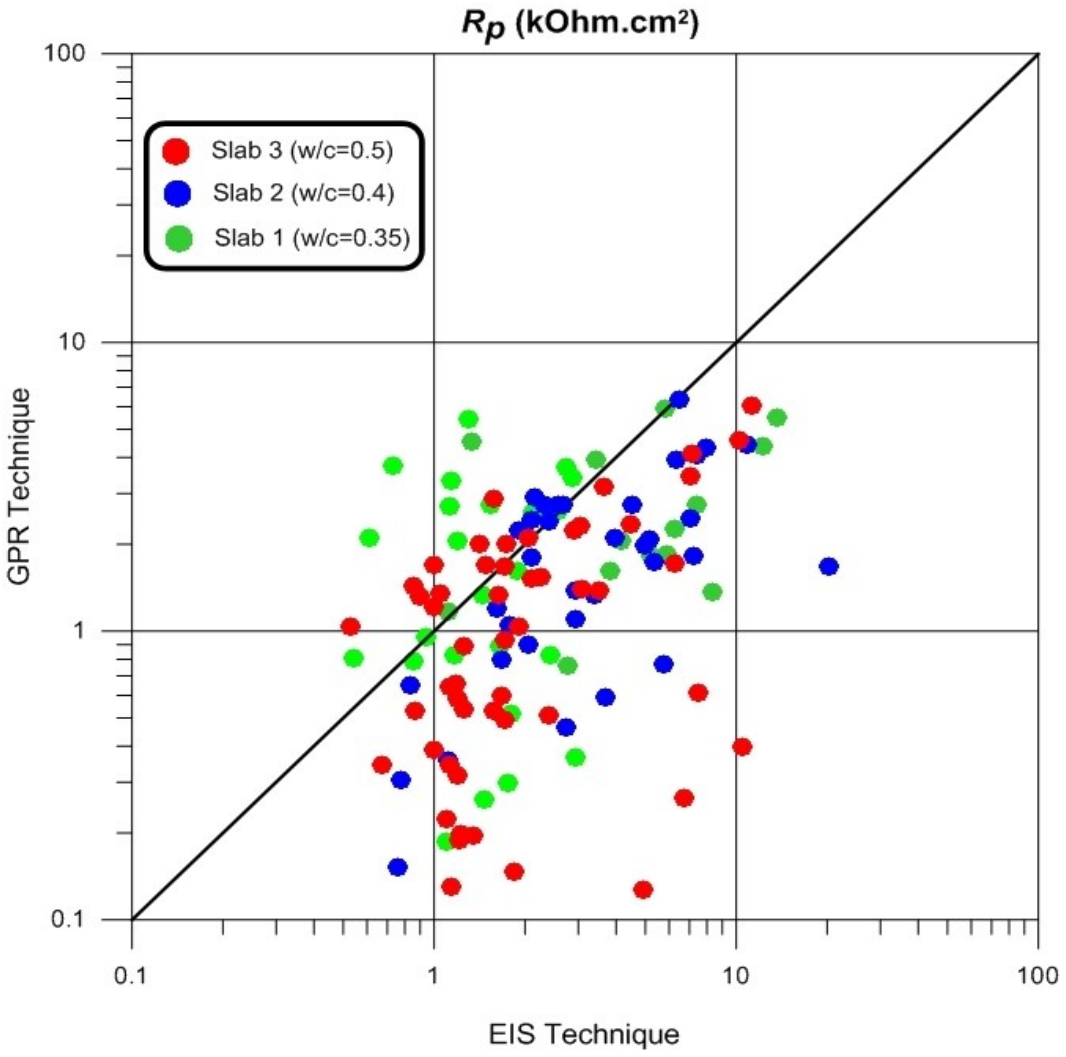

Figure 5-13: Polarization resistance obtained by the GPR technique versus the EIS technique as a function of the concrete water-to-cement ratio.

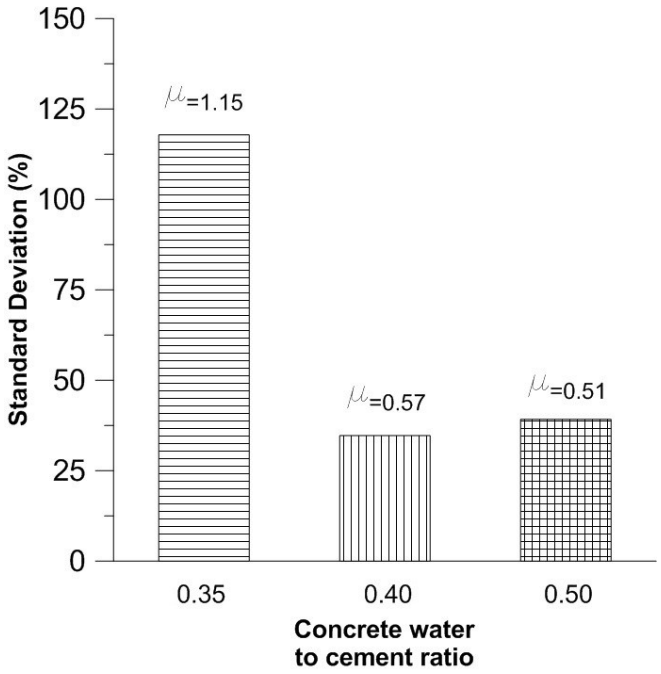

Figure 5-14: Mean and standard deviation of the ratio of GPR to EIS polarization resistances as a function of the concrete water-to-cement ratio.

The polarization resistance values obtained by the GPR and EIS techniques as a function of the concrete saturation condition are shown in Figure 5.15. In general, when the concrete is in dry condition (green symbols), both of the techniques measure higher polarization resistance values. On the other hand, lower polarization resistance values are recorded when the concrete moisture level increases (blue and red symbols).

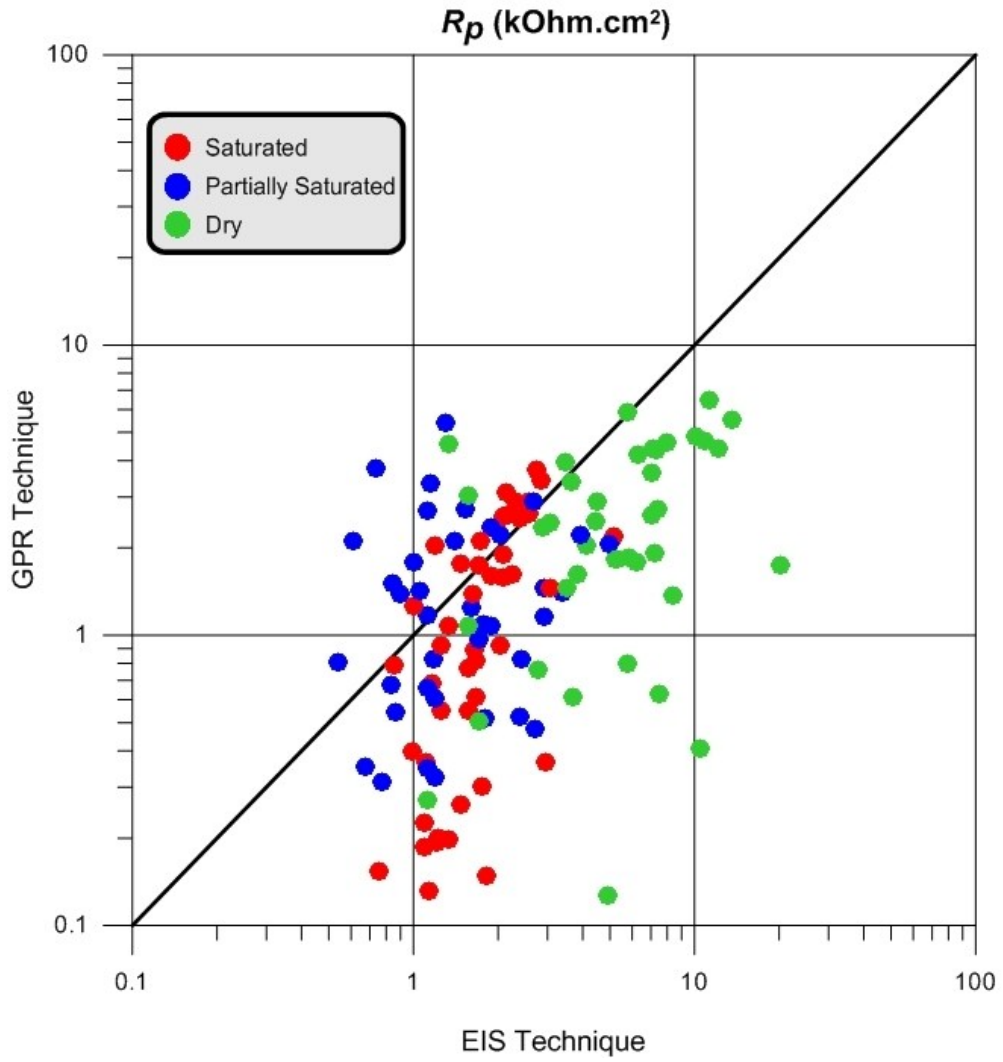

Figure 5-15: Polarization resistance obtained by the GPR technique versus the EIS technique as a function of the concrete saturation condition.

From statistical analysis of the ratio of the polarization resistance values from both techniques (Figure 5.16), the GPR and EIS techniques are better correlated when the concrete moisture content is either low (dry condition) or high. Locations where the concrete is in partially saturated condition display higher scatter in the data.

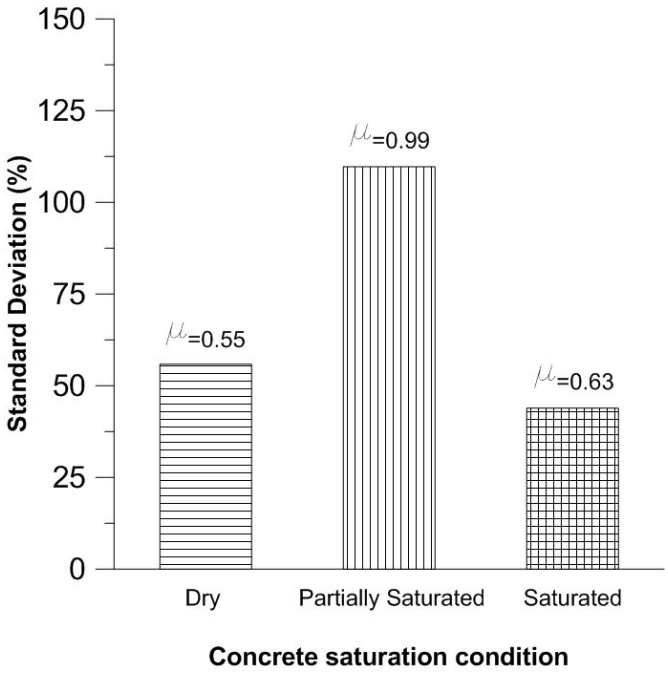

Figure 5-16: Mean and standard deviation of the ratio of GPR to EIS polarization resistances as a function of the concrete saturation condition.

The polarization resistance values obtained by the GPR and EIS techniques as a function of the applied bending moments are shown in Figure 5.17. From this figure, there is no clear indication of the effect of loading on the correlation between GPR and EIS measurements. Unlike the measurements obtained from the LPR technique (Figure 5.9), all the data associated to regions with different loading conditions have the same magnitude of variability (Figure 5.18).

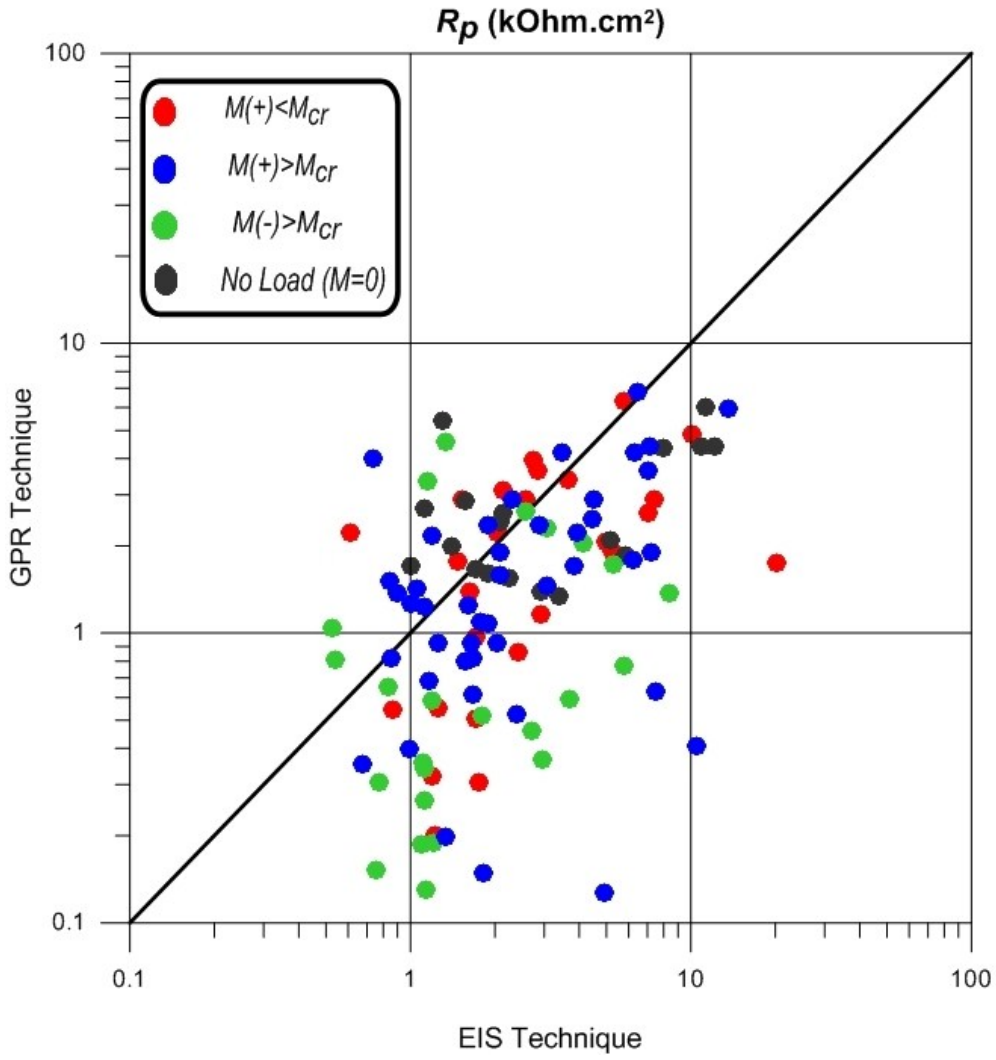

Figure 5-17: Polarization resistance obtained by the GPR technique versus the EIS technique as a function of the applied bending moment.

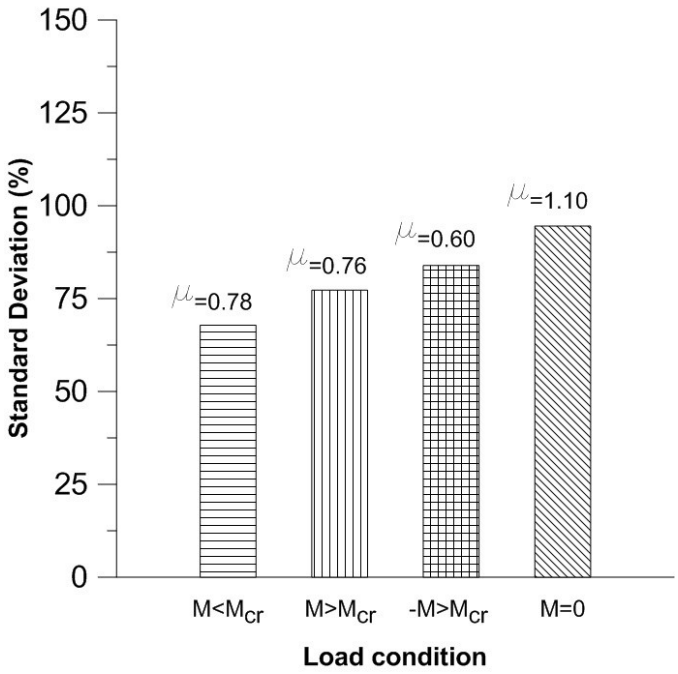

Figure 5-18: Mean and standard deviation of the ratio of GPR to EIS polarization resistances as a function of applied bending moment.

In conclusion, the GPR technique tends to underestimate the polarization resistance in comparison to that obtained from the EIS technique. This means the corrosion rate reported by this technique is higher than the EIS technique. The range of the values measured by the GPR and the EIS techniques are close to each other, and they are between 0.1 to 7 kOhm.cm^2 and 0.5 to 20 kOhm.cm^2, respectively.

5.3 Correlation between Polarization Resistance and Concrete Resistivity

As seen in the previous section, the polarization resistance measured by the GPR and the EIS techniques are better correlated. This section investigates the relationship between concrete electrical resistivity and polarization resistance as measured by the GPR

and EIS techniques. The relation between concrete resistivity and polarization resistance is analyzed as a function of moisture content and loading condition.

5.3.1 Concrete saturation level

The polarization resistance measurements by the GPR technique versus the concrete electrical resistivity measurements by Wenner probe technique are plotted in Figure 5.19. The data points shown in the figures are color coded based on the concrete saturation condition. Figure 5.19 contains about 2,200 measurements carried out with the GPR device and concrete resistivity meter in various concrete saturation conditions.

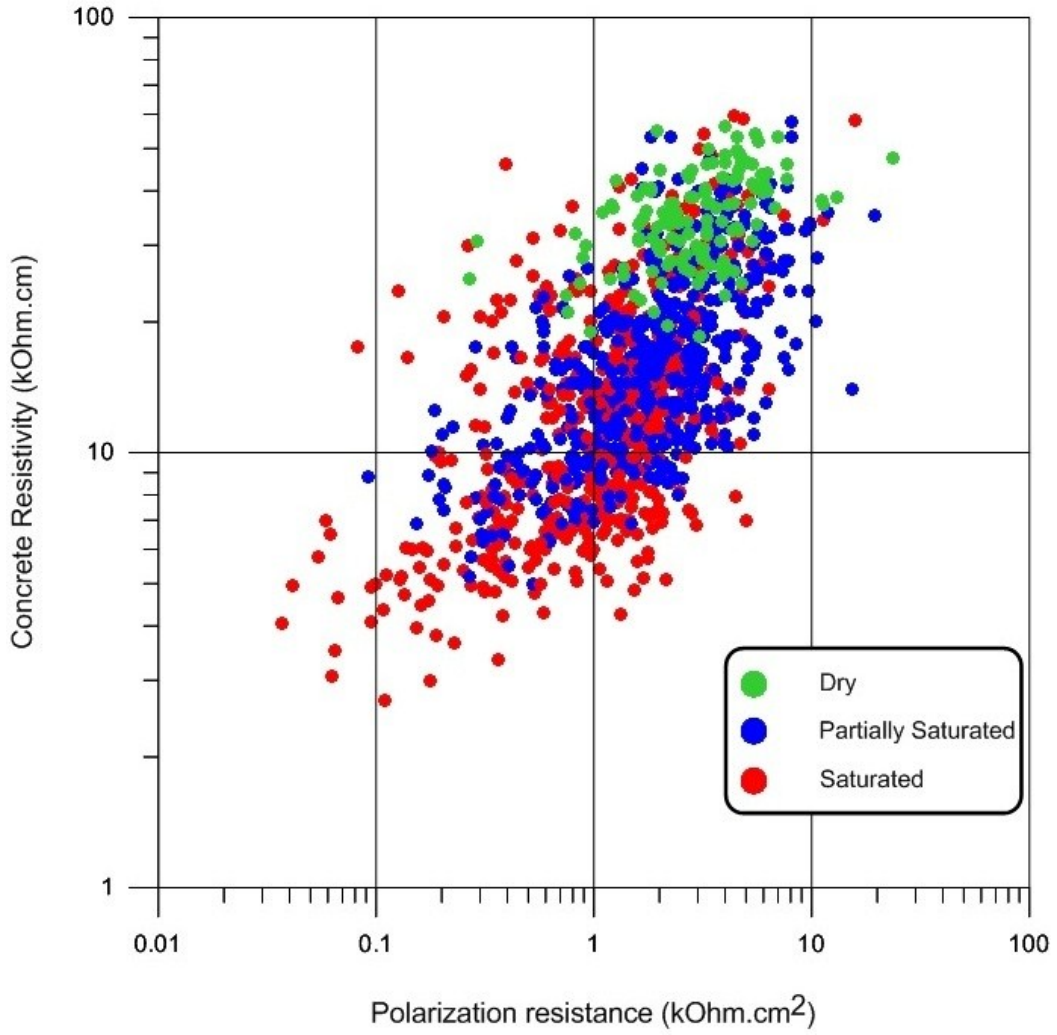

Figure 5-19: Polarization resistance by the GPR technique versus the concrete resistivity by the Wenner probe technique as a function of the concrete saturation condition.

As seen in Figure 5.19 there is a good correlation between the polarization resistance measured by the GPR technique and the concrete electrical resistivity measured by the Wenner probe technique. By shifting the concrete electrical resistivity, the polarization resistance shifts as well. The highest values obtained for the polarization resistance correspond to locations in which the concrete electrical resistivity is higher than 30 kOhm.cm. The results show that the concrete electrical resistivity is a good indicator

of corrosion activity. Thus, measuring concrete electrical resistivity does not only provide information about the resistivity of the concrete, but it can also be indicative of the corrosion kinetics of the embedded reinforcing steel. The lowest and highest values for the concrete electrical resistivity measured in this research were around 3 and 60 kOhm.cm, respectively.

The polarization resistance by the EIS technique versus the concrete electrical resistivity measured by the Wenner probe technique is plotted in Figure 5.20. The data is color coded based on the concrete saturation condition. Note that the number of measurements carried out with the EIS technique is lower than the GPR technique, mainly due to the time EIS measurements take. Furthermore, the moisture content of concrete is likely to change during the measurement timeframe.

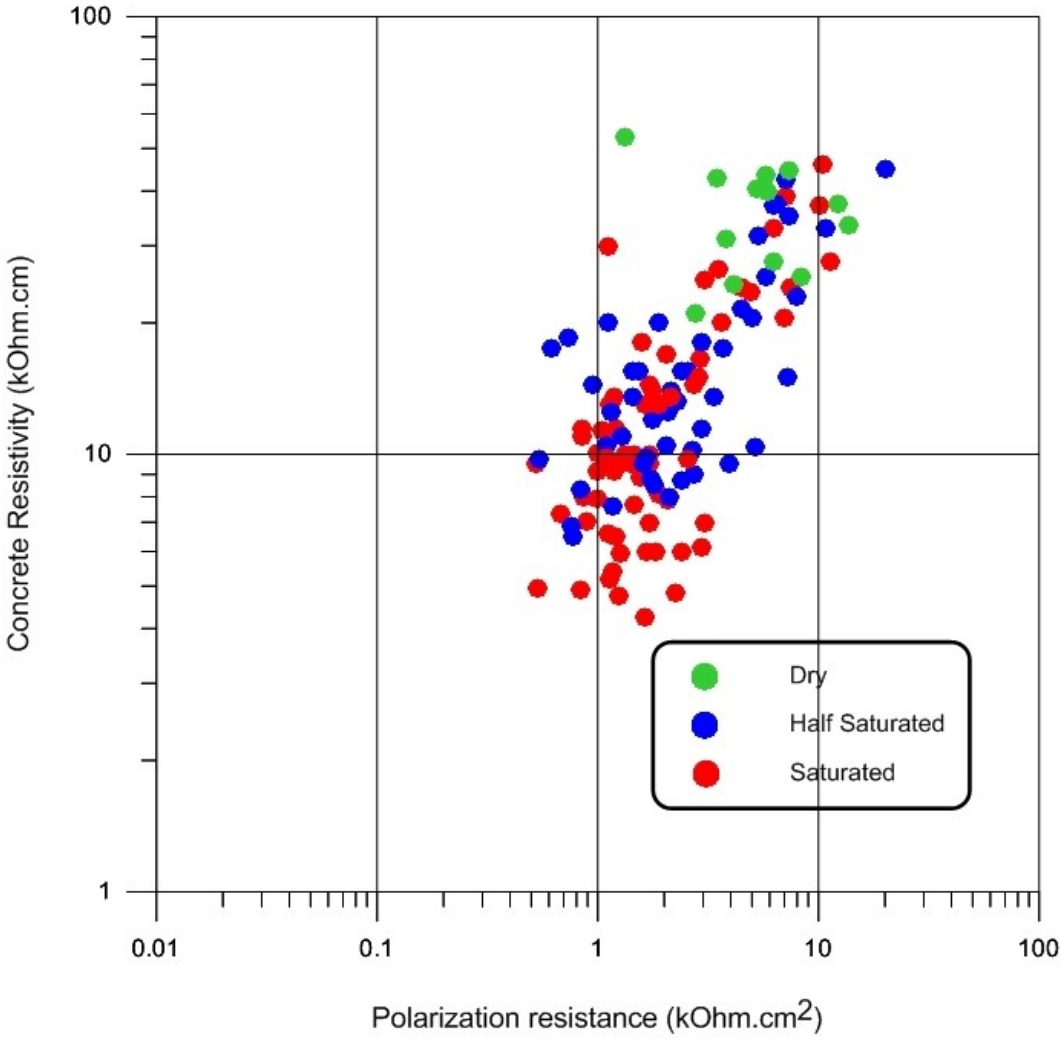

Figure 5-20: Polarization resistance by the EIS technique versus the concrete resistivity by the Wenner probe technique as a function of the concrete saturation condition.

Figure 5.20 also shows that there is a good correlation between the polarization resistance measured by the EIS technique and the concrete electrical resistivity measured by the Wenner probe. However, a trend difference is observed between Figures 5.19 and 5.20 for concrete electrical resistivities below 10 kOhm.cm. For resistivity values below 10 kOhm.cm, the polarization resistance as measured by the GPR technique continues to

decrease. Polarization resistance measurements taken by the EIS technique are not lower than 0.5 kOhm.cm^2 at the same locations. This difference in the data mainly corresponds to measurements in the saturated condition (red symbols).

To investigate this difference, the factors controlling the corrosion process in reinforced concrete should be taken into account. The concrete moisture content has a direct effect on the concrete electrical resistivity; by increasing the concrete moisture content the electrical resistivity decreases. The presence of water is also essential for the corrosion process; however, it might hinder the oxygen supply at cathodic regions at high saturation levels. Thus, the corrosion process can be controlled by lack of oxygen at cathodic areas or when the concrete electrical resistivity is too high due to dry conditions (ohmic control).

The corrosion of the reinforcing steel depends on the anodic curve (Alonso et al. 1988). When the slope of the anodic branch of the corrosion polarization curve drops, due to a reduction of the concrete electrical resistivity, the rate of corrosion increases, as illustrated in Figure 5.21(a). The rate of corrosion is controlled by the rate of current passing from the anode to the cathode, so when the concrete electrical resistivity decreases, the corrosion current flows with lower resistance through the porous structure of concrete. An increase in the concrete moisture content accelerates the corrosion process until oxygen needed for the cathodic reaction becomes limited (Figure 5.21(b)). The amount water and oxygen should be in an equilibrium condition to maximize the corrosion process.

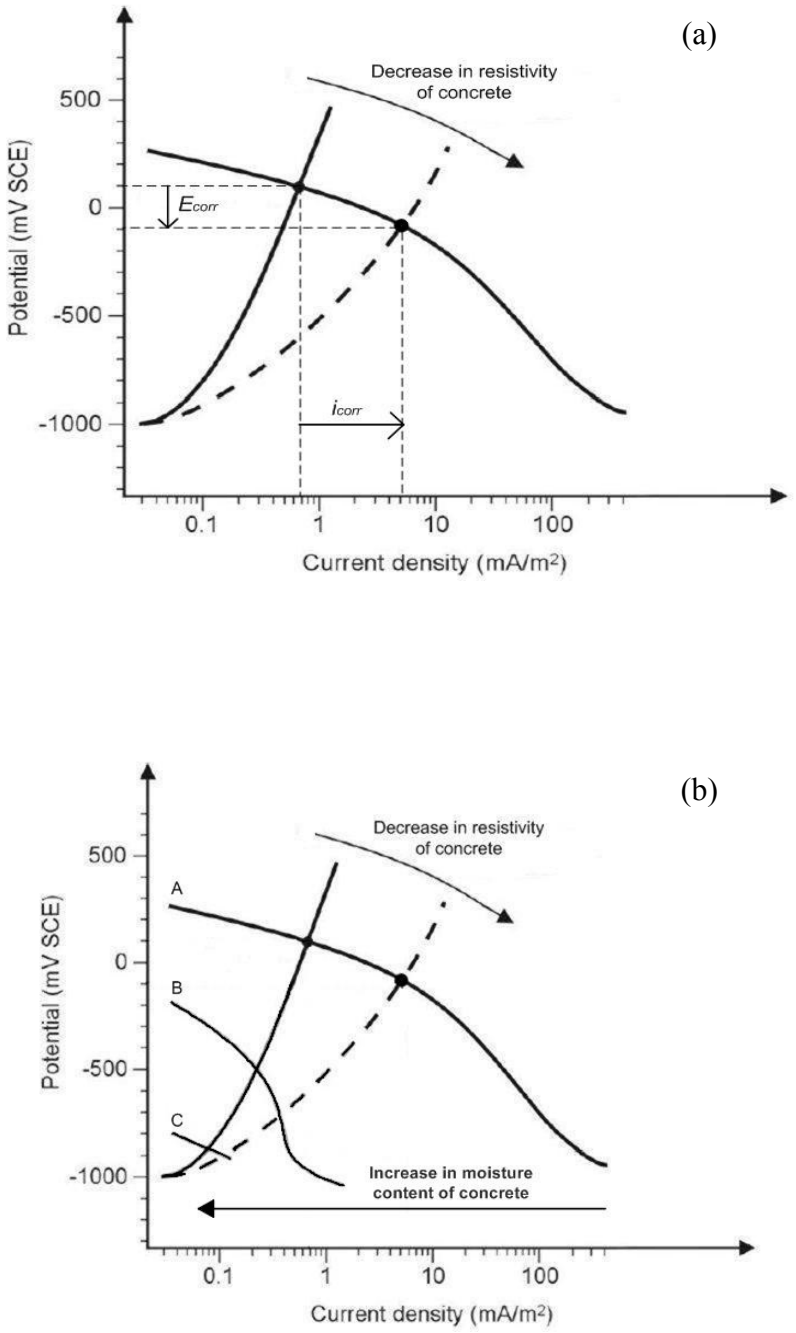

Figure 5-21: Relation between the concrete electrical resistivity and corrosion proces: (A) high oxygen availability (dry concrete); (B) medium oxuygen availability (wet concrete); (C) low oxygen availability (saturated concrete) (modified from Glass et al., 1991).

The GPR technique measures the polarization resistance by polarizing the reinforcement in the anodic direction, and the result is then compared to its free corrosion potential. In fact, after applying a galvanostatic current and compensating it for the ohmic drop, the GPR technique measures the slope of the anodic curve, which corresponds to the polarization resistance. In this experimental study the measurements are carried out in different concrete saturation conditions (dry, partially saturated and saturated). When the concrete electrical resistivity shifts to lower values due to an increase in the concrete moisture level, the slope of the anodic curve shifts to lower values as well. This slope reduction of the anodic curve induces the polarization resistance measured by the GPR technique to decrease, as observed in Figure 5.19.

The main difference between the results measured by the GPR and EIS techniques is observed in the saturated condition. When the concrete is saturated, the concrete electrical resistivity is very low, as observed in a large proportion of red data points in Figures 5.19 and 5.20. However, as mentioned earlier, the presence of oxygen at the rebar surface becomes limited in saturated conditions. Therefore, the corrosion process is controlled by oxygen diffusion through the concrete cover. As the supply of oxygen is decreased, the rate corrosion also decreases, and the polarization resistance should not decrease, even if the concrete electrical resistivity decreases. Measurements from the GPR technique show that by decreasing the concrete electrical resistivity, the corrosion process increases even in the saturated condition. However, measurements from EIS capture the phenomenon in which the rate of corrosion is controlled by oxygen supply at the cathodic regions.

The above analysis shows that the GPR technique can provide reliable information on the kinetics of corrosion when the concrete is not saturated. However, it does not capture the role of the cathodic polarization curve in saturated concrete as the EIS technique does.

5.3.2 Structural loading condition

This section investigates the effect of the structural loading condition by looking at the relation between the concrete electrical resistivity and the polarization resistance as measured by the GPR and EIS techniques. As described earlier, this is accomplished by dividing each concrete slab into four distinct structural zones based on the applied bending moment.

The results of the polarization resistance measurements by the GPR technique versus the concrete electrical resistivity are illustrated in Figure 5.22. This figure only includes data points on which EIS measurements were also taken to facilitate the comparison between both techniques. The data is color coded based on the applied bending moment.

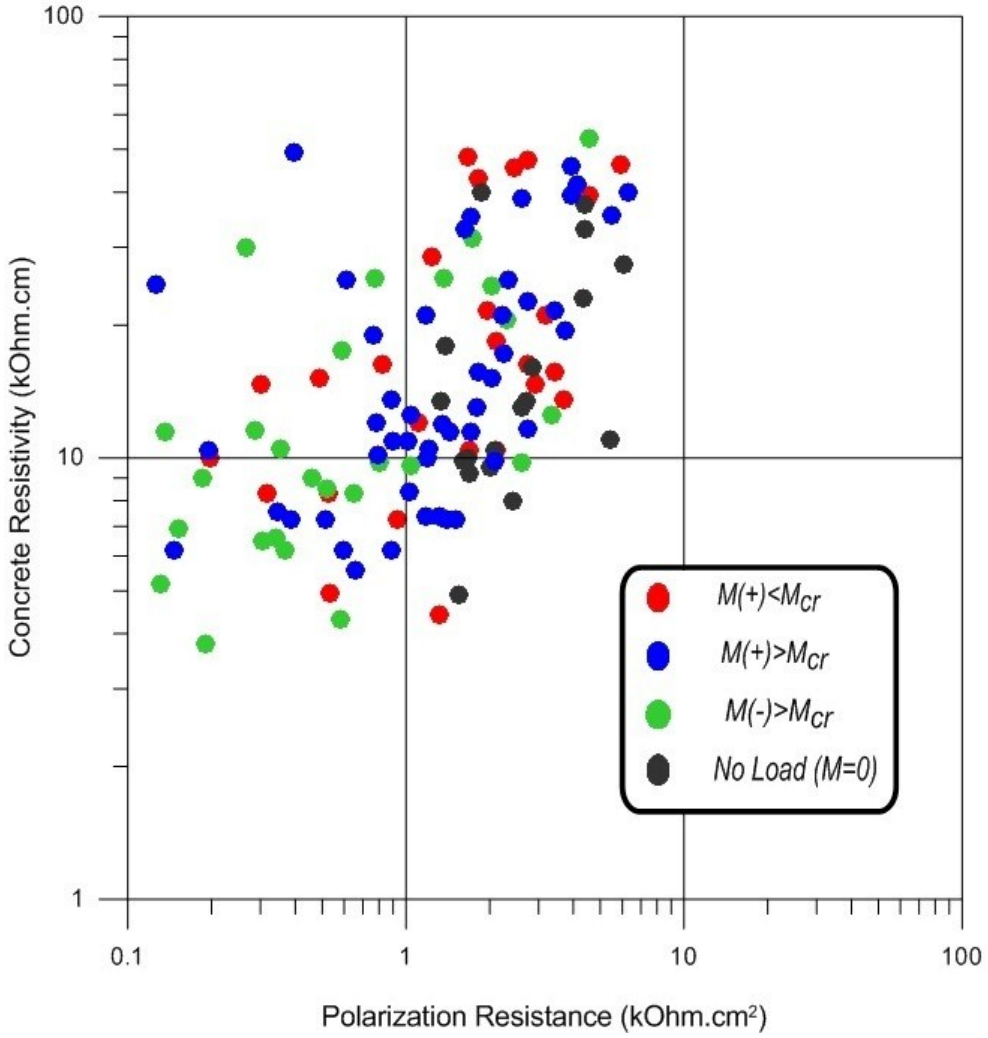

Figure 5-22: Polarization resistance by the GPR technique versus the concrete resistivity by the Wenner probe technique as a function of the applied bending moment.

Although there is no clear indication of the effect of loading on the relationship between concrete resistivity and polarization resistance, in general lower values of resistivity and polarization resistance are associated to regions where the applied bending moment creates tension at the top surface and it is higher than the cracking moment (green data points in Figure 5.22). This is very likely due to the presence of flexural cracks on this region.

The polarization resistance obtained by the EIS technique is plotted against the concrete resistivity as a function of the applied bending moment in Figure 5.23. The data points illustrated in Figure 5.23 correspond to the same locations as those displayed in Figure 5.22. The same observations as in Figure 5.22 are drawn. The results show that the structural loading condition does not have a significant effect on either concrete resistivity or polarization resistance measurements.

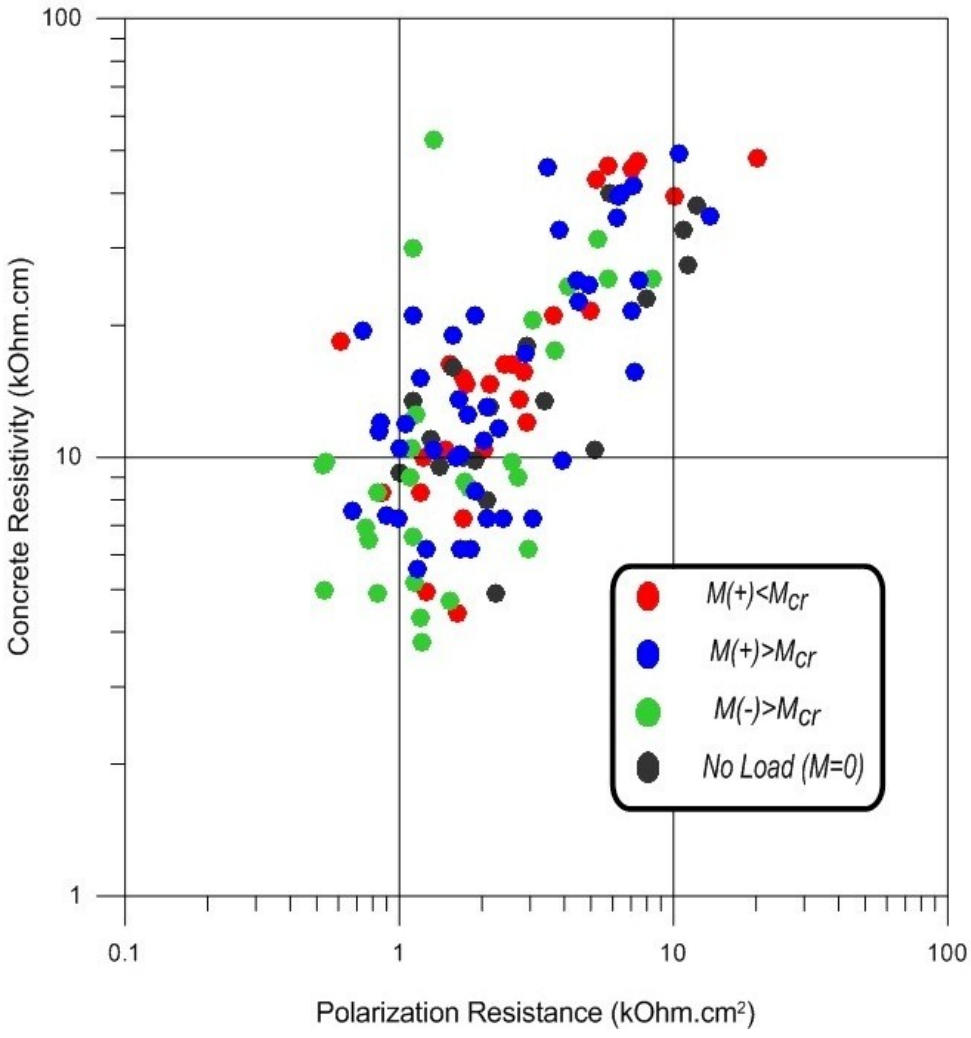

Figure 5-23: Polarization resistance by the EIS technique versus the concrete resistivity by the Wenner probe technique as a function of the applied bending moment.

5.4 Correlation between Polarization Resistance and Half-Cell Potentials

In this section the results of half-cell potential mapping according to the ASTM C876-09 standard criteria are compared to the measured polarization resistance to assess the capability of half-cell potentials to predict the probability of corrosion activity. Whereas half-cell potential measurements provide information about the probability of reinforcement corrosion, polarization resistance measurements provide information on the rate of corrosion activity. As seen before, the polarization resistances from EIS and GPR techniques are better correlated to each other. Therefore, the polarization resistance values measured by these techniques are used in this section.

In order to investigate the relationship between half-cell potential measurements and polarization resistance, the half-cell potential readings are divided into three groups based on the ASTM C876-09 standard criteria:

1. Locations where the potential is more positive than −0.20 V CSE.
2. Locations where the potential is between −0.20 V to −0.35 V CSE.
3. Locations where the potential is more negative than −0.35 V CSE.

As the reference electrode used in this research was the saturated calomel electrode (SCE), the ASTM criteria, which is based on the copper-copper sulfate electrode (CSE), is modified accordingly (see Table 5.1).

Table 5.1: Guidelines for interpretation of half-cell potential mapping as stated in ASTM C876 – 09.

Corrosion Potential (V)		**Probability of corrosion activity**
Vs. Cu/CuSO4	**Vs. SCE**	
$E_{corr} > -0.2$	$E_{corr} > - 0.126$	90% Probability of No Corrosion
$- 0.35 < E_{corr} < - 0.20$	$- 0.276 < E_{corr} < - 0.126$	Corrosion Activity is Uncertain
$E_{corr} < -0.35$	$E_{corr} < - 0.276$	90% Probability of Corrosion

The results of half-cell potential mapping versus the polarization resistance measured by the EIS and GPR techniques are illustrated in Figures 5.24 and 5.25 respectively. In these graphs the corrosion rate is illustrated on the right axis, and the results are color coded based on the concrete saturation condition. These figures also display the limits between the three different regions designated by ASTM C876 – 09 (dashed lines in Figures 5.26 and 5.27).

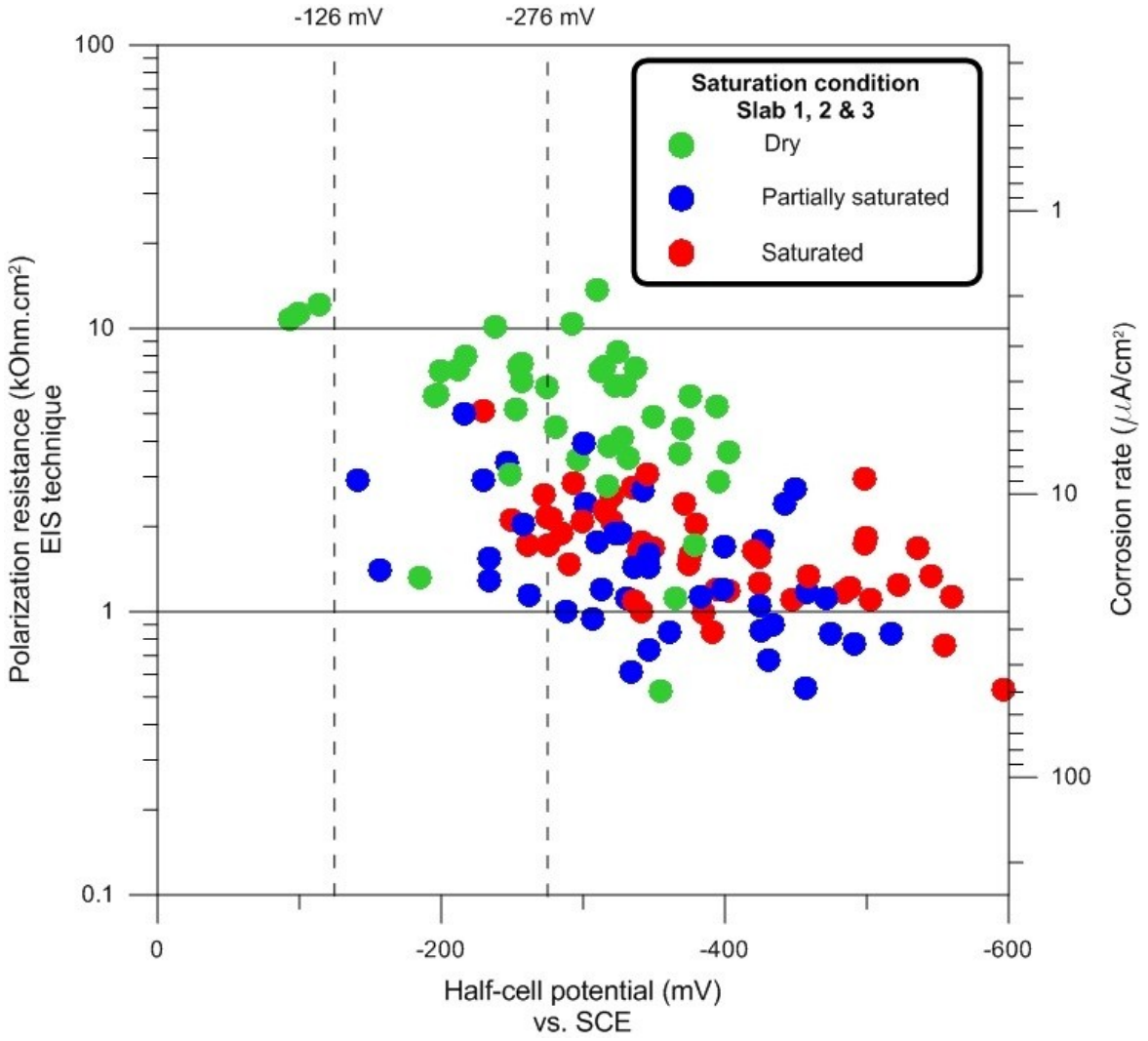

Figure 5-24: Half-cell potential versus polarization resistance measurements by the EIS technique.

As seen in Figure 5.24, half-cell potential readings for saturated and partially saturated conditions correspond to low polarization resistance and high corrosion rates. The ASTM standard criteria do not capture the high polarization resistance and low corrosion rates associated to dry conditions (green data points in Figure 5.24). Figure 5.24 only represents 120 measurements taken with the EIS technique. Since the GPR method allowed taking about 1,500 measurements, the capability of the half-cell potential mapping can be

evaluated better by comparing half-cell potential readings with GPR measurements. The results of half-cell potential mapping versus the GPR polarization resistance, modified according to Eq. 5.1, are illustrated in Figure 5.25.

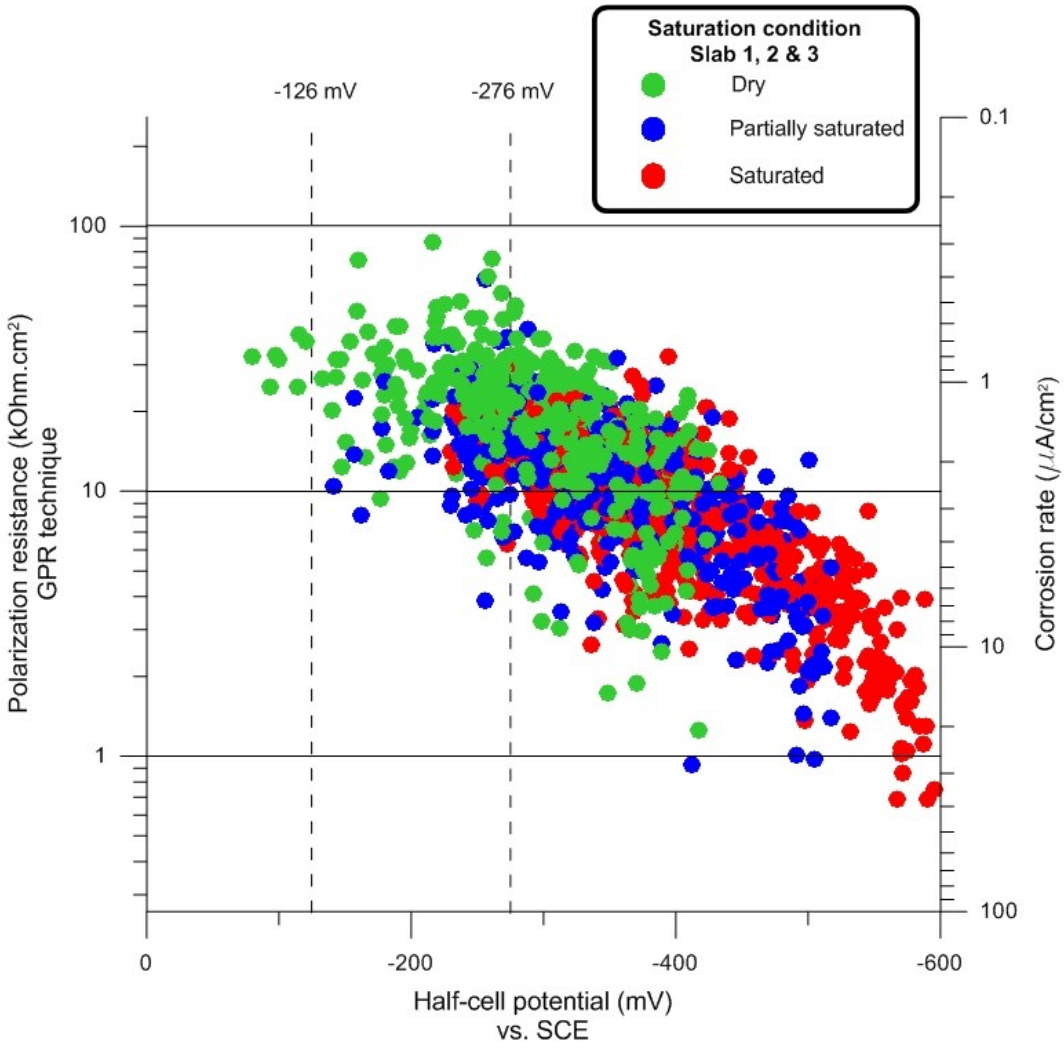

Figure 5-25: Half-cell potential versus the polarization resistance measurements by the GPR technique (modified values).

As observed in Figure 5.25, half–cell potentials shift to more negative values as the polarization resistance decreases. The effect of saturation level on both techniques is obvious; as the moisture content of the concrete increases, both techniques measure lower polarization resistances (higher corrosion rates). However, it is difficult to categorize the

measurements points according to the ASTM C876-09 criteria. A high proportion of measurements, especially those corresponding to dry conditions, falls within the region of uncertain corrosion activity according to the ASTM standard. Even locations where half-cell potential readings identified low probability of corrosion activity (green data symbols with half-cell potential more positive than -126 mV vs. SCE) still have a considerable corrosion rate based on the polarization resistance measurements.

As seen in both Figures 5.24 and 5.25, the ASTM C876-09 criteria cannot evaluate the state of corrosion activity in reinforced concrete structures just by mapping half-cell potentials. These specific half-cell potential values (-126 mV and -276 mV vs. SCE) do not differentiate the state of corrosion activity. In particular, the standard criteria cannot predict the probability of corrosion activity properly when the half-cell potential is more positive than -276 mV vs. SCE. Therefore, it is critical to evaluate corrosion activity with other methods as well.

5.5 Corrosion activity and concrete electrical resistivity

In previous sections, the effects of different parameters on polarization resistances (and corrosion activity) were evaluated by using various electrochemical techniques. From the results, it was observed that the effect of concrete moisture content on corrosion activity is more significant than the other parameters studied in this research. The concrete electrical resistivity is a good indicator of concrete moisture content and quality of concrete. Therefore, evaluating the corrosion activity by measuring the concrete resistivity could be a suitable practice for corrosion detection. In this section the capability of this

technique is investigated in detail. The concrete electrical resistivity measurements are plotted versus the polarization resistance measured by the EIS and GPR techniques in Figure 5.26 and 5.27, respectively. In these graphs, the corrosion rate is illustrated in the right axis, and the data is colour coded as a function of the moisture content. It is observed in both figures that the polarization resistance (and corrosion are) correlates well with the concrete resistivity. A limiting value of concrete resistivity of 15 kOhm.cm is a good indicator of significant change in concrete moisture content (transition from green to blue and red data points). Furthermore, the corrosion activity increases dramatically for concrete resistivities lower than this threshold. It can be concluded that the concrete resistivity, which is an easy non-destructive test to conduct, can provide suitable insight into the state of corrosion activity and be an additional indicator to complement currently used half-cell potential readings.

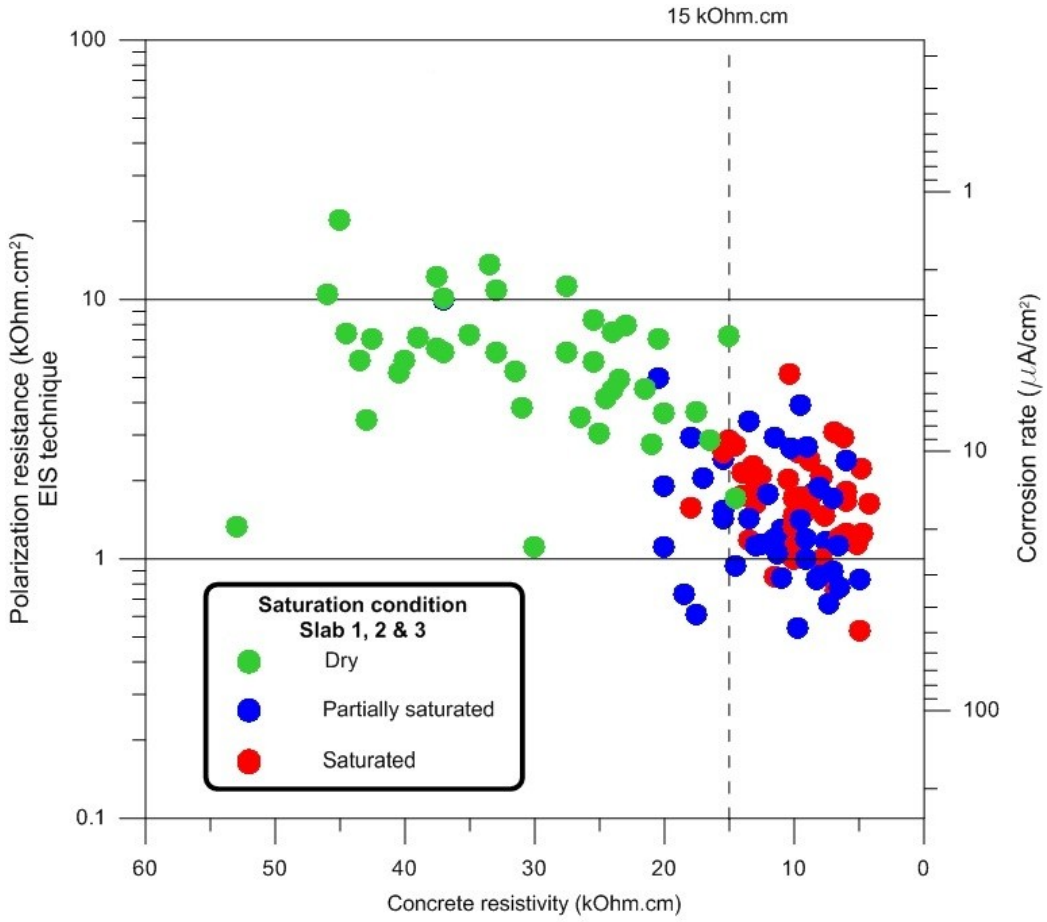

Figure 5-26: Concrete electrical resistivity versus the polarization resistance measurements by the EIS technique.

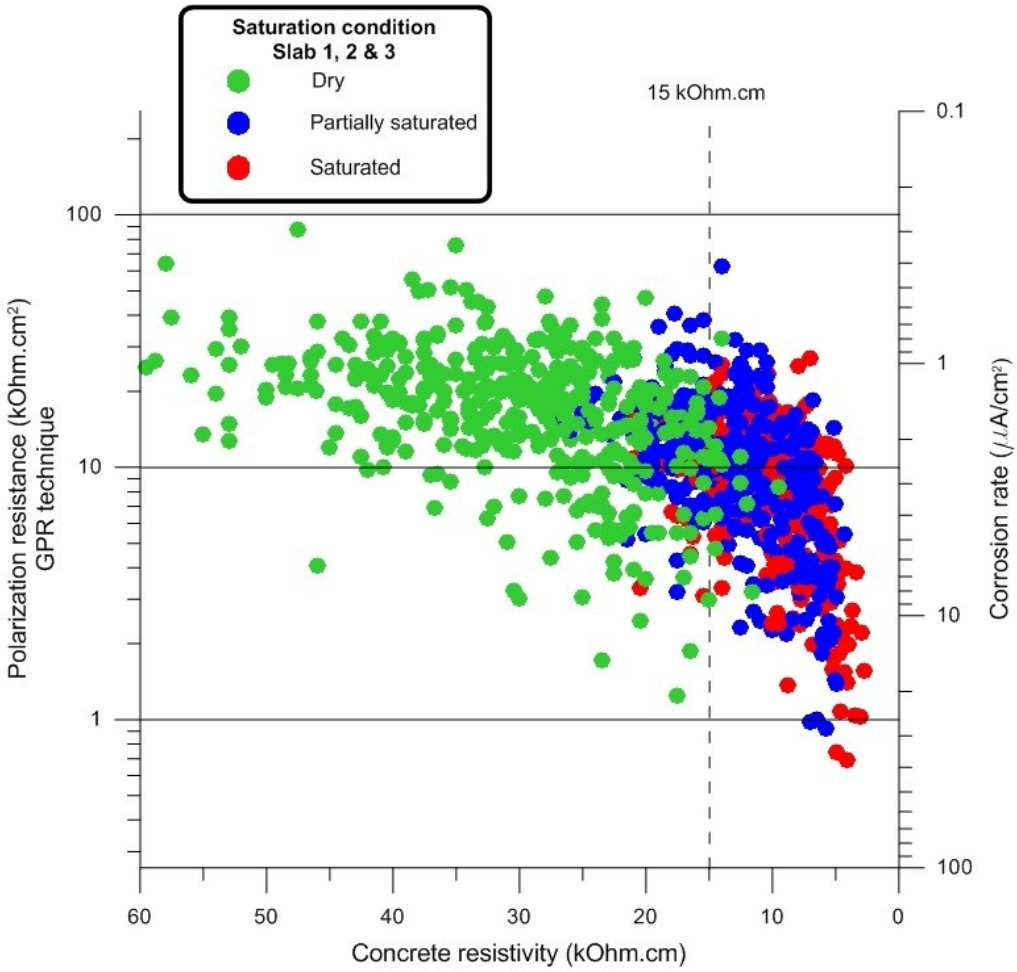

Figure 5-27: Concrete electrical resistivity versus the polarization resistance measurements by the GPR technique (modified values).

6. Conclusions and Future Work

6.1 General

An experimental investigation was carried out to study comparatively the most common corrosion detection techniques used in practice on realistically detailed reinforced concrete slabs that are loaded at service level. The study is designed to investigate important parameters that may affect steel corrosion in reinforced concrete such as w/c of concrete, moisture content of concrete, load-induced cracking and mechanical stresses. To control these parameters systematically and accurately, three large-scale concrete slabs had previously been designed and built in the laboratory. The slabs were loaded and exposed to chloride-containing salts and wetting and drying cycles to initiate reinforcement corrosion. Half-cell potential mapping, as prescribed by ASTM C876-09, was used to predict the probability of steel corrosion in the slabs and to study the validity of the standard in service conditions. Practical and commercially-available linear polarization (LPR) and galvanostatic pulse (GPR) techniques were used to measure corrosion rates in the slabs,

and these measurements were compared with corrosion rate measurements obtained from electrochemical impedance spectroscopy (EIS), which is an advanced technique that is suitable for laboratory studies. It was assumed that corrosion rate measurements through EIS were relatively accurate; therefore, comparisons were carried out against the EIS measurements. Electrical resistivity of concrete was mapped for each slab at different conditions so that its correlation with steel corrosion in the studied slabs is investigated. This chapter presents the main conclusions of this experimental research and recommendations for future work originating from and related to the current research.

6.2 Main conclusions

The experimental study revealed that among the factors studied in this research, concrete moisture content has the highest influence on the corrosion activity of steel in loaded concrete slabs. Among the techniques used in this work concrete electrical resistivity reflects well the variation in concrete moisture content; therefore, it can be considered as a practical way of rating corrosion activity in reinforced concrete members.

Although the effect of loading on the relationship between concrete resistivity and polarization resistance was not clear, in general lower values of resistivity and polarization resistance are associated to regions where the applied bending moment is higher than the cracking moment which creates tension at the surface. This is very likely due to the presence of flexural cracks on this region, which facilitate ingress of aggressive ions and oxygen into the concrete.

Among the polarization resistance techniques which were used to define the rate of corrosion activity, the GPR technique, as compared to LPR, provides relatively closer

results to the measurements by the EIS technique. The polarization resistance measured by the LPR technique ranges from 1 to 500 kOhm.cm^2, whereas the range of data obtained by the EIS technique varies from 0.7 to 20 kOhm.cm^2. Polarization resistance data obtained by the GPR technique varies from 0.1 to 7 kOhm.cm^2. This comparison shows that the LPR technique always underestimates the corrosion activity in comparison to the GPR and EIS technique.

Having said this, it should be noted that the GPR technique can provide reliable information on the kinetics of corrosion when the concrete is not saturated; however, it does not capture the role of the cathodic polarization curve in saturated concrete – hence its measurements should not be regarded as accurate in saturated conditions.

ASTM C876-09 criteria cannot evaluate the state of corrosion activity in reinforced concrete structures just by mapping half-cell potentials. These specific half-cell potential values (-126 mV and -276 mV vs. SCE) do not differentiate the state of corrosion activity. In particular, the standard criteria cannot predict the probability of corrosion activity properly when the half-cell potential is more positive than -276 mV vs. SCE. Therefore, it is critical to evaluate corrosion activity with other methods as well.

6.3 Recommendations for future work

In addition to the present study, other works related to the present study are recommended here for future investigation. These topics are listed as follows:

- Mass loss determination of embedded reinforcing steel to determine the average rate of corrosion.

- The effect of carbonation on the electrochemical techniques, especially concrete electrical resistivity measurements.
- Comparison of experimental results with analytical, empirical and numerical models proposed by other researchers.
- Using the data produced in this research to develop empirical corrosion rate prediction models based on easily measurable and known parameters such as concrete resistivity.

7. References

Alberto A. Sagues (1993). Corrosion measurement techniques for steel in concrete. *Corrosion 93 the annual conference and corrosion show*, paper 353.

Alonso, C., Andrade, C., and Gonzalez, J. (1988). Relation between resistivity and corrosion rate of reinforcemnts in carbonated mortar made with several cement types. *Cement and Concrete Research*, 8(5), p.687.

Angst, U., Elsener, B., Larsen, C. K., and Vennesland, (2009). Critical chloride content in reinforced concrete-A review. *Cement and Concrete Research,* 39(12), p. 1122.

Andrade, C. (1973). New elecrtrochemical technique for the corrosion measurement in reinforced and prestressed concretes. *PhD Thesis Dissertation*, University of Madrid.

Andrade, C. and Alonso, C. (1995). Corrosion rate monitoring in the laboratory and on-site. *Construction and Building Materials*, 10(5), p.315.

Andrade, C., Alonso, C., Gulikers, J., Polder, R., Cigna, R., Vennesland, O., Salta, M., Raharinaivo, R., and Elsener, B. (2004). Test methods for on-site corrosion rate measurement of steel reinforcement in concrete by means of the polarization resistance method. *Materials and Structures*, 37, p.623.

Andrade, C., Alonso, C., and Sarria, J. (2002). Corrosion rate evolution in concrete structures exposed to the atmosphere. *Cement and Concrete Composites*, 24, p.55.

Andrade, C., Castelo, V., Alonso, C., and Gonzalez, J. A. (1984). The determination of the corrosion rate of steel embedded in concrete by the polarization resistance and ac impedance methods. In Chaker, V., editor, Corrosion effect of stray currents and the techniques for evaluating corrosion of rebars in concrete, STP 906. *ASTM International*.

Andrade, C. and Castillo, A. (2003). Evolution of reinforcement corrosion due to climatic variations. *Materials and Corrosion*, 54, p.379.

Andrade, C. and Gonzalez, J. A. (1978). Quantitative measurements of corrosion rate of reinforcing steels embedded in concrete using polarization resistance measurements. *Werkstoffe und Korrosion*, 29(8), p. 515.

Andrade, C., Keddam, M., N´ovoa, X. R., P´erez, M. C., Rangel, C. M., and Takenouti, H. (2001). Electrochemical behaviour of steel rebars in concrete: influence of environmental factors and cement chemistry. *Electrochemical Acta*, 46, p. 3905.

ASTM C 876-77 (1977). Standard test method for half-cell potentials of uncoated reinforced steel in concrete. *ASTM International*.

ASTM C876 - 09 (2009). Standard Test Method for Corrosion Potentials of Uncoated Reinforcing Steel in Concrete. *ASTM International*.

Bentur, A., Diamond, S., and Berke, N.S. (1997). Steel corrosion in concrete. New York, New York, U.S.A.: Chapman & Hall.

Berke, N. S., & Hicks, M. C. (1990). Electrochemical methods of determining the corrosivity of steel in concrete. Corrosion Testing and Evaluation, Eds: Baboian, R., & Dean, S. W., p.425.

Bertolini. L., Elsener, B., Pedeferri, p., Rob P. Polder. (2004) Corrosion of Steel in Concrete.WILEY-VCH Verlag GmbH & Co. KGaA, Weinheim ISBN: 3-527-30800-8.

Bonhoeffer, K. F. and Jena, W. (1951). The electrolytic and chemical passivation and activation of iron. *Journal of Elektrochem*. 59, p.151

Bohni, H. (2005). Corrosion in reinforced concrete structures. Florida, U.S.A.: CRC Press.

Brameshuber, W., Raupach, M., and Schröder, P., (2003). International Symposium (NDT-CE).

Broomfield, J. P. (1997). Corrosion of steel in concrete: Understanding, investigation and repair, *E & FN Spon Press*, New York, NY.

Bungey, J. H. (1989). *Testing of concrete in structures*, 2nd Edition., Chapman & Hall, New York.

Carino, N. (1999). Nondestructive technique to investigate corrosion status in concrete structures. *Journal of performance of constructed facilities*. 13(3), p. 96.

Choi, Y. S., Kim, J. G., & Lee, K. M. (2006). Corrosion behavior of steel bar embedded in fly ash concrete. *Corrosion Science*, 48(7), p. 1733.

Cigna, R., Proverbio, E. and Rocchini, G. (1993). A study of reinforcement behavior in concrete structures using electrochemical techniques. *Corrosion Science*, 35(5-8), p.1579.

Deif, A., Martín-Pérez, B., and Cousin, B. (2008) "Experimental study of chloride penetration in a RC slab sustaining in-service loads", Proc. of the 8th Int. Conf. on Creep, Shrinkage and Durability of Concrete and Concrete Structures, Ed by T. Tanabe, K.Sakata, H. Mihashi, R. Sato, K. Maekawa, and H. Nakamura, Sept. 30th–Oct. 2nd 2008, Ise-Shima, Japan, pp.1107-1113.

Deif, A. (2010). Chloride ingress into reinforced concrete sustaining in-service loads. *PhD Thesis Dissertation*, Department of Civil Engineering, University of Ottawa.

Electrochemical techniques to detect corrosion in concrete structures in nuclear installation, NEA/CSNI/R (2002) 21.

Elsener, B. (2005). Corrosion rate of steel in concrete-Measurements beyond the Tafel law. Corrosion Science, 47(12), p. 3019.

Flis, J., Pickering, H. W., and Osseo-Asare, K. (1995). Assessment of data from three electrochemical instruments for evaluation of reinforcement corrosion rates in concrete bridge components. *Corrosion*, 51(8), p. 601.

Flis, J., Sabol, S., Pickering, H. W., Sehgal, A., Osseo-Asare, K., and Cady, P. (1993). Electrochemical measurements on concrete bridges for evaluation of reinforcement corrosion rates. *Corrosion*, 49(7), p.601.

Feliu, S., Gonzalez, J. A., and Andrade, C. (1996). Electrochemical methods for on-site determination of corrosion rates of rebars. In Berke, N. S., Escalante, E., Nmai, C. K., and Whiting, D., editors, Techniques to assess the corrosion activity of steel reinforced concrete structures, ASTM STP 1276. *ASTM International*.

Feliu, S., Gonzalez, J. A., Andrade, C., and Feliu, V. (1988). On-site determination of the polarization resistance in a reinforced concrete beam. *Corrosion Engineering*, 44(10), p. 761.

Feliu, S., Gonzalez, J. A., Andrade, M. C., and Feliu, V. (1989a). Determining polarisation resistance in reinforced concrete slabs. *Corrosion Science*, 29(1), p.105.

Feliu S., Gonzalez J. A., Feliu S. Jr. and Andrade C., (1990), Confinement of the electrical signal for in situ measurement of polarization resistance in reinforced concrete. *ACI Materials Journal*, p. 457.

Feliu, S., Gonzalez, J. A., Feliu, V., Feliu, S., Escudero, M. L., Rodriguez-Maribona, I. A., Austin, V., Andrade, M. C., Bolano, J. A., and Jimenez, F. (1993). Corrosion detecting probes for use with a corrosion-rate meter for electrochemically determining the corrosion rate of reinforced concrete structures. *United States Patent 5259944*.

Feliu, S., Andrade, A., Gonzalez, J. A., and Alonso, C. (1996). A new method for in-situ measurement of electrical resistivity of reinforced concrete. *Materials and Structures*, V. 29, p. 362.

Feliu, V., Gonzalez, J. A., Andrade, C., and Feliu, S. (1998). Equivalent circuit for modelling the steel-concrete interface. i. experimental evidence and theoretical predictions. *Corrosion Science*, 40(6), p.975.

Feliu, V., Gonzalez, J., and Feliu, S. (2005). Modelling of the steel-concrete interface to obtain information on reinforcement bar corrosion. *Journal of Applied Electrochemistry*, 35, p.429.

GalvaPulse-german instruments, http://www.germann.org

Garcés, P., Andrade, M. C., Saez, A., & Alonso, M. C. (2005). Corrosion of reinforcing steel in neutral and acid solutions simulating the electrolytic environments in the micropores of concrete in the propagation period. Corrosion Science, 47(2), p. 289.

Ge, J., and Isgor, O. B. (2007). Effects of Tafel slope, exchange current density and electrode potential on the corrosion of steel in concrete. *Materials and Corrosion*, 58(8), p.573.

Gepraegs, O. K. and Hansson, C. M. (2004). A comparative evaluation of three commercial instruments for field measurements of reinforcing steel corrosion rates. In Berke, N. S., Thomas, M., Yunping, X., and Veleva, L. L., editors, *Electrochemical Techniques for Evaluating Corrosion Performance and Estimating Service-Life of Reinforced Concrete, ASTM STP 1457*. ASTM International.

Ghods, P. (2010). “Multi-scale investigation of the formation and breakdown of passive films on carbon steel rebar in concrete” *PhD Thesis Dissertation*, Carleton University, Ottawa, ON.

Glass, G. K., Page, C. L., Short. N. R. (1991) Factors affecting the corrosion rate of steel in carbonated mortars, Corrosion Science, 32, p. 1283.

Goni, S., & Andrade, C. (1990). Synthetic concrete pore solution chemistry and rebar corrosion rate in the presence of chlorides. Cement and Concrete Research, 20(4), p.525.

Gonzalez, J., Algaba, S., and Andrade, C. (1980). Corrosion of reinforcing bars in carbonated concrete. *British Corrosion Journal*, 15(3), p.135.

Gonzalez, J. A., Molina, A., Escudero, M. L., and Andrade, C. (1985a). Errors in the electrochemical evaluation of very small corrosion rates - i. polarisation resistance method applied to corrosion of steel in concrete. *Corrosion Science*, 25(10), p.917.

Gonzalez, J. A., Molina, A., Escudero, M. L., and Andrade, C. (1985b). Errors in the electrochemical evaluation of very small corrosion rates - ii. other electrochemical techniques applied to corrosion of steel in concrete. *Corrosion Science*, 25(7), p.519.

Gonzalez, J. A., Feliu, S., Andrade, C., Rodriguez, I., (1991) On-site detection of corrosion in reinforced concrete structures. *Materials and Structures*, 24, p. 346.

Gonzalez, J. A., Feliu, S., Rodffguez, P., Ramlrez , E., Alonso, C., Andrade, C., (1996a) Some questions on the corrosion of steel in concrete - Part 1: when, how and how much steel corrodes. *Materials and Structures*, 29(1), p. 40.

Gonzalez, J. A., Feliu, S., Rodffguez, P., Ramlrez , E., Alonso, C., Andrade, C., (1996b) Some questions on the corrosion of steel in concrete - Part 2: Corrosion mechanism and monitoring, service life prediction and protection methods. *Materials and Structures*, 29(2), p. 97.

Gonzalez, J. A., Miranda, J. M., and Feliu, S. (2004). Considerations on reproducibility of potential and corrosion rate measurements in reinforced concrete. *Corrosion Science*, 46, p.24.

Gowers, K. R. and Millard, S. G. (1993). On-site linear polarization resistance mapping of reinforced concrete structures. *Corrosion Science*, 35(5-8), p.1593.

Gowers, K. R., & Millard, S. G. (1999). Measurement of Concrete Resistivity for Assessment of Corrosion Severity of Steel Using Wenner Technique. *ACI Materials Journal*, 96(5), p. 536.

Hansson, C. (1984). Comments on electrochemical measurements of the rate of corrosion of steel in concrete. *Cement and Concrete Research*, 14, p. 574.

Hansson, C. M., & Sorensen, B. (1990). The threshold concentration of chloride in concrete for the initiation of reinforcement corrosion. Corrosion Rates of Steel in Concrete, Eds: Berke, N. S., Chaker, V., Whiting, D., p. 3.

Hamid, A., Tayyib, j. A., and Shamim khan, M. , (1988), Corrosion rate measurement of reinforcing steel in concrete by electrochemical techniques. *ACI Material Journal*, 85(3), p. 172.

Hausmann, D. A. (1967). Steel corrosion in concrete--how does it occur? *Materials Protection*, 6(11), p. 19.

Ismaili, M. A., Soleymani, H. , Ohtsu, M. (2006). Early detection of corrosion activity in reinforced concrete slab by AE technique. *Proceedings of the 6th Asia-Pacific Structural Engineering and Construction Conference* (APSEC 2006), September 2006, Kuala Lumpur, Malaysia B-64

Jaggi, S., Elsener, B., and B¨ohni, H. (2000). Oxygen reduction on mild steel and stainless steel in alkaline solutions. In j. Mietz, Polder, R., and Elsener, B., editors, Corrosion of Reinforcement in Concrete - Corrosion Mechanisms and Corrosion Protection, *European Federation of Corrosion publications*, 31, p. 3.

John, D. G. (1981). Use of AC impedance technique in studies on steel in concrete in immersed conditions. *British Corrosion Journal*, 16(2), p.102.

Jones, D. A., Greene, N. D. (1966). Electrochemical measurement of low corrosion rates. *Corrosion*, 12. P. 468.

Kaesche, H. (1973). Testing corrosion danger of steel reinforcement due to admixture in concrete. *Zment-Kalk-Gips*, 7, p. 289.

Klinghoffer, O., Frølund, T., Poulsen, E. (2000). Rebar Corrosion Rate Measurements for Service Life Estimates, *Paper presented at the ACI Fall Convention 2000*, Toronto, Canada, Committee 365 "Practical Application of Service Life Models".

Koch, G.H., Brogers, P.H, Thompson, N. Virmani, Y.P and Payer, J.H. (2002). Corrosion cost and preventive strategies in the United States, *FHWA report*; FHWA-RD-01-156, Federal Highway Administration, Washington, DC.

Karadakis, K. (2010). Numerical investigation of the chemistry of the pore solution in the mill scale crevices of carbon steel rebar, *MASc Thesis*, Carleton University, Ottawa, ON.

Lamberte, P., Page, C. L., Vassie, P. R. W. (1991). Investigations of reinforcement corrosion.1. The pore electrolyte phase in chloride-contaminated concrete. *Materials and Structures*, 24, p.24.

Lamberte, P., Page, C. L., Vassie, P. R. W. (1991). Investigations of reinforcement corrosion. 2. Electrochemical monitoring of steel in chloride-contaminated concrete, *Materials and Structures*, 24, p.351.

Law, D. W., Millard, S. G., and Bungey, J. H. (2000). Effect of electrode orientation on linear polarisation measurements using sensor controlled guard ring. *British Corrosion Journal*, 35(2), p.136.

Lehat, A., (2009). The importance of corrosion monitoring for the durability of structures, ARCHES and SPENS Final Seminar – Ljubljana.

Li, L. and Sagues, A. A. (2001). Chloride corrosion threshold of reinforcing steel in alkaline solutions: open-circuit immersion tests. *Corrosion*, 57(1), p.19.

Luping, T. (2002). Calibration of the Electrochemical Methods for the Corrosion Rate Measurement of Steel in Concrete, NORDTEST Project No. 1531-0, *SP Swedish National Testing and Research Institute Building Technology*, SP REPORT 2002:25

Monfore, G. E. (1968). The electrical resistivity of concrete. *Journal of the PCA Research and Development Laboratories*, p. 35.

Murata, T. (2011) Uhlig's Corrosion Handbook, Third Edition (ed R. W. Revie), John Wiley & Sons, Inc., Hoboken, NJ, USA.

Nakamura, E., Watanabe, H., Koga, H., Nakamura, M. and Ikawa, K. (2008). Half-cell potential measurements to assess corrosion risk of reinforcement steels in a pc bridge, *2008 International RILEM Conference*, September 2008 Varenna (LC), Como Lake – Italy.

Newman, J. (1966), Resistance for Flow of current to a disk, *Journal of Electrochem*. Sot., 107, p. 501.

Newton, C. J., & Sykes, j. M. (1988). A galvanostatic pulse technique for investigation of steel corrosion in concrete. *Corrosion Science*, 28(11), p. 1051.

Neville, A. M. (1996). Properties of concrete (4th ed.), John Wiley & Sons Inc.

Nmai, C. K. (2004). Multi-functional organic corrosion inhibitor. *Cement and Concrete Composites*, 26(3), p. 199.

Nygaard. P, Mette, Geiker, R., Elsener, B., (2009) Corrosion rate of steel in concrete: evaluation of confinement techniques for on-site corrosion rate Measurements, *Materials and Structures*, 42, p. 1059.

Oh, B. H., Jang, S. Y. (2005). Experimental investigation on the threshold chloride concentration for corrosion initiation in reinforced concrete structures, *18th International Conference on Structural Mechanics in Reactor Technology (SMiRT 18),* Beijing, China.

Otsuki, N., Madlangbayan, M. S., Nishida, T., Satio, T. and Baccay, M. A. (2009). Temperature Dependency of Chloride Induced Corrosion in Concrete, *Journal of advanced Concrete Technology*. 7(1), p.41.

Page, C. L., Lambert, P., & Vassie, P. R. W. (1991). Investigations of reinforcement corrosion. 1. the pore electrolyte phase in chloride-contaminated concrete. *Materials and Structures*, 24(4), p. 243.

Pedeferri, P., Bertolini, L., (2000), Durability of Reinforced Concrete (in Italian), McGrawHill Italia.

Pettersson, K. (1993). Chloride threshold value and the corrosion rate in reinforced concrete. *Proceedings of Concrete 2000*, V.1, *E&FN Spon*, p. 461.

Pettersson, K. (1996). Factors influencing chloride induced corrosion of reinforcement in concrete. *Durability of Building Materials and Components*, 1, p. 334.

Pettersson, K., & Sandberg, P. (1997). Chloride threshold levels and corrosion rates in cracked high performance concrete exposed in a marine environment. *The 4th*

CANMET/ACI International Conference on Durability of Concrete, Sydney, Australia.

Perez, N. (2004) Electrochemistry and corrosion science, *Kluwer Academic Publishers*, Nederlands.

Polder, R., Tondi, A., and Cigna, R. (1993). Concrete resistivity and corrosion rate of reinforcement, TNO Report 93-BT-r0170.

Polder, R., (2001). Test methods for on-site measurement of resistivity of concrete - a RILEM TC-154 technical recommendation. *Construction and Building Materials*, 15, p.125.

Poupard, O., Ait-Mokjtar, A., & Dumargue, P. (2004). Corrosion by chlorides in reinforced concrete: Determination of chloride concentration threshold by impedance spectroscopy. Cement and Concrete Research, 34, p. 991.

Pour-Ghaz, M., Isgor, O. B., Ghods, P. (2009) Quantitative Interpretation of Half-cell Potential Measurements in Concrete Structures. *ASCE Journal of Materials in Civil Engineering*. 21(9), p. 465.

Qian, S.Y., Chagnon, N. (2001). Evaluation of corrosion of reinforcement in repaired Concrete. *9th International Conference and Exhibition, Structural Faults and Repair*, London, UK.

Raupach, M. (1996). Chloride-induced macrocell corrosion of steel in concrete-theoretical background and practical consequences. *Construction and Building Materials*, 10 (5), p. 329.

Rehm, G., Nürnberger, U., & Fret, R. (1981). Zur korrosion und Spannungsrisßkorrosion von spannstählen bei bauwerken mit nachträglichem verbund. *Bauingenieur*, 56, p.275.

Richardson, M. (2002), Fundamentals of durable reinforced concrete. *Londres e Nova Iorque*, Spon press.

Rodriguez, J., Ortega, L., Garcia, A., Johansson L. and Petterson K., (1994), Proceedings of the International Conference on Concrete Across Borders. Odense, Denmark, Vol. 1, p. 215.

Rodríguez J., Ortega L.M., Garcia A.M., Johansson L. & Petterson K. (1995). On-site corrosion measurements in concrete structures. *Construction Repair*, Nov.-Dec., p. 27.

Saleem, M., Shamee, M., Hussain, S. E., and Maslehuddint. M., (1995). Effect of moisture, chloride and sulphate contamination on the electrical resistivity of Portland cement concrete. *Construction and Building Materials*, 10(3), p. 209.

Sagues, A. (1993). Corrosion measurement techniques for steel in concrete, *Corrosion 93 the annual conference and corrosion show*, paper 353.

Sandberg, P. (1995). Critical evaluation of factors affecting chloride initiated reinforcement corrosion in concrete. *Report TVBM·3068*, University of Lund, Sweden.

Schell, H. C., and Maning, D. G. (1985). Evaluating the performance of cathodic protection systems on reinforced concrete structures. *Material performance*, 24(7), p.18.

Schiessl. P. and Raupach M. (1988). Chloridinduzierte Korrosion von Stahl im Beton. *Beton-Informationen*, 28, p.33.

Schiessl. P. and Raupach M. (1990). Einfluß der Betonzusammensetzung und der Umgebungsbedingungen auf die chloridinduzierte Korrosion von Stahl im Beton, *Beton-Informationen*, 30, p. 43.

Siegel, S., & Castellani Jr, N. J. (1988). Nonparametric statistics, *MacGraw-Hill*, New York, NY.

Song, G. (2000). Theoretical analysis of the measurement of polarisation resistance in reinforced concrete. *Cement and Concrete Composites*, 22, p.407.

Stratfull. R. F. (1957). The Corrosion of Steel in a Reinforced Concrete Bridge, *Corrosion*. 13, p. 173.

Stratfull, Richard F. (1983). Criteria for cathodic protection of bridge decks. Corrosion of reinforcement in concrete construction, *Society of chemical industry/Ellis horwood Ltd.*, London, p. 287.

Stern, M., and Geary, A. L. (1957). Theoretical Analysis of the Shape of Polarization Curves. *Journal of Electrochem*. SOC 104, p. 56.

Stern, M., and Weisert, E. D. (1959). Experimental observations on the relation between polarization resistance and corrosion rate, Proc. Am. SOCT. est. Mat. 59,1280.

Tait, W. S., Handrich, K. A., Tait, S. W., & Martin, J. W. (1993). Analyzing and interpreting electrochemical impedance spectroscopy data from internally coated

steel aerosol containers. Electrochemical Impedance Analysis and Interpretation: *ASTM STP 1188*, Eds.: Scully, J. C., Silverman, D. C., Kendig,M. W., p. 428.

Trabanelli, G., Monticelli, C., Grassi, V., & Frignani, A. (2005). Electrochemical study on inhibitors of rebars corrosion in carbonated concrete. *Cement and Concrete Research*, 35(9), p. 1804.

Tuutti, K. (1982). Corrosion of steel in concrete (Tech. Rep.). Stockholm: *Swedish Cement and Concrete Research Institute*. p.469.

Vassie, P. R. (1984). Reinforcement corrosion and the durability of concrete bridges, *Proceedings of the Institution of Civil Engineers*, Part 1, V.76.

Venu, K., Balakrishnan, K., & Rajagopalan, K. S. (1965). A potentiokinetic polarization study of the behaviour of steel in NaOH-NaCl system. Corrosion Science, 5, p. 59.

Wagner, C. and Traud W. (1938). Qber Die Deutung Von Korrosionsvorgiingen Durch Dber-lagerung Von Electrochemischen Teil- vorgangen Und Uber Die Potentialbildung An Mischelektroden. *Journal of Electrochem,* 44, p. 391.

Weber, J. (1988). Penetration of chloride into concrete on the normal exposure conditions, In dauerhaftigkeit nichtmetallischer anorganischer Baustoffe: Abschluβkolloquium des Forschungsschwer punkt programmes der DFG, Karlsruhe 4-5. *Institut Fur Massivbau Bautechnologie*, Karlsruhe, p.55.

8. Appendix

In this section all the measurements collected using half-cell potential mapping is given.

Table A.1: Half-cell potential (mV) vs. SCE, slab 1 (w/c=0.35) in dry condition.

Location	Distance (cm)	Rebar					
		1	**2**	**3**	**4**	**5**	**6**
1	**10**	-385	-414	-384.5	-355	-296	-214
2	**20**	-350	-381	-358	-339	-296	-243
3	**30**	-323	-334	-312	-313	-312	-281
4	**40**	-295	-287	-302	-287	-287	-261
5	**50**	-272	-255	-250	-234	-248	-245
6	**60**	-271	-261	-261	-178	-195	-229
7	**70**	-275	-290	-268	-180	-195	-237
8	**80**	-296	-303	-279	-281	-250	-243
9	**90**	-311	-333	-298	-277	-249	-148
10	**100**	-346	-350	-291	-284	-226	-143
11	**110**	-316	-352	-300	-297	-219	-178
12	**120**	-282	-321	-328	-320	-285	-210
13	**130**	-318	-345	-338	-323	-300	-307
14	**140**	-346	-367	-346	-298	-269	-296
15	**150**	-350	-350	-307	-243	-216	-253
16	**160**	-332	-326	-306	-232	-218	-268
17	**170**	-323	-310	-310	-296	-275	-274
18	**180**	-308	-298	-301	-287	-235	-208

19	**190**	-300	-280	-270	-266	-230	-205
20	**200**	-312	-331	-269	-254	-180	-221
21	**210**	-317	-330	-295	-252	-223	-165
22	**220**	-324	-319	-287	-260	-255	-260
23	**230**	-295	-302	-277	-269	-258	-270
24	**240**	-289	-309	-293	-151	-217	-259
25	**250**	-291	-311	-292	-180	-185	-280
26	**260**	-322	-317	-303	-302	-304	-331
27	**270**	-349	-328	-293	-309	-329	-350
28	**280**	-359	-332	-307	-322	-367	-356
29	**290**	-348	-305	-319	-286	-335	-324
30	**300**	-350	-291	-284	-294	-285	-313
31	**310**	-355	-319	-299	-308	-328	-325
32	**320**	-337	-313	-279	-313	-325	-317
33	**330**	-308	-290	-281	-234	-260	-289
34	**340**	-280	-270	-273	-183	-180	-259
35	**350**	-241	-269	-255	-244	-245	-246
36	**360**	-244	-235	-241	-240	-240	-241
37	**370**	-224	-211	-208	-241	-200	-151
38	**380**	-233	-217	-195	-193	-175	-154
39	**390**	-227	-228	-192	-188	-160	-147
40	**400**	-209	-197	-187	-177	-114	-140

Table A.2: Half-cell potential (mV) vs. SCE, slab 1 (w/c=0.35) in partially saturated condition.

Location	Distance (cm)	Rebar					
		1	**2**	**3**	**4**	**5**	**6**
1	**10**	-389	-424	-404.0	-384	-333	-331
2	**20**	-372	-413	-383	-352	-275	-302
3	**30**	-347	-363	-348	-354	-338	-325
4	**40**	-306	-329	-335	-323	-302	-306
5	**50**	-297	-302	-308	-255	-282	-288
6	**60**	-312	-326	-344	-244	-249	-277
7	**70**	-307	-338	-330	-266	-234	-297
8	**80**	-351	-363	-344	-325	-305	-310
9	**90**	-353	-394	-364	-345	-278	-253
10	**100**	-395	-405	-345	-339	-266	-231
11	**110**	-382	-414	-351	-347	-258	-282
12	**120**	-328	-354	-381	-369	-358	-341
13	**130**	-346	-363	-385	-377	-363	-410
14	**140**	-384	-388	-346	-322	-332	-393
15	**150**	-381	-377	-344	-255	-254	-334
16	**160**	-368	-349	-328	-252	-251	-337
17	**170**	-367	-346	-347	-331	-328	-355
18	**180**	-368	-395	-350	-358	-304	-288
19	**190**	-446	-437	-353	-356	-273	-293
20	**200**	-469	-501	-370	-355	-259	-305

21	**210**	-458	-460	-350	-304	-284	-256
22	**220**	-442	-404	-329	-298	-315	-337
23	**230**	-383	-382	-325	-298	-303	-320
24	**240**	-359	-380	-338	-217	-241	-295
25	**250**	-366	-378	-348	-261	-262	-375
26	**260**	-418	-404	-382	-378	-407	-428
27	**270**	-477	-457	-404	-406	-455	-472
28	**280**	-506	-461	-423	-441	-473	-469
29	**290**	-502	-439	-448	-402	-445	-427
30	**300**	-481	-434	-431	-415	-445	-480
31	**310**	-468	-439	-425	-428	-473	-489
32	**320**	-440	-410	-379	-405	-456	-458
33	**330**	-393	-386	-390	-318	-386	-428
34	**340**	-357	-365	-350	-282	-295	-376
35	**350**	-341	-348	-343	-342	-345	-351
36	**360**	-335	-318	-329	-338	-325	-339
37	**370**	-334	-306	-304	-302	-293	-253
38	**380**	-355	-349	-313	-312	-285	-258
39	**390**	-338	-322	-287	-276	-231	-255
40	**400**	-345	-336	-307	-276	-234	-285

Table A.3: Half-cell potential (mV) vs. SCE, slab 1 (w/c=0.35) in saturated condition.

Location	Distance (cm)	Rebar					
		1	**2**	**3**	**4**	**5**	**6**
1	**10**	-340	-345	-341.5	-338	-294	-297
2	**20**	-315	-330	-342	-320	-280	-281
3	**30**	-329	-335	-324	-322	-307	-294
4	**40**	-321	-331	-334	-325	-298	-305
5	**50**	-311	-335	-338	-302	-285	-300
6	**60**	-337	-341	-383	-296	-287	-305
7	**70**	-339	-355	-365	-317	-293	-329
8	**80**	-369	-382	-387	-379	-346	-340
9	**90**	-386	-402	-445	-430	-367	-324
10	**100**	-429	-443	-427	-422	-394	-338
11	**110**	-400	-440	-423	-422	-375	-350
12	**120**	-367	-420	-455	-452	-398	-373
13	**130**	-391	-412	-416	-406	-376	-402
14	**140**	-403	-420	-396	-368	-355	-384
15	**150**	-400	-422	-381	-348	-331	-341
16	**160**	-399	-402	-377	-440	-326	-346
17	**170**	-405	-403	-386	-376	-351	-361
18	**180**	-415	-440	-408	-407	-369	-347
19	**190**	-474	-479	-426	-425	-390	-359
20	**200**	-507	-520	-430	-419	-350	-340
21	**210**	-375	-495	-420	-388	-322	-320
22	**220**	-367	-422	-367	-340	-325	-362
23	**230**	-402	-375	-342	-328	-307	-370
24	**240**	-374	-358	-325	-282	-308	-350

25	**250**	-373	-365	-342	-300	-320	-380
26	**260**	-433	-395	-391	-377	-390	-420
27	**270**	-477	-447	-426	-430	-448	-452
28	**280**	-511	-475	-461	-461	-486	-486
29	**290**	-519	-485	-448	-448	-475	-498
30	**300**	-510	-472	-455	-455	-465	-513
31	**310**	-478	-453	-450	-461	-465	-490
32	**320**	-445	-415	-422	-435	-435	-465
33	**330**	-398	-382	-368	-352	-382	-415
34	**340**	-362	-355	-342	-325	-332	-378
35	**350**	-352	-342	-327	-332	-332	-357
36	**360**	-322	-306	-307	-311	-315	-344
37	**370**	-296	-294	-307	-308	-320	-310
38	**380**	-296	-297	-291	-291	-301	-302
39	**390**	-289	-290	-274	-274	-280	-297
40	**400**	-295	-285	-273	-273	-278	-306

Table A.4: Half-cell potential (mV) vs. SCE, slab 2 (w/c=0.4) in dry condition.

Location	Distance (cm)	Rebar					
		1	**2**	**3**	**4**	**5**	**6**
1	**10**	-302	-321	-320	-312	-258	-199
2	**20**	-302	-305	-327	-322	-227	-198
3	**30**	-302	-304	-331	-302	-267	-254
4	**40**	-300	-299	-308	-292	-256	-265
5	**50**	-313	-302	-314	-280	-191	-243
6	**60**	-349	-331	-307	-195	-191	-219
7	**70**	-371	-335	-322	-172	-181	-254
8	**80**	-398	-361	-311	-321	-255	-303
9	**90**	-425	-364	-306	-310	-267	-257
10	**100**	-395	-348	-305	-307	-262	-176
11	**110**	-371	-326	-283	-283	-237	-194
12	**120**	-315	-320	-286	-287	-303	-259
13	**130**	-287	-291	-281	-286	-339	-366
14	**140**	-274	-268	-273	-247	-324	-364
15	**150**	-257	-267	-275	-154	-274	-342
16	**160**	-249	-261	-267	-279	-248	-363
17	**170**	-231	-254	-256	-269	-336	-337
18	**180**	-264	-269	-244	-260	-312	-309
19	**190**	-269	-278	-247	-252	-218	-235
20	**200**	-285	-255	-221	-216	-159	-190
21	**210**	-311	-287	-248	-235	-228	-213

22	**220**	-318	-297	-273	-236	-264	-276
23	**230**	-305	-305	-282	-248	-272	-260
24	**240**	-306	-304	-301	-202	-269	-268
25	**250**	-324	-315	-329	-261	-190	-301
26	**260**	-362	-366	-368	-338	-363	-338
27	**270**	-394	-386	-377	-373	-416	-376
28	**280**	-386	-390	-404	-372	-417	-381
29	**290**	-336	-353	-348	-334	-409	-409
30	**300**	-365	-366	-371	-356	-404	-410
31	**310**	-403	-394	-389	-393	-416	-400
32	**320**	-422	-412	-379	-387	-412	-405
33	**330**	-409	-403	-371	-300	-371	-372
34	**340**	-359	-378	-348	-195	-204	-346
35	**350**	-339	-337	-317	-289	-303	-320
36	**360**	-291	-303	-264	-252	-292	-266
37	**370**	-252	-275	-265	-261	-255	-163
38	**380**	-241	-239	-222	-207	-200	-141
39	**390**	-242	-239	-228	-182	-219	-115
40	**400**	-217	-217	-218	-179	-93	-80

Table A.5: Half-cell potential (mV) vs. SCE, slab 2 (w/c=0.4) in partially saturated condition.

Location	Distance (cm)	Rebar					
		1	**2**	**3**	**4**	**5**	**6**
1	**10**	-306	-356	-339	-342	-298	-230
2	**20**	-318	-334	-332	-325	-292	-249
3	**30**	-304	-320	-308	-306	-294	-287
4	**40**	-302	-326	-295	-289	-272	-278
5	**50**	-317	-339	-302	-254	-216	-266
6	**60**	-342	-357	-314	-202	-199	-260
7	**70**	-400	-376	-327	-285	-240	-276
8	**80**	-452	-429	-353	-330	-296	-292
9	**90**	-492	-483	-353	-324	-283	-252
10	**100**	-500	-452	-349	-339	-241	-205
11	**110**	-476	-393	-306	-304	-217	-216
12	**120**	-387	-362	-307	-301	-280	-277
13	**130**	-338	-327	-310	-304	-313	-340
14	**140**	-327	-318	-290	-207	-292	-334
15	**150**	-301	-292	-269	-233	-236	-352
16	**160**	-289	-275	-270	-283	-260	-354
17	**170**	-281	-279	-266	-301	-316	-346
18	**180**	-300	-289	-270	-300	-291	-316
19	**190**	-308	-318	-278	-288	-246	-275
20	**200**	-339	-320	-275	-268	-238	-245
21	**210**	-373	-339	-268	-246	-240	-249
22	**220**	-355	-316	-276	-259	-282	-290
23	**230**	-319	-323	-286	-270	-278	-288
24	**240**	-320	-331	-310	-206	-252	-300

25	**250**	-350	-342	-354	-285	-231	-325
26	**260**	-409	-400	-406	-387	-376	-379
27	**270**	-474	-453	-452	-457	-459	-449
28	**280**	-479	-470	-481	-469	-474	-468
29	**290**	-455	-464	-460	-423	-451	-485
30	**300**	-465	-472	-494	-480	-473	-506
31	**310**	-491	-488	-478	-482	-503	-509
32	**320**	-499	-473	-447	-457	-451	-491
33	**330**	-463	-445	-435	-404	-430	-470
34	**340**	-391	-403	-398	-319	-326	-431
35	**350**	-348	-339	-349	-334	-339	-382
36	**360**	-307	-318	-297	-308	-316	-312
37	**370**	-272	-296	-283	-286	-255	-216
38	**380**	-248	-274	-266	-259	-254	-192
39	**390**	-265	-300	-269	-250	-248	-178
40	**400**	-241	-246	-258	-249	-141	-162

Table A.6: Half-cell potential (mV) vs. SCE, slab 2 (w/c=0.4) in saturated condition.

Location	Distance (cm)	Rebar					
		1	**2**	**3**	**4**	**5**	**6**
1	**10**	-305	-317	-306	-306	-294	-274
2	**20**	-304	-305	-320	-300	-286	-261
3	**30**	-296	-300	-290	-296	-280	-280
4	**40**	-310	-308	-298	-296	-280	-285
5	**50**	-311	-314	-296	-273	-272	-275
6	**60**	-326	-320	-310	-265	-271	-282
7	**70**	-370	-345	-320	-296	-292	-304
8	**80**	-438	-400	-356	-344	-321	-326
9	**90**	-477	-427	-382	-365	-329	-305
10	**100**	-475	-434	-377	-371	-314	-300
11	**110**	-445	-415	-363	-362	-316	-315
12	**120**	-395	-375	-357	-356	-354	-374
13	**130**	-361	-355	-350	-352	-367	-410
14	**140**	-318	-329	-323	-327	-351	-391
15	**150**	-315	-318	-315	-321	-335	-377
16	**160**	-335	-325	-316	-320	-340	-378
17	**170**	-352	-343	-327	-340	-352	-380
18	**180**	-370	-367	-331	-335	-345	-366
19	**190**	-394	-408	-355	-356	-325	-350
20	**200**	-414	-419	-357	-355	-320	-330
21	**210**	-412	-407	-333	-325	-314	-325
22	**220**	-387	-363	-327	-318	-315	-338
23	**230**	-363	-354	-324	-313	-310	-328
24	**240**	-362	-353	-335	-295	-306	-314
25	**250**	-374	-371	-361	-342	-320	-345

26	**260**	-432	-418	-415	-405	-400	-413
27	**270**	-503	-481	-477	-477	-485	-498
28	**280**	-532	-513	-507	-497	-516	-528
29	**290**	-525	-529	-525	-508	-530	-537
30	**300**	-543	-547	-578	-527	-528	-545
31	**310**	-555	-550	-548	-534	-520	-545
32	**320**	-535	-527	-502	-503	-492	-530
33	**330**	-475	-472	-457	-429	-424	-490
34	**340**	-425	-428	-403	-370	-374	-415
35	**350**	-380	-375	-360	-355	-352	-360
36	**360**	-318	-310	-320	-318	-310	-305
37	**370**	-270	-285	-290	-289	-265	-250
38	**380**	-245	-262	-257	-257	-258	-237
39	**390**	-250	-263	-250	-250	-240	-232
40	**400**	-241	-250	-253	-246	-230	-232

Table A.7: Half-cell potential (mV) vs. SCE, slab 1 (w/c=0.35) in dry condition.

Location	Distance (cm)	Rebar					
		1	**2**	**3**	**4**	**5**	**6**
1	**10**	-386	-368	-285	-285	-201	-264
2	**20**	-339	-337	-344	-333	-292	-269
3	**30**	-326	-327	-300	-264	-284	-280
4	**40**	-328	-327	-300	-264	-284	-280
5	**50**	-320	-310	-297	-221	-238	-250
6	**60**	-332	-314	-300	-120	-265	-248
7	**70**	-356	-345	-312	-261	-265	-248
8	**80**	-369	-363	-303	-258	-260	-234
9	**90**	-424	-400	-321	-306	-259	-212
10	**100**	-433	-375	-327	-311	-279	-120
11	**110**	-386	-354	-320	-311	-250	-188
12	**120**	-381	-373	-355	-330	-259	-328
13	**130**	-395	-379	-370	-349	-333	-268
14	**140**	-404	-394	-367	-363	-358	-297
15	**150**	-414	-392	-370	-257	-290	-330
16	**160**	-413	-397	-383	-337	-286	-382
17	**170**	-409	-386	-350	-318	-353	-381
18	**180**	-405	-400	-366	-327	-338	-378
19	**190**	-390	-373	-332	-319	-258	-292
20	**200**	-386	-335	-252	-242	-133	-195
21	**210**	-362	-342	-288	-259	-253	-178
22	**220**	-329	-315	-285	-269	-283	-297
23	**230**	-332	-318	-289	-257	-304	-288
24	**240**	-339	-334	-313	-197	-305	-347
25	**250**	-372	-362	-336	-248	-265	-378

26	**260**	-375	-354	-347	-339	-387	-372
27	**270**	-384	-363	-355	-358	-389	-394
28	**280**	-350	-346	-348	-367	-405	-392
29	**290**	-356	-324	-328	-321	-383	-405
30	**300**	-375	-362	-373	-360	-367	-402
31	**310**	-365	-381	-376	-387	-408	-409
32	**320**	-399	-364	-364	-365	-404	-393
33	**330**	-417	-391	-375	-327	-373	-382
34	**340**	-415	-411	-361	-214	-288	-345
35	**350**	-391	-373	-326	-314	-287	-332
36	**360**	-356	-349	-311	-307	-311	-293
37	**370**	-365	-339	-305	-304	-265	-267
38	**380**	-329	-302	-285	-269	-266	-123
39	**390**	-337	-321	-287	-239	-167	-98
40	**400**	-311	-341	-286	-272	-143	-100

Table A.8: Half-cell potential (mV) vs. SCE, slab 3 (w/c=0.5) in partially saturated condition.

Location	Distance (cm)	Rebar					
		1	**2**	**3**	**4**	**5**	**6**
1	**10**	-441	-399	-322	-322	-245	-278
2	**20**	-364	-393	-335	-331	-275	-261
3	**30**	-355	-332	-319	-287	-277	-293
4	**40**	-341	-323	-289	-265	-268	-269
5	**50**	-353	-324	-278	-248	-258	-241
6	**60**	-375	-340	-317	-188	-263	-251
7	**70**	-381	-351	-294	-278	-286	-299
8	**80**	-424	-370	-308	-288	-309	-315
9	**90**	-443	-422	-373	-331	-295	-309
10	**100**	-469	-428	-377	-363	-331	-265
11	**110**	-405	-406	-397	-400	-369	-348
12	**120**	-395	-396	-415	-425	-425	-432
13	**130**	-425	-426	-424	-431	-452	-429
14	**140**	-457	-450	-440	-457	-435	-448
15	**150**	-444	-448	-434	-405	-412	-442
16	**160**	-405	-418	-407	-351	-346	-455
17	**170**	-415	-398	-361	-344	-381	-429
18	**180**	-413	-409	-374	-333	-340	-428
19	**190**	-414	-400	-356	-343	-295	-322
20	**200**	-403	-371	-314	-313	-281	-296
21	**210**	-379	-337	-291	-286	-241	-256
22	**220**	-361	-365	-295	-290	-293	-224
23	**230**	-373	-336	-317	-301	-300	-320
24	**240**	-392	-395	-369	-265	-324	-401

25	**250**	-435	-421	-398	-313	-346	-462
26	**260**	-472	-445	-434	-436	-469	-477
27	**270**	-505	-493	-471	-474	-517	-505
28	**280**	-494	-487	-484	-459	-518	-520
29	**290**	-512	-491	-480	-450	-480	-412
30	**300**	-504	-500	-493	-464	-462	-415
31	**310**	-517	-510	-496	-485	-500	-498
32	**320**	-512	-503	-493	-477	-487	-494
33	**330**	-511	-497	-470	-449	-440	-470
34	**340**	-498	-501	-468	-375	-327	-426
35	**350**	-460	-461	-421	-375	-351	-383
36	**360**	-417	-409	-371	-355	-325	-321
37	**370**	-405	-388	-353	-348	-301	-299
38	**380**	-377	-374	-307	-300	-257	-174
39	**390**	-373	-333	-291	-269	-157	-183
40	**400**	-355	-337	-288	-284	-180	-157

Table A.9: Half-cell potential (mV) vs. SCE, slab 3 (w/c=0.5) in saturated condition.

Location	Distance (cm)	Rebar					
		1	**2**	**3**	**4**	**5**	**6**
1	**10**	-441	-420	-381	-381	-342	-353
2	**20**	-396	-418	-385	-385	-351	-365
3	**30**	-390	-392	-373	-357	-338	-353
4	**40**	-393	-378	-350	-336	-308	-331
5	**50**	-392	-381	-327	-307	-290	-297
6	**60**	-421	-369	-330	-285	-293	-294
7	**70**	-439	-389	-341	-318	-308	-303
8	**80**	-485	-434	-397	-368	-315	-332
9	**90**	-507	-462	-455	-441	-330	-300
10	**100**	-527	-476	-418	-413	-323	-294
11	**110**	-497	-478	-452	-441	-374	-315
12	**120**	-502	-501	-503	-470	-398	-346
13	**130**	-536	-522	-528	-500	-395	-362
14	**140**	-525	-522	-513	-485	-392	-368
15	**150**	-520	-514	-484	-425	-386	-385
16	**160**	-511	-489	-455	-397	-368	-410
17	**170**	-502	-488	-459	-418	-387	-456
18	**180**	-489	-477	-451	-411	-372	-421
19	**190**	-468	-453	-424	-410	-367	-345
20	**200**	-467	-422	-367	-365	-301	-315
21	**210**	-445	-399	-379	-372	-318	-313
22	**220**	-428	-418	-385	-363	-323	-374
23	**230**	-431	-420	-394	-370	-336	-383
24	**240**	-453	-443	-412	-356	-369	-395
25	**250**	-482	-472	-452	-394	-402	-471

26	**260**	-550	-530	-521	-515	-512	-550
27	**270**	-590	-571	-560	-548	-550	-575
28	**280**	-584	-578	-567	-548	-567	-572
29	**290**	-572	-571	-555	-545	-540	-560
30	**300**	-587	-581	-577	-527	-524	-552
31	**310**	-596	-583	-575	-566	-553	-573
32	**320**	-589	-584	-576	-558	-532	-560
33	**330**	-572	-570	-543	-510	-588	-525
34	**340**	-546	-546	-504	-545	-524	-464
35	**350**	-484	-460	-421	-412	-396	-424
36	**360**	-448	-426	-400	-392	-360	-374
37	**370**	-404	-384	-374	-371	-337	-320
38	**380**	-377	-366	-337	-335	-316	-270
39	**390**	-355	-360	-329	-324	-310	-269
40	**400**	-343	-327	-316	-303	-276	-261

In this section all the measurements collected using concrete electrical resistivity is given.

Table A.10: Concrete electrical resistivity (kΩ.cm^2), slab 1 (w/c=0.35) in dry condition.

Location	Distance (cm)	Rebar					
		1	**2**	**3**	**4**	**5**	**6**
1	**10**	18.5	19.5	25.0	32.0	34.0	27.5
3	**30**	30.0	30.5	26.5	27.5	32.5	36.5
5	**50**	40.5	44.5	48.5	40.5	44.0	43.0
7	**70**	27.5	29.5	38.5	46.0	43.5	37.5
9	**90**	24.5	27.0	35.5	38.5	36.5	36.0
11	**110**	37.5	41.0	46.0	42.5	38.0	46.5
13	**130**	31.0	39.5	40.0	44.5	49.5	38.5
15	**150**	26.0	43.0	46.5	43.0	47.5	40.5
17	**170**	26.5	33.5	37.0	43.0	46.5	35.5
19	**190**	29.0	25.5	32.3	48.8	52.0	41.5
21	**210**	21.0	28.5	36.5	43.5	54.0	55.0
23	**230**	39.5	42.0	50.0	46.5	44.5	40.5
25	**250**	37.5	33.5	37.5	56.0	53.0	32.5
27	**270**	26.5	24.5	31.0	39.0	35.5	30.5
29	**290**	23.0	21.0	28.0	33.0	25.5	25.5
31	**310**	26.0	28.0	30.5	35.5	42.0	34.5
33	**330**	23.0	19.0	22.5	33.5	37.5	32.0

35	**350**	33.0	30.0	30.0	30.5	30.5	26.0
37	**370**	23.0	26.5	27.8	29.3	34.0	37.5
40	**400**	31.5	40.0	40.5	37.0	37.5	32.5

Table A.11: Concrete electrical resistivity (kΩ.cm^2), slab 1 (w/c=0.35) in partially saturated condition.

Location	Distance (cm)	Rebar					
		1	**2**	**3**	**4**	**5**	**6**
1	**10**	11.5	12.5	16.0	15.5	13.0	11.5
3	**30**	21.5	19.0	15.0	14.5	17.5	20.5
5	**50**	16.0	15.5	19.5	21.5	16.5	16.5
7	**70**	14.5	18.0	17.5	15.5	15.5	20.0
9	**90**	14.5	13.5	16.5	19.5	17.5	16.5
11	**110**	14.5	17.0	19.8	17.3	15.5	13.0
13	**130**	15.5	15.5	18.5	19.0	15.5	14.5
15	**150**	11.5	14.5	17.5	17.0	14.5	17.5
17	**170**	14.5	18.5	19.5	20.0	22.0	20.0
19	**190**	12.5	13.0	14.3	14.8	15.5	15.5
21	**210**	7.6	7.5	11.0	17.0	18.0	14.0
23	**230**	19.5	20.5	20.0	19.0	17.0	16.5
25	**250**	13.0	11.5	12.0	9.5	12.5	17.5
27	**270**	10.3	9.8	11.0	12.0	12.0	11.0

29	**290**	6.5	8.0	7.3	6.9	6.9	8.5
31	**310**	10.9	9.4	11.0	12.0	11.0	9.6
33	**330**	8.6	8.0	11.5	12.5	10.5	13.5
35	**350**	16.0	13.0	12.5	13.0	11.0	12.0
37	**370**	12.0	13.0	14.3	14.8	14.5	12.5
40	**400**	20.0	13.5	13.0	11.0	11.0	13.5

Table A.12: Concrete electrical resistivity (kΩ.cm^2), slab 1 (w/c=0.35) in saturated condition.

Location	Distance (cm)	Rebar					
		1	**2**	**3**	**4**	**5**	**6**
1	**10**	14.0	12.0	12.5	12.5	11.0	12.0
3	**30**	16.0	15.5	15.5	21.0	20.5	14.5
5	**50**	14.5	13.0	16.5	19.5	16.5	16.0
7	**70**	13.0	13.5	14.0	14.5	15.0	15.5
9	**90**	13.8	12.8	16.3	16.8	16.0	14.0
11	**110**	13.6	11.1	11.8	11.3	12.0	11.5
13	**130**	11.5	14.5	19.0	20.5	18.0	13.5
15	**150**	9.6	7.6	10.6	14.5	15.5	14.0
17	**170**	13.5	14.5	16.5	18.0	17.5	15.5
19	**190**	6.2	7.4	10.9	13.0	14.0	12.5
21	**210**	7.7	9.4	12.0	14.0	14.0	12.0

23	**230**	19.0	19.5	17.5	15.5	16.0	16.0
25	**250**	14.3	9.7	9.8	9.8	9.8	11.4
27	**270**	9.8	9.3	8.8	9.4	10.4	9.9
29	**290**	4.8	4.5	5.0	6.7	6.7	6.2
31	**310**	8.8	7.9	8.1	7.7	7.7	8.6
33	**330**	8.9	8.1	8.3	9.3	9.7	9.8
35	**350**	12.0	11.0	11.0	12.0	12.0	11.5
37	**370**	7.3	9.2	11.5	12.5	12.5	12.0
40	**400**	13.0	9.8	9.8	12.5	13.5	12.0

Table A.13: Concrete electrical resistivity (kΩ.cm^2), slab 2 (w/c=0.4) in dry saturated condition.

Location	Distance (cm)	Rebar					
		1	**2**	**3**	**4**	**5**	**6**
1	**10**	40.5	40.0	32.0	32.0	41.0	42.5
3	**30**	36.0	37.0	36.0	35.0	36.0	39.5
5	**50**	25.0	26.0	42.0	41.0	45.0	47.5
7	**70**	24.5	27.0	37.0	41.5	53.0	53.0
9	**90**	22.5	29.0	31.3	29.8	30.0	34.0
11	**110**	27.5	26.0	26.5	36.5	35.5	28.5
13	**130**	39.5	33.0	21.5	25.0	29.0	22.0
15	**150**	37.5	22.0	28.5	27.5	17.5	18.5
17	**170**	53.0	57.5	41.0	27.0	20.0	15.0
19	**190**	23.5	20.0	33.3	33.8	32.5	26.0
21	**210**	37.0	37.5	32.0	21.5	23.5	25.0
23	**230**	31.0	32.0	33.5	33.0	33.0	40.0
25	**250**	26.5	35.0	40.5	35.0	28.0	30.0
27	**270**	31.5	30.0	26.5	22.5	26.5	25.5
29	**290**	15.5	18.0	21.0	21.0	18.0	16.5
31	**310**	17.5	21.0	24.5	19.0	16.5	15.5
33	**330**	16.5	18.5	26.5	20.5	18.5	26.5
35	**350**	23.0	19.5	21.5	24.5	32.5	32.5
37	**370**	25.0	22.5	21.0	25.0	24.5	22.5
40	**400**	30.0	23.0	27.5	32.0	33.0	28.5

Table A.13: Concrete electrical resistivity (kΩ.cm^2), slab 2 (w/c=0.4) in dry saturated condition.

Location	Distance (cm)	Rebar					
		1	**2**	**3**	**4**	**5**	**6**
1	**10**	40.5	40.0	32.0	32.0	41.0	42.5
3	**30**	36.0	37.0	36.0	35.0	36.0	39.5
5	**50**	25.0	26.0	42.0	41.0	45.0	47.5
7	**70**	24.5	27.0	37.0	41.5	53.0	53.0
9	**90**	22.5	29.0	31.3	29.8	30.0	34.0
11	**110**	27.5	26.0	26.5	36.5	35.5	28.5
13	**130**	39.5	33.0	21.5	25.0	29.0	22.0
15	**150**	37.5	22.0	28.5	27.5	17.5	18.5
17	**170**	53.0	57.5	41.0	27.0	20.0	15.0
19	**190**	23.5	20.0	33.3	33.8	32.5	26.0
21	**210**	37.0	37.5	32.0	21.5	23.5	25.0
23	**230**	31.0	32.0	33.5	33.0	33.0	40.0
25	**250**	26.5	35.0	40.5	35.0	28.0	30.0
27	**270**	31.5	30.0	26.5	22.5	26.5	25.5
29	**290**	15.5	18.0	21.0	21.0	18.0	16.5
31	**310**	17.5	21.0	24.5	19.0	16.5	15.5
33	**330**	16.5	18.5	26.5	20.5	18.5	26.5
35	**350**	23.0	19.5	21.5	24.5	32.5	32.5
37	**370**	25.0	22.5	21.0	25.0	24.5	22.5
40	**400**	30.0	23.0	27.5	32.0	33.0	28.5

Table A.14: Concrete electrical resistivity (kΩ.cm^2), slab 2 (w/c=0.4) in partially saturated condition

Location	Distance (cm)	Rebar					
		1	**2**	**3**	**4**	**5**	**6**
1	**10**	14.0	13.0	14.3	12.8	12.5	11.5
3	**30**	16.0	19.0	21.5	19.0	20.0	24.5
5	**50**	15.5	14.5	16.5	18.5	20.5	23.0
7	**70**	11.9	12.9	20.0	18.5	17.5	22.0
9	**90**	7.9	13.3	18.0	20.0	16.0	11.5
11	**110**	10.3	12.0	15.5	20.5	19.0	12.5
13	**130**	13.0	13.0	12.0	17.0	19.5	17.5
15	**150**	9.5	9.5	12.5	10.5	9.2	9.7
17	**170**	15.5	19.5	26.0	24.5	14.3	9.6
19	**190**	17.0	10.5	12.3	12.8	12.0	9.0
21	**210**	21.5	24.0	26.5	25.0	21.0	18.5
23	**230**	24.0	22.5	19.5	17.5	18.0	19.5
25	**250**	13.8	10.3	11.5	13.5	13.5	17.0
27	**270**	8.3	11.5	10.8	9.8	8.0	9.0
29	**290**	6.4	6.3	7.5	10.0	12.0	10.3
31	**310**	6.5	8.5	8.5	7.8	8.9	8.9
33	**330**	7.6	8.6	10.5	11.0	12.5	11.1
35	**350**	12.5	11.5	14.0	16.5	17.5	18.0
37	**370**	11.5	10.5	13.0	15.0	13.0	14.5
40	**400**	20.5	13.5	17.5	20.0	18.0	17.0

Table A.15: Concrete electrical resistivity (kΩ.cm^2), slab 2 (w/c=0.4) in saturated condition.

Location	Distance (cm)	Rebar					
		1	**2**	**3**	**4**	**5**	**6**
1	**10**	13.9	10.4	13.0	14.0	13.5	14.0
3	**30**	19.5	16.5	16.0	15.5	14.5	13.0
5	**50**	13.5	11.5	14.0	15.0	15.5	15.5
7	**70**	11.0	9.0	12.5	13.0	11.5	14.5
9	**90**	8.4	9.5	11.3	11.8	12.5	13.0
11	**110**	10.0	8.7	9.5	13.3	14.0	13.0
13	**130**	14.5	8.8	9.8	16.0	16.0	14.5
15	**150**	13.2	8.7	11.0	10.9	9.4	10.5
17	**170**	21.5	17.0	16.0	16.0	12.5	10.5
19	**190**	13.0	12.0	11.4	10.3	10.4	9.3
21	**210**	14.5	14.5	15.0	15.0	12.5	10.5
23	**230**	20.5	18.5	14.0	13.5	13.5	13.5
25	**250**	8.8	8.8	10.8	10.3	10.1	12.1
27	**270**	10.5	10.0	9.3	9.8	9.3	8.8
29	**290**	5.0	5.5	7.8	8.8	7.7	6.5
31	**310**	6.9	5.2	5.8	6.3	7.1	7.8
33	**330**	7.3	7.0	7.3	6.9	7.4	7.5
35	**350**	9.8	8.0	9.7	10.5	11.0	12.5
37	**370**	9.0	8.8	10.0	10.7	11.0	11.5
40	**400**	11.5	8.0	9.5	11.0	10.4	11.4

Table A.16: Concrete electrical resistivity (kΩ.cm^2), slab 3 (w/c=0.5) in dry condition.

Location	Distance (cm)	Rebar					
		1	**2**	**3**	**4**	**5**	**6**
1	**10**	12.5	20.0	24.0	14.0	17.5	18.0
3	**30**	22.0	23.0	21.5	23.5	28.5	29.5
5	**50**	26.5	28.0	39.0	42.5	37.0	36.5
7	**70**	16.0	18.5	20.5	27.0	31.5	30.5
9	**90**	14.5	16.5	24.8	32.3	41.5	39.0
11	**110**	14.0	12.0	12.5	15.5	27.0	31.0
13	**130**	16.5	14.5	16.5	23.5	27.5	24.5
15	**150**	15.0	22.5	24.0	24.0	33.0	33.0
17	**170**	22.5	27.0	36.5	42.5	39.0	27.5
19	**190**	17.5	20.5	29.0	39.0	58.0	46.0
21	**210**	22.5	20.5	27.0	37.0	59.5	54.0
23	**230**	26.0	27.5	34.0	34.0	27.0	24.0
25	**250**	25.5	26.0	23.5	25.0	30.0	23.0
27	**270**	17.0	11.6	9.6	17.5	20.5	17.0
29	**290**	14.5	14.5	16.0	20.5	20.0	17.0
31	**310**	30.0	32.5	31.0	23.0	22.5	25.5
33	**330**	17.5	18.5	15.0	15.5	21.0	16.5
35	**350**	15.5	20.0	22.0	22.5	28.5	26.5
37	**370**	21.0	20.5	23.0	26.5	28.5	36.0
40	**400**	19.0	20.5	16.0	15.5	21.0	27.5

Table A.17: Concrete electrical resistivity (kΩ.cm^2), slab 3 (w/c=0.5) in partially-saturated condition.

Location	Distance (cm)	Rebar					
		1	**2**	**3**	**4**	**5**	**6**
1	**10**	7.3	7.0	7.0	7.0	8.2	7.3
3	**30**	12.5	10.5	11.0	12.0	12.0	13.5
5	**50**	12.5	13.0	16.5	18.0	17.0	17.0
7	**70**	8.3	10.2	11.0	12.5	14.0	14.0
9	**90**	7.0	9.6	12.8	12.3	11.0	10.5
11	**110**	8.3	6.9	7.2	8.1	6.8	5.1
13	**130**	11.4	8.0	5.5	7.3	8.6	6.0
15	**150**	7.1	7.6	7.1	7.1	7.5	6.0
17	**170**	13.5	11.5	11.0	12.0	11.0	8.4
19	**190**	6.6	6.9	10.5	13.5	13.0	8.1
21	**210**	11.5	13.0	13.0	11.0	8.5	6.5
23	**230**	7.0	7.0	11.5	16.0	15.0	13.5
25	**250**	8.0	6.7	7.8	9.2	8.5	6.8
27	**270**	5.1	6.1	6.6	5.7	5.7	7.0
29	**290**	6.0	6.5	5.2	4.3	6.1	5.8
31	**310**	4.9	5.6	5.0	6.7	7.1	6.3
33	**330**	5.7	5.0	5.6	8.0	8.5	6.6
35	**350**	8.1	6.9	9.3	13.0	15.5	13.0
37	**370**	7.8	7.1	8.4	10.8	11.5	11.5
40	**400**	8.2	8.1	9.2	11.0	10.5	9.5

Table A.18: Concrete electrical resistivity (kΩ.cm^2), slab 3 (w/c=0.5) in saturated condition.

Location	Distance (cm)	Rebar					
		1	**2**	**3**	**4**	**5**	**6**
1	**10**	5.2	4.3	5.6	6.5	7.5	6.7
3	**30**	8.7	7.1	7.5	9.6	10.5	10.0
5	**50**	7.9	7.3	9.3	9.5	10.0	11.5
7	**70**	6.1	7.5	10.1	12.0	11.5	11.5
9	**90**	5.4	6.6	8.7	9.6	8.6	7.9
11	**110**	6.6	7.1	7.4	7.8	7.9	7.4
13	**130**	6.0	4.8	4.6	6.0	7.8	8.5
15	**150**	5.1	5.4	5.4	6.0	7.2	7.9
17	**170**	8.8	9.6	10.0	10.5	10.5	7.9
19	**190**	5.3	5.4	5.9	5.7	7.0	7.0
21	**210**	8.5	8.4	9.3	9.8	9.5	9.7
23	**230**	9.1	9.3	9.1	9.2	9.6	9.6
25	**250**	6.1	6.4	6.4	6.5	6.4	5.7
27	**270**	4.1	4.7	5.2	4.9	4.0	3.5
29	**290**	2.7	3.1	3.7	3.8	3.4	3.0
31	**310**	5.0	4.7	4.1	4.5	5.0	5.3
33	**330**	4.4	4.2	5.1	6.0	6.7	6.1
35	**350**	7.2	6.8	7.1	7.8	8.8	8.9
37	**370**	5.8	5.1	6.3	7.7	8.3	8.6
40	**400**	6.5	6.0	4.9	7.3	9.5	10.0

-In this section all the measurements collected using GPR technique is given.

Table A.19: Corrosion rate measurement with GPR device (μA/cm^2), slab 1 (w/c=0.35) in dry condition.

Location	Distance (cm)	Rebar					
		1	**2**	**3**	**4**	**5**	**6**
1	**10**	8.5	12.0	21.9	31.8	12.3	10.4
3	**30**	12.9	4.9	6.3	6.6	6.0	7.1
5	**50**	8.0	5.7	6.5	4.7	4.1	5.7
7	**70**	11.5	8.1	2.0	4.9	4.4	5.0
9	**90**	5.4	7.6	12.5	9.4	3.9	15.0
10	**100**	14.0	6.7	4.5	4.5	2.3	4.3
11	**110**	7.7	4.4	3.4	3.4	2.3	5.1
13	**130**	16.0	4.3	4.2	9.2	5.7	9.0
15	**150**	9.4	9.5	7.4	6.7	1.1	14.2
17	**170**	18.9	4.7	6.3	6.6	6.5	11.4
19	**190**	12.9	6.7	5.6	5.6	4.5	4.9
20	**200**	96.3	11.9	7.8	7.8	3.7	5.6
21	**210**	34.0	9.9	21.3	9.7	4.7	13.3
23	**230**	8.0	6.0	7.8	5.5	13.0	4.3
25	**250**	7.9	11.8	11.6	6.5	5.7	5.6
27	**270**	10.0	12.7	11.4	16.3	10.9	16.2
29	**290**	34.9	13.8	8.1	5.7	8.3	18.9
30	**300**	30.0	8.6	8.6	15.7	10.6	8.8
31	**310**	14.1	29.0	89.6	23.6	20.4	15.4
33	**330**	16.9	27.0	15.9	16.1	7.6	9.5
35	**350**	13.4	28.1	13.4	10.5	6.8	5.9
37	**370**	6.5	6.7	8.2	8.2	9.8	11.2

39	**390**	5.4	4.5	2.9	2.9	1.4	4.3
40	**400**	7.9	14.3	15.0	21.7	5.9	7.8

Table A.20: Corrosion rate measurement with GPR device (μA/cm^2), slab 1 (w/c=0.35) in partially saturated condition.

Location	Distance (cm)	Rebar					
		1	**2**	**3**	**4**	**5**	**6**
1	**10**	115.0	63.2	38.8	38.8	14.4	11.6
3	**30**	47.8	26.5	13.5	25.4	90.8	20.8
5	**50**	23.6	15.8	19.7	23.3	9.8	12.6
7	**70**	27.1	20.2	28.6	13.2	9.5	44.7
9	**90**	20.5	19.7	15.4	15.4	11.0	23.8
10	**100**	26.1	21.6	12.6	12.6	3.5	8.6
11	**110**	18.2	14.0	9.6	9.6	5.1	12.6
13	**130**	19.4	7.2	5.8	11.5	16.1	10.1
15	**150**	19.7	31.5	61.8	16.7	17.0	12.3
17	**170**	30.0	6.4	23.3	22.1	12.2	18.0
19	**190**	140.0	26.8	15.1	15.1	3.3	8.8
20	**200**	144.0	13.7	9.2	9.2	4.8	11.4
21	**210**	31.3	30.2	20.6	12.8	5.0	1.7
23	**230**	18.8	11.2	18.9	16.4	8.2	12.6
25	**250**	10.9	24.1	20.5	13.3	7.8	8.9
27	**270**	43.2	32.2	32.1	25.7	32.7	129.0
29	**290**	76.0	75.0	45.0	36.2	17.4	50.0
30	**300**	35.0	24.0	32.0	29.1	17.0	24.3
31	**310**	16.7	23.8	22.0	65.3	47.0	28.9

33	**330**	12.0	22.2	21.8	11.0	9.5	8.4
35	**350**	13.0	12.1	18.6	15.7	6.5	7.8
37	**370**	6.8	10.6	8.1	8.1	5.5	5.6
39	**390**	6.8	8.2	5.9	5.9	3.6	7.5
40	**400**	10.0	9.6	11.9	9.4	4.8	8.3

Table A.21: Corrosion rate measurement with GPR device (μA/cm^2), slab 1 (w/c=0.35) in saturated condition.

Location	Distance (cm)	Rebar					
		1	**2**	**3**	**4**	**5**	**6**
1	**10**	26.0	19.6	19.5	19.3	19.0	16.2
2	**20**	12.3	15.1	13.8	12.5	7.8	7.0
3	**30**	11.5	12.8	9.9	17.8	9.1	22.3
4	**40**	17.8	11.0	11.6	20.5	13.7	17.2
5	**50**	12.2	7.0	21.1	11.6	10.4	16.9
6	**60**	17.5	10.2	26.5	11.7	8.1	12.3
7	**70**	29.3	24.4	41.6	14.0	7.6	16.6
8	**80**	65.0	16.3	29.0	29.5	10.5	26.9
9	**90**	60.0	50.0	45.9	37.6	10.9	21.8
10	**100**	37.2	45.5	24.8	24.8	4.2	10.0
11	**110**	17.3	8.5	7.5	7.5	6.5	13.3
12	**120**	29.9	10.2	13.3	24.0	8.6	16.3
13	**130**	33.0	12.9	19.5	85.8	17.5	27.5
14	**140**	29.0	23.4	14.5	22.4	16.0	41.7
15	**150**	22.7	21.7	17.3	17.9	11.8	86.6
16	**160**	19.3	10.3	26.4	15.3	15.9	33.3
17	**170**	35.8	12.7	56.4	33.8	20.4	94.6
18	**180**	26.0	12.7	56.4	28.4	16.0	45.2
19	**190**	60.0	45.7	27.9	27.9	10.1	12.3

20	**200**	112.0	63.1	35.1	35.1	7.1	18.7
21	**210**	99.5	81.6	31.1	25.0	5.6	20.2
22	**220**	70.6	25.4	33.5	22.1	12.5	14.7
23	**230**	17.4	17.4	35.8	16.6	11.0	19.5
24	**240**	10.7	15.4	14.0	15.5	7.7	13.0
25	**250**	8.2	14.7	23.1	17.3	9.9	14.3
26	**260**	17.6	37.8	41.1	24.4	11.4	46.3
27	**270**	24.0	139.3	37.9	24.2	15.9	81.1
28	**280**	36.7	43.7	41.4	36.7	35.2	48.2
29	**290**	82.2	74.0	45.7	28.6	32.9	71.1
30	**300**	57.7	24.3	42.1	43.3	52.3	57.0
31	**310**	26.7	61.9	23.7	34.1	39.2	34.1
32	**320**	19.0	44.7	35.9	26.8	17.9	36.5
33	**330**	19.9	38.0	27.0	24.4	14.3	16.9
34	**340**	21.5	26.7	17.2	23.1	10.0	18.4
35	**350**	21.2	40.0	22.6	22.1	10.7	14.1
36	**360**	14.8	24.4	31.6	18.6	17.8	16.8
37	**370**	9.2	13.7	13.0	13.0	12.2	8.9
38	**380**	9.0	13.7	9.7	9.7	5.6	8.7
39	**390**	10.7	11.2	7.9	7.9	4.6	8.7
40	**400**	18.3	16.1	13.2	36.8	10.0	13.6

Table A.22: Corrosion rate measurement with GPR device (μA/cm^2), slab 2 (w/c=0.4) in dry condition.

Location	Distance (cm)	Rebar					
		1	**2**	**3**	**4**	**5**	**6**
1	**10**	15.6	13.6	13.4	13.4	13.2	10.6
3	**30**	7.9	7.3	7.8	5.3	6.3	6.8
5	**50**	7.9	4.6	6.3	3.4	15.6	7.6
7	**70**	10.0	5.9	6.6	4.0	11.6	14.3
9	**90**	12.4	7.6	7.1	7.1	6.7	7.5
10	**100**	17.3	14.2	8.8	8.8	3.4	4.0
11	**110**	13.6	5.8	4.0	4.0	2.2	4.2
13	**130**	4.4	4.4	9.5	5.0	8.9	12.2
15	**150**	4.1	4.7	14.3	3.5	6.5	6.4
17	**170**	3.2	3.2	6.5	4.8	7.8	12.3
19	**190**	2.7	2.5	2.7	2.7	2.8	3.5
20	**200**	4.8	4.2	3.3	3.3	2.5	6.3
21	**210**	5.9	4.2	7.6	5.4	3.3	8.5
23	**230**	4.3	4.5	5.3	6.4	7.7	8.7
25	**250**	3.9	6.4	5.8	1.3	7.4	13.4
27	**270**	15.0	10.8	19.3	7.6	28.0	33.7
29	**290**	14.2	12.6	24.4	8.4	7.0	6.5
30	**300**	59.0	44.0	43.9	9.3	10.8	9.8
31	**310**	44.0	35.0	18.6	44.0	12.2	36.8
33	**330**	16.7	8.1	12.6	7.5	8.6	10.5
35	**350**	9.1	7.7	11.9	6.2	7.3	10.2
37	**370**	7.3	4.1	4.6	4.6	5.1	5.5
39	**390**	4.7	6.5	4.6	4.6	2.6	3.2
40	**400**	5.6	6.0	8.9	4.6	5.9	4.2

Table A.23: Corrosion rate measurement with GPR device (μA/cm^2), slab 2 (w/c=0.4) in partially saturated condition.

Location	Distance (cm)	Rebar					
		1	**2**	**3**	**4**	**5**	**6**
1	**10**	28.8	4.2	9.5	9.5	14.7	23.5
3	**30**	33.9	22.7	36.1	10.1	14.8	11.3
5	**50**	29.6	15.6	14.2	6.2	13.2	13.2
7	**70**	15.0	11.4	11.7	9.2	11.4	11.0
9	**90**	91.3	27.8	19.7	19.7	11.5	9.2
10	**100**	54.3	24.6	14.7	14.7	4.7	8.4
11	**110**	51.5	15.0	9.3	9.3	3.6	6.8
13	**130**	13.8	13.8	24.8	12.0	19.6	28.2
15	**150**	12.4	17.6	33.7	6.6	11.5	16.7
17	**170**	9.8	7.5	12.6	8.6	14.7	21.7
19	**190**	9.5	7.5	6.2	6.2	4.8	20.4
20	**200**	13.3	14.0	9.6	9.6	5.1	15.4
21	**210**	12.3	11.1	10.7	10.3	5.2	12.5
23	**230**	8.1	7.0	13.5	14.1	16.1	17.8
25	**250**	8.7	9.5	15.4	14.5	21.0	15.5
27	**270**	40.0	34.0	37.1	22.2	22.7	56.3
29	**290**	42.2	41.5	22.0	22.2	22.7	21.0
30	**300**	67.4	127.3	56.7	48.0	83.7	58.6
31	**310**	85.2	73.7	126.0	70.0	150.0	61.9
33	**330**	34.0	31.6	44.6	24.5	20.0	29.6
35	**350**	26.0	21.3	36.7	16.3	16.6	15.5
37	**370**	16.4	12.1	10.9	10.9	9.6	9.8
39	**390**	21.5	12.6	9.1	9.1	5.5	9.5
40	**400**	13.1	19.4	28.0	15.9	18.8	26.0

Table A.24: Corrosion rate measurement with GPR device (μA/cm^2), slab 2 (w/c=0.4) in saturated condition.

Location	Distance (cm)	Rebar					
		1	**2**	**3**	**4**	**5**	**6**
1	**10**	25.8	23.3	20.9	18.6	13.8	8.9
2	**20**	18.0	11.3	8.8	11.0	7.0	9.0
3	**30**	20.4	17.7	19.5	14.8	11.4	14.0
4	**40**	15.9	17.3	25.2	9.6	11.9	15.0
5	**50**	13.5	13.5	13.5	7.3	9.5	16.8
6	**60**	10.7	11.5	11.9	7.7	12.8	13.5
7	**70**	19.4	19.5	14.4	11.4	22.4	19.4
8	**80**	38.7	19.5	12.8	11.0	17.7	19.8
9	**90**	125.0	32.1	16.1	19.8	14.3	19.8
10	**100**	128.7	18.7	12.4	12.4	6.0	7.9
11	**110**	24.4	30.2	18.3	18.3	6.4	13.2
12	**120**	14.5	14.7	21.1	18.8	12.1	16.5
13	**130**	9.6	14.5	32.8	16.2	31.5	45.4
14	**140**	9.4	10.7	24.4	10.3	17.0	29.0
15	**150**	9.5	13.2	28.7	10.6	14.5	18.6
16	**160**	10.7	8.6	32.6	11.1	17.0	22.1
17	**170**	10.0	11.3	22.7	17.1	17.7	29.1
18	**180**	10.5	13.8	27.6	17.0	16.9	37.4
19	**190**	11.0	11.6	9.0	9.0	6.3	17.4

20	**200**	15.0	28.4	17.7	17.7	7.0	19.6
21	**210**	33.1	27.9	27.7	16.5	10.8	31.0
22	**220**	12.8	16.2	27.6	37.4	24.3	56.7
23	**230**	11.0	12.0	28.0	24.2	22.5	43.0
24	**240**	11.7	8.3	17.0	23.2	15.1	29.6
25	**250**	10.1	10.8	14.3	20.7	19.1	23.7
26	**260**	28.9	64.0	42.7	22.4	21.3	42.8
27	**270**	73.0	57.2	70.1	64.7	69.7	283.0
28	**280**	323.6	87.7	77.9	69.2	48.3	83.2
29	**290**	49.2	64.2	47.5	39.3	40.8	67.7
30	**300**	141.4	235.4	226.0	60.4	95.0	201.0
31	**310**	170.5	96.4	95.4	84.0	86.2	133.8
32	**320**	53.0	41.8	71.8	25.4	24.9	51.9
33	**330**	32.2	31.6	80.0	26.0	26.3	42.5
34	**340**	32.0	19.9	33.7	16.4	23.7	29.4
35	**350**	26.8	19.4	33.3	24.9	24.2	34.0
36	**360**	18.9	14.8	32.9	23.0	22.1	27.0
37	**370**	12.6	11.0	10.8	10.8	10.6	11.2
38	**380**	13.7	13.3	10.9	10.9	8.5	8.4
39	**390**	11.7	14.5	22.4	13.0	7.7	7.7
40	**400**	9.2	10.7	20.4	13.0	12.5	14.9

Table A.25: Corrosion rate measurement with GPR device (μA/cm^2), slab 3 (w/c=0.5) in dry condition.

Location	Distance (cm)	Rebar					
		1	**2**	**3**	**4**	**5**	**6**
1	**10**	24.0	8.2	4.1	4.1	-	10.7
3	**30**	17.0	46.7	36.2	18.3	9.3	7.0
5	**50**	8.7	10.7	9.1	6.4	5.7	6.1
7	**70**	10.3	13.1	7.6	4.9	5.6	7.9
9	**90**	35.0	20.2	13.8	13.8	7.3	6.3
10	**100**	18.0	8.5	5.4	5.4	2.3	3.5
11	**110**	19.1	30.8	17.4	17.4	4.0	5.7
13	**130**	11.6	53.0	185.0	205.8	8.1	31.6
15	**150**	18.0	72.7	11.1	42.6	11.0	15.2
17	**170**	20.3	21.0	9.9	17.5	11.4	59.4
19	**190**	12.6	8.6	5.1	5.1	1.7	65.5
20	**200**	14.0	13.3	9.4	9.4	5.4	8.5
21	**210**	12.8	14.7	17.1	6.7	5.9	8.1
23	**230**	11.5	8.9	9.3	10.3	8.4	10.5
25	**250**	11.7	22.3	27.0	31.2	12.3	20.0
27	**270**	75.3	90.9	25.0	19.6	128.0	35.1
29	**290**	18.3	15.2	12.6	11.3	20.7	16.7
30	**300**	42.9	31.2	13.3	22.0	41.3	18.2

31	**310**	98.2	37.0	49.3	41.0	62.7	49.5
33	**330**	317.5	-	99.7	7.5	69.0	44.0
35	**350**	23.8	76.6	45.3	22.0	15.3	18.7
37	**370**	19.9	11.2	8.7	8.7	6.1	8.9
39	**390**	14.4	5.6	4.4	4.4	3.1	4.1
40	**400**	9.6	12.9	9.1	7.5	5.3	4.3

Table A.26: Corrosion rate measurement with GPR device ($\mu A/cm^2$), slab 3 (w/c=0.5) in partially saturated condition.

Location	Distance (cm)	Rebar					
		1	**2**	**3**	**4**	**5**	**6**
1	**10**	26.3	28.0	19.3	19.3	10.5	12.4
3	**30**	33.7	28.4	37.4	42.9	16.4	14.8
5	**50**	22.0	41.9	31.4	25.1	12.3	26.1
7	**70**	34.1	45.2	15.2	11.4	14.9	17.6
9	**90**	62.0	32.1	23.5	23.5	14.8	25.4
10	**100**	65.8	19.6	15.8	15.8	12.0	13.2
11	**110**	21.1	19.9	14.4	14.4	8.8	12.2
13	**130**	19.2	49.3	52.0	75.4	54.3	75.8
15	**150**	25.5	31.1	19.7	22.0	17.6	50.8
17	**170**	16.7	82.3	18.1	17.1	17.6	34.1
19	**190**	18.5	12.8	9.6	9.6	6.3	25.2
20	**200**	19.8	38.8	23.0	23.0	7.1	29.7
21	**210**	21.3	15.1	16.1	16.3	11.6	70.6
23	**230**	22.6	17.8	21.2	15.1	31.2	33.7

25	**250**	57.1	22.9	28.5	80.0	15.9	28.5
27	**270**	147.0	190.0	76.0	75.8	48.2	442.0
29	**290**	151.0	423.0	67.0	44.5	28.0	475.0
30	**300**	164.0	160.0	31.0	77.1	43.8	45.1
31	**310**	275.0	128.0	95.5	112.0	71.8	94.1
33	**330**	83.7	262.3	66.3	25.1	21.0	40.6
35	**350**	22.3	40.9	37.5	25.1	21.0	40.6
37	**370**	21.4	38.6	24.0	24.0	9.4	12.8
39	**390**	24.9	11.8	9.3	9.3	6.8	15.6
40	**400**	14.1	20.6	15.3	11.3	5.5	13.0

Table A.27: Corrosion rate measurement with GPR device ($\mu A/cm^2$), slab 3 (w/c=0.5) in saturated condition.

Location	Distance (cm)	Rebar					
		1	**2**	**3**	**4**	**5**	**6**
1	**10**	15.3	19.6	16.4	16.4	13.1	14.0
2	**20**	15.2	23.9	17.3	17.3	10.6	12.3
3	**30**	23.8	30.8	25.0	27.7	16.2	19.2
4	**40**	63.1	34.5	25.8	25.7	17.1	23.7
5	**50**	18.8	27.8	41.0	17.6	15.4	20.1
6	**60**	24.3	23.9	23.4	14.4	14.6	17.4
7	**70**	26.9	57.5	21.5	16.2	13.8	20.3
8	**80**	66.3	87.5	33.8	21.8	24.6	17.8

9	**90**	102.6	36.0	26.4	26.4	16.8	17.1
10	**100**	55.0	35.6	21.2	21.2	6.7	8.0
11	**110**	33.0	41.8	23.8	23.8	5.8	9.5
12	**120**	35.6	72.1	51.6	61.5	19.4	42.9
13	**130**	43.6	48.8	148.0	177.3	37.9	58.8
14	**140**	79.5	80.6	58.4	60.0	38.1	80.3
15	**150**	61.9	70.9	39.4	29.2	25.3	67.1
16	**160**	61.9	62.4	32.4	31.7	31.4	122.7
17	**170**	61.5	131.9	133.0	44.7	26.0	84.7
18	**180**	148.8	66.1	35.9	62.8	18.4	59.5
19	**190**	31.5	24.3	14.8	14.8	5.2	18.6
20	**200**	38.3	52.0	32.9	32.9	13.8	27.3
21	**210**	39.9	26.6	19.6	23.6	20.3	31.7
22	**220**	35.1	28.9	28.3	21.3	26.0	36.0
23	**230**	65.9	42.2	35.7	26.2	116.6	63.7
24	**240**	38.1	27.2	29.4	26.6	30.7	72.7
25	**250**	49.9	34.7	43.1	39.3	27.3	82.5
26	**260**	191.3	83.0	110.6	67.7	79.7	211.5
27	**270**	701.0	389.0	198.5	83.5	170.0	404.0
28	**280**	-	178.0	703.9	186.0	97.8	521.0
29	**290**	235.0	415.0	113.0	137.0	70.8	147.0
30	**300**	374.0	167.4	225.7	171.3	102.0	157.2

31	**310**	632.0	193.0	273.5	161.6	135.0	232.0
32	**320**	301.0	299.7	214.0	76.2	76.2	182.8
33	**330**	241.0	68.0	203.0	48.2	69.7	111.6
34	**340**	86.0	49.6	131.7	25.0	36.8	44.6
35	**350**	42.8	64.9	87.6	37.0	48.8	48.8
36	**360**	34.0	79.1	43.3	54.7	55.0	29.8
37	**370**	26.9	22.5	20.2	20.2	17.9	19.9
38	**380**	.5.3	30.4	21.3	21.3	12.2	16.6
39	**390**	23.2	9.5	8.2	8.2	6.9	15.3
40	**400**	23.6	26.0	16.8	15.0	13.0	15.6

-In this section all the measurements collected using LPR technique is given.

Table A.28: Corrosion rate measurement with LPR device (μA/cm^2), slab 1 (w/c=0.35) in dry condition.

Location	Distance (cm)	Rebar					
		1	**2**	**3**	**4**	**5**	**6**
1	**10**	3.70	0.93	0.69	0.69	0.45	0.73
5	**50**	0.10	0.20	0.49	1.05	1.40	0.30
9	**90**	0.62	0.30	0.60	0.60	0.90	0.76
13	**130**	0.10	0.42	0.08	0.21	0.89	0.51
17	**170**	0.77	0.28	0.28	0.26	0.56	0.90
23	**230**	-	0.34	0.19	0.36	0.54	-
25	**250**	0.20	0.96	0.42	0.37	-	0.10
29	**290**	0.77	-	0.96	0.57	0.62	0.76
33	**330**	0.58	0.70	0.61	0.59	-	0.53
35	**350**	0.12	0.10	0.21	0.53	0.41	0.67
40	**400**	0.44	-	0.19	0.43	0.41	0.71

Table A.29: Corrosion rate measurement with LPR device (μA/cm^2), slab 1 (w/c=0.35) in partially saturated condition.

Location	Distance (cm)	Rebar					
		1	**2**	**3**	**4**	**5**	**6**
1	**10**	1.85	1.71	1.16	1.16	0.62	0.76
5	**50**	0.25	0.69	0.56	0.62	0.62	0.30
9	**90**	0.76	0.56	0.41	0.41	0.25	0.31
13	**130**	-	0.25	0.17	0.50	0.64	-
17	**170**	0.51	0.50	0.45	0.38	0.42	0.51
23	**230**	0.60	0.32	18.90	0.98	0.43	0.47
25	**250**	0.78	-	0.45	1.12	0.27	0.30
29	**290**	0.87	3.84	0.89	1.63	1.32	2.34
35	**350**	0.86	0.68	0.52	-	0.37	0.40
40	**400**	1.16	0.84	0.75	0.46	0.32	0.38

Table A.30: Corrosion rate measurement with LPR device (μA/cm^2), slab 1 (w/c=0.35) in saturated condition.

Location	Distance (cm)	Rebar					
		1	**2**	**3**	**4**	**5**	**6**
1	**10**	1.35	1.09	0.80	0.80	0.50	0.54
3	**30**	0.06	0.40	0.52	0.58	0.42	0.43
5	**50**	0.26	0.52	0.19	0.39	0.49	0.39

7	**70**	1.00	0.96	0.19	0.05	0.06	0.43
9	**90**	0.29	8.64	4.3	4.3	-	0.18
11	**110**	1.20	4.4	2.96	2.96	1.51	0.96
13	**130**	-	0.16	0.72	0.05	2.30	-
15	**150**	2.31	0.11	1.17	0.44	0.89	0.89
17	**170**	0.15	0.82	-	0.70	1.5	1.2
19	**190**	1.82	0.8	1.5	1.5	2.23	1.29
21	**210**	1.83	1.01	0.8	0.8	0.61	0.89
23	**230**	0.20	0.26	0.74	0.48	0.25	0.30
25	**250**	0.94	1.50	-	3.86	0.70	1.65
27	**270**	2.91	3.43	1.05	3.68	2.06	0.92
29	**290**	13.38	4.95	2.05	1.82	8.77	1.97
31	**310**	1.24	0.70	4.97	63.48	1.66	1.53
33	**330**	0.45	17.31	0.82	0.82	0.33	0.81
35	**350**	0.74	1.15	0.84	1.10	1.04	0.54
37	**370**	1.20	0.10	1.1	1.1	0.30	0.20
40	**400**	1.37	0.96	1.34	1.05	0.84	0.61

Table A.31: Corrosion rate measurement with LPR device (μA/cm^2), slab 2 (w/c=0.4) in dry condition.

Location	Distance (cm)	Rebar					
		1	**2**	**3**	**4**	**5**	**6**
1	**10**	0.28	0.48	0.30	0.30	0.13	0.18
5	**50**	-	0.15	0.13	0.36	0.15	0.11
9	**90**	0.15	0.76	0.32	0.21	-	0.23
13	**130**	1.01	0.70	0.41	0.41	0.13	0.33
17	**170**	0.53	0.55	0.70	0.23	0.22	0.25
23	**230**	0.34	0.23	0.17	0.30	0.36	0.44
25	**250**	0.16	0.15	0.16	0.55	0.41	0.18
29	**290**	-	0.26	0.80	0.43	0.46	-
33	**330**	2.12	4.64	1.35	0.37	0.39	2.01
35	**350**	0.52	0.31	0.79	0.60	0.22	0.63
40	**400**	0.69	1.07	0.34	0.15	0.14	0.21

Table A.32: Corrosion rate measurement with LPR device (μA/cm^2), slab 2 (w/c=0.4) in partially saturated condition.

Location	Distance (cm)	Rebar					
		1	**2**	**3**	**4**	**5**	**6**
1	**10**	1.41	2.07	1.21	1.21	0.36	0.95
5	**50**	0.24	0.29	2.86	0.36	0.51	0.29

9	**90**	1.35	1.54	0.88	0.88	0.21	0.46
13	**130**	1.129	1.045	0.91	0.779	0.35	-
17	**170**	0.91	0.55	0.45	0.68	0.49	1.07
23	**230**	0.25	0.27	0.52	0.55	0.32	0.18
25	**250**	1.84	2.12	-	1.23	-	0.29
29	**290**	1.44	0.81	3.13	1.78	1.88	2.70
35	**350**	0.18	0.98	0.81	0.83	0.62	0.57
40	**400**	1.33	3.46	0.79	0.34	0.45	0.81

Table A.33: Corrosion rate measurement with LPR device ($\mu A/cm^2$), slab 2 (w/c=0.4) in saturated condition.

Location	Distance (cm)	Rebar					
		1	**2**	**3**	**4**	**5**	**6**
1	**10**	1.25	1.40	1.28	1.28	1.15	0.25
3	**30**	0.22	0.16	0.39	0.15	0.17	-
5	**50**	0.41	0.34	0.55	0.35	0.24	0.03
7	**70**	0.93	1.01	0.38	0.48	0.87	0.39
9	**90**	1.85	0.70	0.35	0.35	-	0.28
11	**110**	0.92	0.94	0.93	0.93	0.92	0.52
13	**130**	0.37	0.27	0.13	0.90	0.95	-
15	**150**	0.44	0.55	0.50	0.50	1.20	0.72
17	**170**	0.20	0.20	0.23	0.30	1.15	1.09

19	**190**	1.10	0.98	0.92	0.92	0.92	0.01
21	**210**	1.20	0.92	0.98	0.98	1.54	0.51
23	**230**	0.31	0.41	0.72	1.32	0.57	1.28
25	**250**	2.90	1.40	1.13	1.14	1.05	1.63
27	**270**	0.54	4.00	1.20	1.40	4.44	0.77
29	**290**	1.65	1.05	5.00	2.54	8.65	1.06
31	**310**	2.47	3.48	0.59	0.15	8.65	1.38
33	**330**	0.95	1.26	1.66	0.91	1.67	0.38
35	**350**	1.10	0.94	0.06	0.08	0.25	0.30
37	**370**	0.77	0.85	0.7	0.7	0.45	0.30
40	**400**	0.45	1.32	1.10	0.84	0.10	0.18

Table A.34: Corrosion rate measurement with LPR device (μA/cm^2), slab 3 (w/c=0.5) in dry condition.

Location	Distance (cm)	Rebar					
		1	**2**	**3**	**4**	**5**	**6**
1	**10**	1.20	1.66	0.91	0.91	0.16	0.41
5	**50**	0.33	0.53	-	0.43	0.25	0.25
9	**90**	0.65	0.40	0.50	0.50	0.61	0.80
13	**130**	0.36	0.60	-	0.81	0.32	0.50
17	**170**	0.90	0.65	0.81	0.95	-	-
23	**230**	0.3	0.32	0.20	0.33	0.27	0.28
25	**250**	0.78	1.74	0.72	0.90	0.60	1.16

29	**290**	1.18	1.35	3.11	0.97	1.03	2.16
33	**330**	1.60	1.30	-	0.93	0.92	-
35	**350**	0.89	0.85	0.43	0.82	0.26	0.57
40	**400**	0.99	0.67	0.60	0.32	0.18	0.13

Table A.35: Corrosion rate measurement with LPR device (μA/cm^2), slab 3 (w/c=0.5) in partially saturated condition.

Location	Distance (cm)	Rebar					
		1	**2**	**3**	**4**	**5**	**6**
1	**10**	3.26	3.36	1.92	1.92	0.47	1.00
5	**50**	0.62	1.00	17.30	0.64	0.69	0.57
9	**90**	2.42	1.81	-	-	0.67	0.93
13	**130**	1.60	0.10	2.56	0.89	3.04	-
17	**170**	1.52	1.56	1.04	0.94	0.91	2.65
23	**230**	0.42	0.12	0.90	0.25	1.10	2.33
25	**250**	0.60	4.30	2.85	3.84	7.46	3.84
29	**290**	2.50	3.84	2.46	2.16	6.92	3.15
35	**350**	0.81	5.76	1.58	1.01	0.70	1.03
40	**400**	1.07	3.06	1.01	0.94	0.71	0.83

Table A.36: Corrosion rate measurement with LPR device ($\mu A/cm^2$), slab 3 (w/c=0.5) in saturated condition.

Location	Distance (cm)	Rebar					
		1	**2**	**3**	**4**	**5**	**6**
1	**10**	1.30	3.30	2.13	2.13	0.96	2.02
3	**30**	0.27	2.33	1.10	3.72	0.56	0.45
5	**50**	1.11	4.96	1.77	2.30	0.53	0.35
7	**70**	3.98	1.12	5.40	1.10	1.00	0.66
9	**90**	1.92	1.03	0.71	0.71	0.39	4.30
11	**110**	2.87	4.77	3.04	3.04	1.30	-
13	**130**	1.20	0.83	2.17	11.10	8.67	2.46
15	**150**	3.46	1.04	3.46	18.10	0.57	1.70
17	**170**	1.75	2.61	1.57	1.25	0.50	1.13
19	**190**	2.42	3.1	1.83	1.83	0.6	0.65
21	**210**	0.12	3.50	2.11	2.11	0.72	0.13
23	**230**	0.8	0.45	0.56	0.75	3.80	1.97
25	**250**	8.64	9.20	2.01	-	3.65	6.04
27	**270**	8.60	3.90	5.73	4.00	0.72	4.86
29	**290**	7.92	11.50	1.08	1.28	8.72	0.29
31	**310**	17.20	4.30	1.64	2.15	5.60	4.20
33	**330**	34.40	30.40	27.97	2.16	2.02	3.05
35	**350**	2.50	-	17.74	0.83	0.90	2.20
37	**370**	1.50	4.57	2.78	2.78	0.98	0.64
40	**400**	3.25	2.40	2.52	1.63	1.09	0.52